

DIPARTIMENTO DI FISICA

DOTTORATO DI RICERCA IN FISICA
XXIX CICLO

Constraints on the spontaneous collapse mechanism:
theory and experiments

Settore scientifico-disciplinare FIS/02

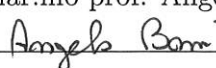
DOTTORANDO:
Marko Toroš

RESPONSABILE DOTTORATO DI RICERCA:
Chiar.mo prof. Livio Lanceri (Univ. Trieste)

FIRMA: 

RELATORE:

Chiar.mo prof. Angelo Bassi (Univ. Trieste)

FIRMA: 

ANNO ACCADEMICO 2015/2016

Contents

1	Introduction	1
1.1	The measurement problem	1
1.2	Spontaneous collapse models	3
1.3	Thesis structure	4
I	Theoretical constraints	6
2	General structure	7
2.1	Introduction	7
2.2	Gaussian stochastic processes	7
2.2.1	Stochastic differential equation	7
2.3	Constraints	9
2.3.1	Probabilistic Interpretation	9
2.3.2	Collapse of the state vector	12
2.3.3	Covariance	14
2.3.4	Stationary process	16
2.4	Classification of collapse models	16
2.5	Conclusion and discussion	18
3	CD map and cdCSL model	19
3.1	Introduction	19
3.2	CD Map	20
3.2.1	Conditions (i), (iii), (iv)	20
3.2.2	Condition (v)	20
3.3	cdCSL	23
3.4	Conclusions	25
II	Experimental constraints	26
4	Matter-Wave Interferometry: theory	27
4.1	Introduction	27
4.2	Derivation of the interference pattern	29
4.2.1	Paraxial approximation	29
4.2.2	Separability	32
4.2.3	Far-field	36
4.2.4	Talbot Lau near-field	37

4.3	Summary of Collapse Models and of the interference pattern	39
4.3.1	Continuous Spontaneous Localization	39
4.3.2	Diósi-Penrose	39
4.3.3	Dissipative CSL	40
4.3.4	Colored CSL	42
4.3.5	Quantum mechanics with universal position localization	45
4.4	Center-of-mass motion for a rigid object and the amplification mechanism . .	46
4.4.1	Adler's formula	47
4.4.2	Homogeneous thin disk approximation	48
4.4.3	2D Lattice disk	49
4.4.4	Comparison and other collapse models	50
4.4.5	Localization requirement of macroscopic objects	51
5	Matter-Wave Interferometry: experiments	54
5.1	Introduction	54
5.2	Limits of validity of the CD bounds	54
5.3	Experimental data analysis	56
5.3.1	Far-field	57
5.3.2	Near-field KDTL	57
5.3.3	Comparison of near and far field experiments.	58
5.4	Parameter space bounds	59
6	Conclusion	62
7	Acknowledgments	63
	Appendices	64
A	Galilean covariant Gaussian maps	65
A.1	Introduction	65
A.2	Map	65
A.3	Covariance	66
A.3.1	Translation-covariance	67
A.3.2	Boost-covariance	68
A.3.3	Translation-boost Covariance	69
A.3.4	Rotation Covariance	69
A.3.5	Markovian limits	70
A.4	Discussion and conclusions	71
B	Canonical quantum mechanics	72
B.1	Canonical quantum mechanics	72
B.1.1	Canonical Poincaré covariant quantum mechanics	72
B.1.2	The non-relativistic limit	74
C	Relativity and classicalization maps	76
C.1	Introduction	76
C.2	Covariance of relativistic maps	76
C.2.1	Map decompositions	77
C.2.2	Covariance	78

<i>CONTENTS</i>	iii
C.2.3 Non-relativistic translations and boosts	79
C.2.4 Relativistic translations and boosts	79
C.2.5 Physical insight	81
C.3 Implications	82
C.3.1 Non-unitary modification of canonical quantum mechanics	82
C.3.2 Macroscopicity measure	83
C.4 Conclusions	84
D Relativistic corrections	85
D.1 Introduction	85
D.2 Dynamical map	85
D.3 rcdCSL	86
D.4 Higher order corrections	87
D.5 Comparison with fully relativistic collapse models	88
Bibliography	89

List of Figures

4.1	The common structure of diffraction experiments	28
4.2	The grating structure	32
4.3	The experimental setup	37
4.4	Comparison of dCSL D functions (temperature)	42
4.5	Comparison of dCSL D functions (boost)	43
4.6	Comparison of D functions	45
4.7	Macro-molecule approximations	48
4.8	Amplification mechanism	50
4.9	Lambda scaling	51
5.1	Limits of validity (temperature)	55
5.2	Limits of validity (temperature and boosts)	56
5.3	Experimental fits	57
5.4	CSL interferometry bounds	58
5.5	CD parameter diagram	60
5.6	QMUPL parameter diagram	61
5.7	DP parameter diagram	61
C.1	Relativistic systems	82

Nomenclature

cCSL	colored continuous spontaneous localization
cdCSL	colored and dissipative continuous spontaneous localization
cdQMUPL	colored and dissipative quantum mechanics with universal position localization
CP	completely positive
cQMUPL	colored quantum mechanics with universal position localization
CSL	continuous spontaneous localization
dCSL	dissipative continuous spontaneous localization
DP	Diósi - Penrose
dQMUPL	dissipative quantum mechanics with universal position localization
GRW	Ghirardi Rimini Weber
KDTL	Kapitza Dirac Talbot Lau
QMUPL	Quantum mechanics with universal position localization
TP	trace preserving

Chapter 1

Introduction

We motivate the construction of spontaneous collapse models. We first look at the measurement problem in orthodox quantum mechanics (Sec. 1.1); we then briefly discuss the main ideas of spontaneous collapse models (Sec. 1.2). For a more complete discussion see [1, 2, 3] and references therein. We conclude by summarizing the structure of the thesis (Sec. 1.3).

1.1 The measurement problem

A physical theory consists of a mathematical formalism and of an interpretation. The mathematical formalism is a set of abstract objects with precise rules on how to manipulate them, while the interpretation connects the abstract mathematical objects with the physical world. Specifically, in quantum mechanics we have the Hilbert space formalism given by the wave function, the observables as self-adjoint operators and by the Schrödinger equation. On the other hand, there is a multitude of different interpretations of quantum mechanics: we will now first discuss the orthodox interpretation, where the state vector is complete and exhaustive description of an individual system [4].

Let us first discuss the problem of macroscopic linear superpositions. For the moment we postpone the discussion on what is macroscopic and what is microscopic: we loosely define as a macroscopic distance the minimal resolution of the human eye and objects as macroscopic, if they are visible by the naked eye. We consider a macroscopic system S described by states in the Hilbert space \mathcal{H} . In particular, we consider two states $|\psi_1\rangle, |\psi_2\rangle$, corresponding to two different macroscopic configurations, i.e. the supports of $|\psi_1\rangle, |\psi_2\rangle$ in the configuration space are disjoint and the distance between them is macroscopic: the distance between the two positions of the center of mass in the two states, e.g. the book at the left edge of the table and at the right edge of the table, respectively. We now consider the following state:

$$|\psi\rangle = \frac{1}{\sqrt{2}} (|\psi_1\rangle + |\psi_2\rangle), \quad (1.1)$$

which is a possible state according to the theory. We are confronted with a paradoxical situation: how can the book exist at two different positions on the table? Because of the linearity of the theory (quantum superposition principle), even if the whole universe is carefully included in the above argument, the conclusion of macroscopic linear superpositions is unavoidable: this is known as the problem of macro-objectification [5].

An attempt to bypass the problem of macro-objectification has been made within the orthodox interpretation: it has been suggested that microscopic and macroscopic objects are

governed by intrinsically different laws, namely quantum mechanics and classical mechanics, respectively. In particular, a microscopic system, when left undisturbed by macroscopic objects, evolves according to the usual Schrödinger equation:

$$i\hbar \frac{d}{dt} |\psi_t\rangle = \hat{H} |\psi_t\rangle, \quad (1.2)$$

where \hat{H} is the usual Hamiltonian operator. On the other hand, when a microscopic object S , completely described by $|\psi\rangle$, interacts with a macroscopic object M (the measuring apparatus), one postulates a completely different evolution, namely the wave-function collapse postulate. To formulate it, we associate to M a hermitian operator \hat{A} with eigenvalues denoted by a . In addition, we associate to both S and M a random variable \mathcal{A} with probability density function given by

$$p(\mathcal{A} = a) = |\langle a | \psi \rangle|^2. \quad (1.3)$$

We prescribe that, when the microscopic system S interacts with the macroscopic system M , the state changes instantaneously, and in a random way, to an eigenstate of \hat{A} :

$$|\psi\rangle \rightarrow |a\rangle, \quad (1.4)$$

where a is chosen randomly by the random variable \mathcal{A} according to the Born rule in Eq. (1.3). This resolution to the macro-objectification problem thus assumes two very different evolutions for the state vector: a continuous and deterministic Schrödinger equation (1.2) and the discontinuous and random wave-function collapse axiom in Eq. (1.4). However, we are now forced to confront the question: what is the distinction between microscopic and macroscopic? Since there does not seem to be an unambiguous answer, we are left with the ambiguity in the use of the prescriptions given by Eqs. (1.2) or (1.4), i.e. when it is not clear whether M is microscopic or macroscopic, it is not clear whether to use Eq. (1.2) or Eq. (1.4) for the evolution of the wave function of the microscopic system S . This is known as the measurement problem.

The measurement problem, although bypassing the macro-objectification problem, leads to either an arbitrary or ambiguous distinction between microscopic and macroscopic systems. In fact, one can argue in a simple way, although not by any means conclusively, that such a distinction is doomed to be flawed [3]: a macroscopic object is composed by microscopic objects, e.g. a book is composed by atoms, and thus there should not be an intrinsic distinction between microscopic and macroscopic objects. On the other hand, the effective dynamics for the composite (macroscopic) object can be quantitatively very different from the dynamics of its constituents. We now explore this possibility.

Consider a composite macroscopic object: we want to describe the dynamics of the composite object using the degrees of freedom of its constituents, e.g. we want to describe the dynamics of a book in terms of individual atoms. In particular, we ask the following question: can we construct a dynamics such that the behavior for constituent microscopic objects resembles quantum mechanics, while the center of mass position of the macroscopic objects evolves approximately classically? We introduce the solution based on this idea, namely spontaneous collapse models, in the following section. Specifically, the Schrödinger dynamics is modified by additional terms: on one hand, for microscopic objects, these terms are tiny, while on the other hand, for macroscopic objects, these terms combine, and effectively classicalize the dynamics for the center of mass position of the macroscopic object.

1.2 Spontaneous collapse models

The literature on collapse model is vast: see [6, 7] and references therein. In this section we discuss heuristically some of the common features of collapse models. In particular, we show how collapse models solve the measurement problem.

The central idea of collapse models is a modification of the dynamics: the Schrödinger equation is modified by stochastic and nonlinear terms. In particular, the dynamics is determined by the pair $(|\psi_t\rangle, h_t)$, where h_t is a noise (field), while the system is completely determined by $|\psi_t\rangle$. Loosely speaking, the measurement problem is solved by combining the Schrödinger evolution with the wave function collapse postulate given by Eqs. (1.2), (1.4), respectively, in a single dynamical law.

For concreteness, let us introduce the collapse mechanism with reference to the first collapse model introduced in the literature, namely the Ghirardi-Rimini-Weber (GRW) model [8]: the other collapse models share the same basic features. The GRW model is parametrized by two parameters: a collapse rate λ and a characteristic localization length r_C . The values suggested by GRW are: $\lambda = 10^{-16}\text{s}^{-1}$ and $r_C = 10^{-7}m$ for a reference object of mass 1amu . h_t is in this case a Poisson stochastic process with mean λ that generates events of wave function collapse at random times: when a collapse event is triggered, the wave function gets multiplied (and thus localized) by a Gaussian with mean \mathbf{z} and standard deviation r_C , where \mathbf{z} is chosen randomly with probability density function

$$\|\hat{L}(\mathbf{z})|\psi_t\rangle\|^2, \quad (1.5)$$

and

$$\hat{L}(\mathbf{z}) = (\pi r_C)^{-3/4} \exp(-(\hat{\mathbf{x}} - \mathbf{z})^2 / 2r_C^2) \quad (1.6)$$

is called the localization operator ($\hat{\mathbf{x}}$ is the position operator). Let us consider a composite object, completely described by $|\psi_t\rangle$, of mass $m \approx Nm_0$, where N denotes the number of nucleons. It can be shown, that the effective dynamics for the center of mass wave function $|\psi_t^{CM}\rangle$ scales with the number of particles N , i.e. the effective collapse rate is given by $\Gamma = (m/m_0)\lambda$. We have the following picture

$$(|\psi_t\rangle, h_t) \longrightarrow (|\psi_t^{CM}\rangle, h_t^{CM}), \quad (1.7)$$

where h_t^{CM} is a Poisson stochastic process with mean Γ . In this way we re-obtain the quantum mechanical predictions for microscopic objects, while, on the other hand, for larger objects the dynamics gradually becomes classical (within experimental errors). This scaling of the dynamical law for the center of mass, known as the amplification mechanism, gives the correct classical limit and solves the macro-objectification problem.

Collapse models are usually seen as phenomenological, emerging from an underlying theory: it has been suggested that the noise effectively describes fast degrees of freedom of an underlying theory, as in Trace dynamics [9], or that it originates from a fundamental instability of the system [10]. So far, the only derivation of the collapse dynamics has been given in the framework of Bohmian mechanics [11]. In Bohmian mechanics, an N particle system is completely determined by the pair $(|\psi_t\rangle, (X_1, \dots, X_N))$, where X_1, \dots, X_N denote the positions of the particles, and the wave function $|\psi_t\rangle$ guides the evolution of the positions X_1, \dots, X_N . Let us define the center of mass position as:

$$X^{CM} = \frac{\sum_{i=1}^N m_i X_i}{\sum_{i=1}^N m_i}, \quad (1.8)$$

where m_i denotes the mass of particle i . It has been argued that the trajectory of particle i becomes classical as the center of mass conditional wave function $|\psi_t^{CM}\rangle$, a well defined object in Bohmian mechanics, becomes well-localized by the interaction with the environment. It has been shown, loosely speaking after the integration of the environment degrees of freedom, that $|\psi_t^{CM}\rangle$ has a GRW dynamics. We have the following picture:

$$(|\phi_t\rangle, (X_1, \dots, X_N, Y_1, \dots, Y_M)), \longrightarrow (|\psi_t^{CM}\rangle, X^{CM}, h_t^{CM}), \quad (1.9)$$

where $|\phi_t\rangle$ is the state vector associated to the total $N + M$ particle system (system and environment).

To summarize, two are the main features of the collapse dynamics: stochasticity and non-linearity. It is straightforward to argue why stochasticity is necessary: we want to re-obtain the quantum mechanical predictions in accordance with the Born rule given in Eq. (1.3). On the other hand, as we will see, non-linearity is necessary to obtain well-localized states in the classical limit. In addition, non-linearity implies stochasticity for the state vector evolution if we request the condition of non-superluminal signaling [12]. However, there still remains a large freedom in the construction of collapse models: this has led to a multitude of different collapse models and model dependent experimental tests. This thesis will address this issues.

1.3 Thesis structure

In this thesis, based on the discussion in Sec. 1.2, we have asked the following two natural questions:

1. Can we single out a particular collapse model using theoretical arguments?
2. Is there a model independent experimental test?

We give answers to these questions in Part I (Chapters 2 and 3) and Part II (Chapters 4 and 5) of this thesis, respectively. We summarize below each chapter of the thesis (the references correspond to papers in preparation).

I 2: Gaussian collapse models [13]. We discuss the general structure of Gaussian spontaneous collapse models. We constrain the dynamics based on a set of minimal requests: (i) probabilistic interpretation, (ii) collapse of state vector, (iii) covariance under space-time transformations and (iv) stationary initial conditions. We classify the most well-known collapse models in the literature.

I 3: CD map and cdCSL model [14]. We obtain the most general modification of the von-Neumann map, namely the CD map, by imposing the following constraints: (i) probabilistic interpretation, (iii) translational and rotational covariance, (iv) stationary initial conditions and (v) asymptotic Gibbs state. By imposing two additional constraints: (ii) collapse of the state vector and (vi) noise field over physical space, we construct a colored and dissipative generalization of the continuous spontaneous localization (CSL) model, namely the cdCSL model.

II 4 Theoretical interference patterns [15, 16]. We present a simple derivation of the interference pattern in matter-wave interferometry as predicted by a class of master equations, by using the density matrix formalism. We apply the obtained formulae to the CD map. In addition, we apply the obtained formulae to the most relevant collapse models. We discuss the separability of the collapse models dynamics along the 3 spatial directions, the validity of the paraxial approximation and the amplification mechanism. We obtain analytical expressions both in the far field and near field limits. These results agree with those already derived with the Wigner function formalism.

II 5 Matter-wave experiments [15, 16]. We compare the theoretical predictions with the experimental data taken from the two most relevant matter-wave experiments: the 2012 far-field experiment and the 2013 Kapitza Dirac Talbot Lau (KDTL) near-field experiment of Arndt's group. We show the region of the parameter space for the CD map, which is excluded by these experiments. In addition, we obtain bounds on the free parameters for the most relevant collapse models. We argue that matter-wave experiments provide model insensitive bounds, valid for a wide family of dissipative and non-Markovian generalizations.

In the appendices we discuss the covariance of dynamical maps: we generalize Holevo structures to non-Markovian maps (Appendix A) and we discuss Poincaré covariance (Appendices B, C and D). We summarize below each appendix of the thesis (the references correspond to papers in preparation).

A: Covariance of Gaussian maps [17]. We discuss the covariance of general non-Markovian Gaussian maps under Galilean transformations. In particular, we characterize translational and Galilei boost covariant maps. We show that in the Markovian limit we reobtain the characterization due to Holevo.

B: Foldy framework [14]. We introduce the canonical Poincaré covariant quantum mechanics. We briefly discuss the relation with the Foldy - Wouthuysen transformation and with standard non-relativistic Galilei covariant quantum mechanics.

C: Classicalization maps and Relativity [18]. We argue the impossibility of translation and Lorentz covariant classicalization maps, when particle/antiparticle interaction are suppressed. We briefly discuss the implications for relativistic open quantum systems, for non-unitary modifications of quantum mechanics and for measures of macroscopicity.

D: rCD and rcdCSL [14]. We discuss relativistic generalizations of the CD map and of the cdCSL model, namely the rCD map and rcdCSL model, respectively. We obtain explicit expressions for the $1/c^2$ relativistic corrections.

Part I

Theoretical constraints

Chapter 2

General structure

2.1 Introduction

Collapse models are largely viewed to be phenomenological models with the origin of the noise still an open question. In particular, in the past decades several collapse models have been proposed, and the term "the zoo of collapse models" has been coined [7]. However, all collapse models have been constructed from a similar mathematical structure: a noise field coupled non-linearly to the wave function. These models all satisfy four basic requests: (i) probabilistic interpretation (trace always equal to one), (ii) the state vector evolves towards an eigenstate of the collapse operator, (iii) translational covariance and (iv) stationary initial conditions of the noise field. The main differences between them can be categorized in terms of the additional request imposed on top of the basic requests (i)-(iv). We will discuss in detail the requests (i)-(iv) and the classification of collapse models. In particular, spontaneous collapse models can be classified in four subgroups based on the (non) Markovian and (non) dissipative character of the evolution. Non-Markovian collapse models have been investigated in [19, 20]: we will re-derive them in a new way and extend the results to complex noise fields and non-hermitian operators. In addition, we will show the connection between (non) dissipation effects, complex noise fields and covariance under Galilean boosts.

In Sec. 2.2 we introduce the general Gaussian modification of the Schrödinger dynamics and the usual collapse models notation. In particular, we obtain the most general Gaussian continuous spontaneous collapse model. In Sec. 2.3 we impose constraint on the dynamics. In Sec. 2.4 we classify the most well-known collapse models. In Sec. 2.5 we discuss some open questions.

2.2 Gaussian stochastic processes

In this section we discuss the most general completely positive map derived from a diffusion process on Hilbert space.

2.2.1 Stochastic differential equation

We consider the probability space $(\Omega, \sigma, \mathbb{Q})$. A generic Gaussian diffusion process for the wave function in Hilbert space $\mathcal{H} = L^2(\mathbb{R}^3)$ is described by the following stochastic differential

equation:

$$i\hbar\partial_t|\psi_t\rangle = (\hat{H} + \hat{A}_t)|\psi_t\rangle \quad (2.1)$$

where \hat{H} is a self-adjoint operator describing the standard quantum mechanical evolution and \hat{A}_t is a Gaussian operator valued \mathbb{Q} -stochastic process defined by its means and correlation functions:

$$\mathbb{E}_{\mathbb{Q}}[\hat{A}_t], \mathbb{E}_{\mathbb{Q}}[\hat{A}_t^\dagger] \quad \mathbb{E}_{\mathbb{Q}}[\hat{A}_t\hat{A}_s], \mathbb{E}_{\mathbb{Q}}[\hat{A}_t^\dagger\hat{A}_s]. \quad (2.2)$$

For later convenience we introduce the centered operator valued stochastic process:

$$\hat{A}_t^c = \hat{A}_t - \mathbb{E}_{\mathbb{Q}}[\hat{A}_t]. \quad (2.3)$$

We thus rewrite Eq.(2.1) as:

$$i\hbar\partial_t|\psi_t\rangle = (\hat{H} + \hat{A}_t^c + \hat{O}_t)|\psi_t\rangle, \quad (2.4)$$

where

$$\hat{O}_t = \mathbb{E}_{\mathbb{Q}}[\hat{A}_t]. \quad (2.5)$$

In order to show how collapse models can be derived from the above equations, it is convenient to rewrite the Gaussian operator valued stochastic process exploiting Weyl decomposition [21], *i.e.*

$$\hat{A}_t = \int d\alpha \int d\beta g_t(\alpha, \beta) e^{\frac{i}{\hbar}(\alpha\hat{x} + \beta\hat{p})}, \quad (2.6)$$

where $g_t(\alpha, \beta)$ is a complex Gaussian stochastic field, determined by mean and correlations:

$$\begin{aligned} \mathbb{E}_{\mathbb{Q}}[g_t(\alpha, \beta)], & \quad \mathbb{E}_{\mathbb{Q}}[g_t^*(\alpha, \beta)] \\ \mathbb{E}_{\mathbb{Q}}[g_t(\alpha_1, \beta_1)g_s(\alpha_2, \beta_2)], & \quad \mathbb{E}_{\mathbb{Q}}[g_t^*(\alpha_1, \beta_1)g_s(\alpha_2, \beta_2)]. \end{aligned} \quad (2.7)$$

This complex stochastic field can be rewritten, without loss of generality, as the product:

$$g_t(\alpha, \beta) = \tilde{h}_t(\alpha, \beta)K(\alpha, \beta), \quad (2.8)$$

where $\tilde{h}_t(\alpha, \beta)$ is a complex stochastic field and $K(\alpha, \beta)$ is a complex valued field. Denoting the inverse Fourier transform of the stochastic field as

$$\tilde{h}_t(\alpha, \beta) = \int dx \int dp h_t(x, p) e^{-i(\alpha x + \beta p)}, \quad (2.9)$$

one can eventually rewrite the generic stochastic process \hat{A}_t as

$$\hat{A}_t = \int dx \int dp h_t(x, p) \hat{B}(x, p), \quad (2.10)$$

where

$$\hat{B}(x, p) = \int d\alpha d\beta K(\alpha, \beta) e^{i(\alpha(\hat{x}-x) + \beta(\hat{p}-p))}. \quad (2.11)$$

In particular, the relations in Eqs. (2.6)-(2.11) apply also for stochastic processes with zero mean.

The definition in Eq. (2.10) thus splits in a general way the operator valued stochastic process \hat{A}_t in the operator field $\hat{B}(x, p)$ and a complex valued \mathbb{Q} -stochastic process field $h_t(x, p)$ determined by

$$\mathbb{E}_{\mathbb{Q}}[h_t(x, p)], \mathbb{E}_{\mathbb{Q}}[h_t^*(x, p)] \quad \mathbb{E}_{\mathbb{Q}}[h_t(x_1, p_1)h_s(x_2, p_2)], \mathbb{E}_{\mathbb{Q}}[h_t^*(x_1, p_1)h_s(x_2, p_2)]. \quad (2.12)$$

We can thus rewrite Eq. (2.1) as

$$i\hbar\partial_t|\psi_t\rangle = \left(\hat{H} + \int dx dp h_t(x, p)\hat{B}(x, p) \right) |\psi_t\rangle. \quad (2.13)$$

Introducing now the centered Gaussian stochastic field

$$h_t^c(x, p) = h_t(x, p) - \mathbb{E}_{\mathbb{Q}}[h_t(x, p)] \quad (2.14)$$

we rewrite Eq. (2.13) as

$$i\hbar\partial_t|\psi_t\rangle = \left(\hat{H} + \hat{O}_t + \int dx dp h_t^c(x, p)\hat{B}(x, p) \right) |\psi_t\rangle. \quad (2.15)$$

This equation can be understood as the dynamics of a quantum state interacting with a classical noise field \hat{h}_t on phase-space (x, p) , through the coupling operator field $\hat{B}(x, p)$.

We also introduce, for later convenience, the zero mean noise field

$$g_t^c(\alpha, \beta) = g_t(\alpha, \beta) - \mathbb{E}_{\mathbb{Q}}[g_t(\alpha, \beta)] \quad (2.16)$$

where g_t is introduced in Eq. (2.6).

2.3 Constraints

2.3.1 Probabilistic Interpretation

The diffusion process described by Eq. (2.1) is completely general and, except for the Gaussianity of the stochastic field, no constraint has been imposed. The first important request that Eq. (2.1) should satisfy is that

$$\text{Tr}[\rho_t] = 1 \quad (2.17)$$

To check whether this condition is verified it is convenient to work in the interaction picture. In particular, from Eq. (2.1) we obtain:

$$i\hbar\partial_t|\psi_t^I\rangle = \hat{A}_t^I|\psi_t^I\rangle \quad (2.18)$$

with

$$\hat{A}_t^I = e^{\frac{i}{\hbar}\hat{H}t}\hat{A}e^{-\frac{i}{\hbar}\hat{H}t}. \quad (2.19)$$

However, for ease of presentation, we omit the index I in the following calculation performed in the interaction picture. The solution of Eq. (2.18), with initial condition $|\psi_0\rangle$, can be formally written in the form

$$|\psi_t\rangle = \mathcal{T}(e^{-\frac{i}{\hbar} \int \hat{A}_\tau d\tau})|\psi_0\rangle. \quad (2.20)$$

Exploiting this equation, under the assumption that the initial state $|\psi_0\rangle$ is noise independent, the statistical operator describing the system at time t , *i.e.*

$$\rho_t = \mathbb{E}_{\mathbb{Q}}[|\psi_t\rangle\langle\psi_t|] \quad (2.21)$$

is described by:

$$\rho_t = \mathcal{M}_0^t[\rho_0], \quad (2.22)$$

where the averaged dynamical map \mathcal{M}_0^t , that connects the statistical operator at time 0 with the statistical operator at time t , is defined as:

$$\mathcal{M}_0^t[\cdot] = \mathbb{E}_{\mathbb{Q}} \left[\mathcal{T}(e^{-\frac{i}{\hbar} \int \hat{A}_\tau d\tau}) \cdot \mathcal{T}(e^{\frac{i}{\hbar} \int \hat{A}_\tau^\dagger d\tau}) \right]. \quad (2.23)$$

It is convenient to introduce the left right formalism, denoting by subscript L(R) the operator acting on $\hat{\rho}$ from left (right) *e.g.* $\hat{A}_L \hat{B}_R \rho = \hat{A} \rho \hat{B}$ [22, 23, 24]. With this notation ρ_t can be rewritten as:

$$\mathcal{M}_t = \mathbb{E}_{\mathbb{Q}} \left[\mathcal{T}(e^{-\frac{i}{\hbar} \int_0^t d\tau (\hat{A}_{L,\tau} - \hat{A}_{R,\tau}^\dagger)}) \right], \quad (2.24)$$

where \mathcal{T} acts separately on left and right operators. We rewrite the above Eq. (2.24) with the centered stochastic process \hat{A}^c defined in Eq. (2.3). Exploiting the Gaussianity of the stochastic operator and the Isserlis theorem [25], we rewrite Eq. (2.24) as:

$$\begin{aligned} \mathcal{M}_0^t = \mathcal{T} \exp \left(-\frac{i}{\hbar} \int_0^t d\tau (\hat{O}_{L,\tau} - \hat{O}_{R,\tau}) \right. \\ \left. - \frac{1}{2\hbar^2} \int_0^t d\tau \int_0^t ds \mathbb{E}_{\mathbb{Q}}[\mathcal{T}(\hat{A}_{\tau,L}^c - \hat{A}_{\tau,R}^{c\dagger})(\hat{A}_{s,L}^c - \hat{A}_{s,R}^{c\dagger})] \right). \end{aligned} \quad (2.25)$$

We time order the exponent using the Heavyside theta function and, after some algebra, we obtain:

$$\begin{aligned} \mathcal{M}_0^t = \mathcal{T} \exp \left[-\frac{i}{\hbar} \int_0^t d\tau (\hat{O}_{L,\tau} - \hat{O}_{R,\tau}^\dagger) \right. \\ \left. - \frac{1}{\hbar^2} \int_0^t d\tau \int_0^t ds (\mathbb{E}_{\mathbb{Q}}[\hat{A}_{\tau,L}^c \hat{A}_{s,L}^c] \theta_{\tau s} - \mathbb{E}_{\mathbb{Q}}[\hat{A}_{s,L}^c \hat{A}_{\tau,R}^{c\dagger}] + \mathbb{E}_{\mathbb{Q}}[\hat{A}_{s,R}^{c\dagger} \hat{A}_{\tau,R}^{c\dagger}] \theta_{s\tau}) \right]. \end{aligned} \quad (2.26)$$

We now exploit the cyclicity of the trace in Eq. (2.26) and transform right operators to left ones. At the end we obtain the following expression with only (the usual) left operators

$$\begin{aligned} \text{Tr}[\rho_t] = \text{Tr}[\mathcal{T} \exp \left[-\frac{i}{\hbar} \int_0^t d\tau (\hat{O}_\tau - \hat{O}_\tau^\dagger) \right. \\ \left. - \frac{1}{\hbar^2} \int_0^t d\tau \int_0^t ds (\mathbb{E}_{\mathbb{Q}}[\hat{A}_\tau^c \hat{A}_s^c] \theta_{\tau s} - \mathbb{E}_{\mathbb{Q}}[\hat{A}_\tau^{c\dagger} \hat{A}_s^c] + \mathbb{E}_{\mathbb{Q}}[\hat{A}_\tau^{c\dagger} \hat{A}_s^{c\dagger}] \theta_{s\tau}) \right] \rho_0]. \end{aligned} \quad (2.27)$$

The request of unitary trace leads to the following equality

$$\hat{O}_\tau = \hat{C}_\tau + \frac{i}{\hbar} \int_0^\tau ds \left(\mathbb{E}_\mathbb{Q}[\hat{A}_\tau^c \hat{A}_s^c] - \mathbb{E}_\mathbb{Q}[\hat{A}_\tau^{c\dagger} \hat{A}_s^c] \right) \theta_{\tau s} \quad (2.28)$$

under the time ordered exponential, where \hat{C}_τ is an arbitrary hermitian operator. However, we can set $\hat{C}_\tau = 0$, as we will discuss below, without loss of generality. We now insert Eq. (2.28) back into Eq. (2.26), and obtain

$$\mathcal{M}_0^t = T \left[e^{-\frac{1}{\hbar^2} \int_0^t ds \int_0^t d\tau \left(E_Q[\hat{A}_{\tau,L}^{c\dagger} \hat{A}_{s,L}^c] \theta_{\tau s} - E_Q[\hat{A}_{\tau,R}^{c\dagger} \hat{A}_{s,L}^c] + E_Q[\hat{A}_{s,R}^c \hat{A}_{\tau,R}^{c\dagger}] \theta_{s\tau} \right)} \right]. \quad (2.29)$$

We now compare \hat{O}_τ from Eq. (2.28) with the definition in (2.5). To this end we have to derive the stochastic differential equation for the state vector, that generates the dynamics in Eq. (2.20). Loosely speaking, we have to take \hat{O}_τ out of the time order operator. Taking the time derivative of Eq. (2.20), where \hat{O}_t and \hat{A}_c have been replaced by Eqs. (2.28), (2.10), respectively, we obtain:

$$\begin{aligned} i\hbar \partial_t |\psi_t\rangle &= \int dx dp h_t^c(x, p) \hat{B}_t(x, p) |\psi_t\rangle + \hat{C}_t |\psi_t\rangle \\ &+ \frac{i}{\hbar} \int_0^t ds \int dx_1 \int dp_1 \int dx_2 \int dp_2 \left(\mathbb{E}_\mathbb{Q}[h_t^c(x_1, p_1) h_s^c(x_2, p_2)] \hat{B}_t(x_1, p_1) \right. \\ &\left. - \mathbb{E}_\mathbb{Q}[h_t^{c*}(x_1, p_1) h_s^c(x_2, p_2)] \hat{B}_t^\dagger(x_1, p_1) \right) \\ &\cdot \mathcal{T} \left\{ \hat{B}_s(x_2, p_2) \exp \left(-\frac{i}{\hbar} \int_0^t d\tau \int dx \int dp h_\tau^c(x, p) \hat{B}_\tau(x, p) + \hat{O}_\tau \right) \right\} |\psi_0\rangle, \end{aligned} \quad (2.30)$$

We now formally replace the operator $\hat{B}_s(x_2, p_2)$ with the functional derivative over the noise field $i\hbar \delta / \delta h_s^c(x_2, p_2)$ to take it outside the time order operator. Thus, by comparing Eq. (2.30) and Eq. (2.15), we obtain the relation:

$$\begin{aligned} \hat{O}_t = \hat{C}_t - \int_0^t ds \int dx_1 \int dp_1 \int dx_2 \int dp_2 \left(\mathbb{E}_\mathbb{Q}[h_t^c(x_1, p_1) h_s^c(x_2, p_2)] \hat{B}_t(x_1, p_1) \right. \\ \left. - \mathbb{E}_\mathbb{Q}[h_t^{c*}(x, p) h_s^c(x, p)] \hat{B}_t^\dagger(x_1, p_1) \right) \frac{\delta}{\delta h_s^c(x_2, p_2)} \end{aligned} \quad (2.31)$$

This equation combined with the definition of \hat{O}_t given in Eq. (2.5), shows that that the requirement of trace preservation, necessary for a probabilistic interpretation of the average dynamics \mathcal{M}_t , restricts the class of possible stochastic fields: the average value is determined by the covariance of the process. Because of the noise functional derivative in the above equation, the average value of the noise is in general not only determined by the noise fluctuations, but also by the dynamics of the quantum mechanical state, as if a back reaction mechanism induced by the dynamics is present in the noise field.

The freedom of the hermitian operator \hat{C}_t is not surprising: hermitian operators do not change the norm of the state vector and thus do not alter the condition of trace preservation. From another perspective, \hat{C}_t can be viewed as the hermitian part of $\int dx dp \mathbb{E}_\mathbb{Q}[h_t(x, p)] \hat{B}_t(x, p)$ that can be absorbed in the usual Hamiltonian operator.

2.3.2 Collapse of the state vector

The evolution of the \mathbb{Q} -state vector $|\psi_t\rangle$ given by Eq. (2.15) in general does not preserve the norm. However, we can introduce the normalized \mathbb{Q} -state vector:

$$|\phi_t\rangle = |\psi_t\rangle / \langle\psi_t|\psi_t\rangle^{1/2}, \quad (2.32)$$

which has a stochastic and non-linear evolution.

Using the fact that $\mathbb{E}_{\mathbb{Q}}[\langle\psi_t|\psi_t\rangle] = 1$ we define a second probability measure \mathbb{P} , through the Radon-Nikodym derivative [26]:

$$\frac{d\mathbb{P}}{d\mathbb{Q}} = \langle\psi_t|\psi_t\rangle. \quad (2.33)$$

Rewriting then Eq. (2.21) in terms of the normalized state vector $|\phi_t\rangle$ and the probability measure \mathbb{P} , we immediately obtain the following relation:

$$\hat{\rho}(t) = E_{\mathbb{P}}[|\phi_t\rangle\langle\phi_t|]. \quad (2.34)$$

We now require that the dynamics of the normalized state vector $|\phi_t\rangle$, evolves $|\phi_t\rangle$ to an eigenstate of a specific operator when $\hat{H} = 0$ (collapse of the wave-function). Indeed, a good collapse model should evolve a macroscopic object towards a well-localized state on a time scale, where the free dynamics can be safely neglected, as otherwise quantum effects could modify the classical motion of the macroscopic object (in the sense that the macro-object is not always localized in space anymore). Setting $\hat{H} = 0$, the state $|\phi_t\rangle$ should evolve to a position eigenstate and the collapse should be compatible with the usual Born rule. The case when \hat{B} are a set of commuting hermitian operators and h_t^c is a imaginary-valued \mathbb{Q} -stochastic field has been investigated in [19, 20]. In particular, it has been shown that the \mathbb{P} -state ϕ_t collapses according to the Born rule when we set $\hat{H} = 0$: we now analyze the case of generic \hat{B} and h_t^c fields referring to this special case.

In order to investigate the collapse mechanism we decompose the stochastic process field in the real and imaginary part:

$$h_t^c = h_t^{c(\text{Re})} + ih_t^{c(\text{Im})}. \quad (2.35)$$

We also decompose the operator in its hermitian and anti-hermitian part:

$$\hat{B} = \hat{B}^{(+)} + i\hat{B}^{(-)}, \quad (2.36)$$

where

$$\hat{B}^{(+)} = \frac{1}{2}(\hat{B} + \hat{B}^\dagger), \quad (2.37)$$

$$i\hat{B}^{(-)} = \frac{1}{2}(\hat{B} - \hat{B}^\dagger). \quad (2.38)$$

In this way we obtain:

$$\hat{A}_t = \hat{L}_t + i\hat{J}_t \quad (2.39)$$

where

$$\hat{L}_t(x, p) = h_t^{c(\text{Re})}(x, p)\hat{B}^{(+)}(x, p) - h_t^{c(\text{Im})}(x, p)\hat{B}^{(-)}(x, p), \quad (2.40)$$

$$\hat{J}_t(x, p) = h_t^{c(\text{Im})}(x, p)\hat{B}^{(+)} + h_t^{c(\text{Re})}(x, p)\hat{B}^{(-)}. \quad (2.41)$$

The \hat{L}_t term, which generates a unitary evolution, can be absorbed in the Hamiltonian operator \hat{H} . On the other hand, the \hat{J}_t term generates a non-unitary evolution and, as we will show, can lead to the collapse of the normalized \mathbb{P} -state $|\phi_t\rangle$. In particular, we have two stochastic noise fields $h_t^{c(\text{Im})}$, $h_t^{c(\text{Re})}$ that compete in the localization in eigenstates of the operator fields $\hat{B}^{(+)}$, $\hat{B}^{(-)}$, respectively.

Let us consider first the case $h_t^{c(\text{Re})} = 0$ and $\hat{B}^{(-)} = 0$. We obtain

$$\hat{J}_t = h_t^{c(\text{Im})}(x, p)\hat{B}^{(+)}(x, p) \quad (2.42)$$

and $\hat{L}_t = 0$. In addition, we assume that the operator field $\hat{B}^{(+)}$ has a common set of eigenstates. In this way we obtain the collapse model considered in [19, 20]. We now sketch, following [19, 20], the calculation that leads to the collapse of the state vector according to the usual Born rule when we set $\hat{H} = 0$. From Eq. (2.32) and Eq. (2.30), where we set $\hat{C} = 0$ without loss of generality as discussed above, after some algebra, we obtain the closed equation for the \mathbb{P} -state:

$$\begin{aligned} i\hbar\partial_t|\phi_t\rangle &= \int dx dp h_t^c(x, p) \left(\hat{B}(x, p) - \langle \hat{B}(x, p) \rangle_t \right) |\phi_t\rangle \\ &+ \frac{2i}{\hbar} \int dx_1 \int dp_1 \int dx_2 \int dp_2 \int_0^t ds \mathbb{E}_{\mathbb{Q}}[h_t^c(x_1, p_1)h_s^c(x_2, p_2)] \\ &\cdot \left(\hat{B}(x_1, p_1)\hat{B}(x_2, p_2) - \langle \hat{B}(x_1, p_1)\hat{B}(x_2, p_2) \rangle_t \right) |\phi_t\rangle \end{aligned} \quad (2.43)$$

where $\langle \cdot \rangle_t$ denotes $\langle \phi_t | \cdot | \phi_t \rangle$.

It is straightforward to obtain the master equation using Eq. (2.34):

$$\begin{aligned} \partial_t \hat{\rho}_t &= -\frac{2}{\hbar^2} \int dx_1 \int dp_1 \int dx_2 \int dp_2 \int_0^t ds \mathbb{E}_{\mathbb{Q}}[h_t^c(x_1, p_1)h_s^c(x_2, p_2)] \\ &\cdot \left(\hat{B}(x_1, p_1)\hat{\rho}_t\hat{B}(x_2, p_2) + \hat{B}(x_2, p_2)\hat{\rho}_t\hat{B}(x_1, p_1) \right. \\ &\left. - \hat{B}(x_1, p_1)\hat{B}(x_2, p_2)\hat{\rho}_t - \hat{\rho}_t\hat{B}(x_2, p_2)\hat{B}(x_1, p_1) \right), \end{aligned} \quad (2.44)$$

One can then easily show that

$$\partial_t \mathbb{E}_{\mathbb{P}}[\langle \hat{B}^2(x, p) \rangle_t] = 0. \quad (2.45)$$

On the other hand, using the Furutsu-Novikov formula

$$\mathbb{E}_{\mathbb{Q}}[F[h^c]h_t^c(x, p)] = \int_0^t ds \int dx_1 \int dp_1 \mathbb{E}_{\mathbb{Q}}[h_t^c(x, p)h_s^c(x_1, p_1)] \mathbb{E}_{\mathbb{Q}}\left[\frac{\delta F[h^c]}{\delta h_s^c(x_1, p_1)}\right] \quad (2.46)$$

where F is a generic functional of the centered Gaussian noise field h^c , we obtain

$$\begin{aligned} \partial_t \mathbb{E}_{\mathbb{P}}[\langle \hat{B}(x, p) \rangle_t^2] = & 8 \int dx_1 \int dp_1 \int dx_2 \int dp_2 \left[\int_0^t ds \mathbb{E}_{\mathbb{Q}}[h_t^c(x_1, p_1) h_s^c(x_2, p_2)] \right] \\ & \cdot \mathbb{E}_{\mathbb{P}} \left[\langle (\hat{B}(x_1, p_1) - \langle \hat{B}(x_1, p_1) \rangle_t) \hat{B}(x, p) \rangle_t \right. \\ & \left. \langle (\hat{B}(x_2, p_2) - \langle \hat{B}(x_2, p_2) \rangle_t) \hat{B}(x, p) \rangle_t \right] \end{aligned} \quad (2.47)$$

Because $\left[\int_0^t ds \mathbb{E}_{\mathbb{Q}}[h_t^c(x_1, p_1) h_s^c(x_2, p_2)] \right]$ is a positive semi-definite kernel, it is now straightforward to show

$$\lim_{t \rightarrow \infty} \mathbb{E}_{\mathbb{P}}[\text{Var}[\hat{B}(x, p)]_t] = 0, \quad (2.48)$$

where

$$\text{Var}[\hat{B}(x, p)]_t = \langle \hat{B}^2(x, p) \rangle_t - \langle \hat{B}(x, p) \rangle_t^2 \quad (2.49)$$

is the usual variance. Thus one can conclude

$$\lim_{t \rightarrow \infty} \text{Var}[\hat{B}(x, p)]_t = 0 \quad \mathbb{P} - \text{a.s.} . \quad (2.50)$$

The case $h_t^{c(\text{Im})} = 0$ and $\hat{B}^{(+)} = 0$ is completely analogous. Let us discuss also the other possibilities when $h_t^{c(\text{Re})} \neq 0$ or $h_t^{c(\text{Im})} \neq 0$. In case $\hat{B}^{(+)} \neq 0$, $\hat{B}^{(-)} \neq 0$ but $[\hat{B}^{(+)}, \hat{B}^{(-)}] = 0$ the collapse mechanism is unaltered: the noise field(s) force the collapse to a common eigenstate. Only the case $\hat{B}^{(+)} \neq 0$, $\hat{B}^{(-)} \neq 0$ and $[\hat{B}^{(+)}, \hat{B}^{(-)}] \neq 0$ might be problematic for the collapse mechanism and one has to check explicitly the collapse mechanism for specific choices of the operators (for example the collapse might be only partial).

2.3.3 Covariance

In this section we discuss covariance of spontaneous collapse models under the action of the Galilei group symmetries: translations, rotations and boosts. In particular, we require covariance¹ of the dynamical map \mathcal{M}_t , given by Eq. (2.29), for the statistical operator ρ_t :

$$\mathcal{M}_t = \mathcal{G}^{-1} \circ \mathcal{M}_t \circ \mathcal{G} \quad (2.51)$$

where the Galilei group is represented as:

$$\mathcal{G}[\cdot] = \hat{U}^\dagger \cdot \hat{U} \quad (2.52)$$

¹On the other hand we could also discuss the covariance of the dynamical map for the \mathbb{P} -state ϕ_t , but this is at the present moment to restrictive: for microscopic objects we only have access to ρ_t , while on the other hand, for macroscopic objects, the collapse mechanism keeps the objects localized without affecting their overall motion in physical space, to within experimental errors, which is governed only by the usual Hamiltonian \hat{H} [27, 28]. In addition, requiring the covariance of the dynamical map for the \mathbb{P} -state ϕ_t leads to only trivial dynamical maps.

and \hat{U} denotes a unitary transformation generated by the operators given in Eqs. (A.6), (A.7) and (A.8). The general structure of Gaussian dynamics, covariant under translations, rotations and boosts, has been discussed in Appendix A: we use these results to characterize the Gaussian noise field $h(x, p)$ and the complex function $K(\alpha, \beta)$ (see Sec. (2.2.1)). Specifically, comparing Eqs. (A.3) and (2.29), where we use the expression in Eq. (2.10) for \hat{A}^c , we obtain the following correspondence:

$$D(\alpha_1, \beta_1, \alpha_2, \beta_2, \tau, s) \leftrightarrow \mathbb{E}_{\mathbb{Q}}[g_{\tau}^{c*}(\alpha_1, \beta_1)g_s^c(\alpha_2, \beta_2)]. \quad (2.53)$$

2.3.3.1 Translations

From Eq. (A.18), using the correspondence in Eq. (2.53), we obtain:

$$\mathbb{E}_{\mathbb{Q}}[g_{\tau}^{c*}(\alpha_1, \beta_1)g_s^c(\alpha_2, \beta_2)] = \delta(\alpha_1 - \alpha_2)\mathbb{E}_{\mathbb{Q}}[g_{\tau}^{c*}(\alpha_1, \beta_1)g_s^c(\alpha_2, \beta_2)] \quad (2.54)$$

Recalling Eq. (2.6) and Eq. (2.8) we immediately find the following condition for the Fourier transform of the noise covariance:

$$\mathbb{E}_{\mathbb{Q}}[\tilde{h}_{\tau}^*(\alpha_1, \beta_1)\tilde{h}_s(\alpha_2, \beta_2)] = \delta(\alpha_1 - \alpha_2)\tilde{D}_T(\alpha_1, \beta_1, \alpha_2, \beta_2, \tau, s), \quad (2.55)$$

where \tilde{D}_T is a complex valued function. Performing now the inverse Fourier transform we immediately obtain:

$$\mathbb{E}_{\mathbb{Q}}[h_{\tau}^{c*}(x_1, p_1)h_s^c(x_2, p_2)] = D_T(x_1 - x_2, p_1, p_2, \tau, s), \quad (2.56)$$

where D_T is a complex valued function.

2.3.3.2 Boosts

From Eq. (A.24), using the correspondence in Eq. (2.53), recalling Eq. (2.6) and Eq. (2.8), performing the inverse Fourier transform we immediately obtain (analogous calculation as in Sec. 2.3.3.1):

$$\mathbb{E}_{\mathbb{Q}}[h_{\tau}^{c*}(x_1, p_1)h_s^c(x_2, p_2)] = D_B(x_1, x_2, p_1 - p_2, \tau, s), \quad (2.57)$$

where D_B is a complex valued function.

2.3.3.3 Rotations

From Eq. (A.32), using the correspondence in Eq. (2.53), we obtain:

$$\mathbb{E}_{\mathbb{Q}}[g_{\tau}^{c*}(R\alpha_1, R\beta_1)g_s^c(R\alpha_2, R\beta_2)] = \mathbb{E}_{\mathbb{Q}}[g_{\tau}^{c*}(\alpha_1, \beta_1)g_s^c(\alpha_2, \beta_2)], \quad (2.58)$$

where R is a generic rotation matrix. From this condition, once Eqs. (2.8) and (2.9) are used to rewrite $g_t(\alpha, \beta)$, we obtain the following two requirements:

$$\mathbb{E}_{\mathbb{Q}}[h_{\tau}^{c*}(Rx_1, Rp_1)h_s^c(Rx_2, Rp_2)] = \mathbb{E}_{\mathbb{Q}}[h_{\tau}^{c*}(x_1, p_1)h_s^c(x_2, p_2)], \quad (2.59)$$

$$K^*(R\alpha_1, R\beta_1)K(R\alpha_2, R\beta_2) = K^*(\alpha_1, \beta_1)K(\alpha_2, \beta_2). \quad (2.60)$$

2.3.4 Stationary process

We have constructed the map \mathcal{M}_0^t in Eq. (2.29). We now want construct the map $\mathcal{M}_u^{u+t}[\cdot]$ from u to $u+t$ and impose that it is independent from the initial time u . In particular, we request

$$\mathcal{M}_u^{u+t}[\cdot] = \mathcal{M}_0^t[\cdot], \quad (2.61)$$

We repeat the calculation of Sec. 2.3.1 for the initial and final times $u, u+t$, respectively. In particular, Eq. (2.19) changes to:

$$\hat{A}_{t-u}^I = e^{\frac{i}{\hbar}\hat{H}(t-u)} \hat{A} e^{-\frac{i}{\hbar}\hat{H}(t-u)}. \quad (2.62)$$

We immediately see from Eq. (2.29), that the request (2.61) gives the following constraint:

$$\mathbb{E}_{\mathbb{Q}}[\hat{A}_t^{c\dagger} \hat{A}_s^c] = \mathbb{E}_{\mathbb{Q}}[\hat{A}_{t+u}^{c\dagger} \hat{A}_{s+u}^c] \quad (2.63)$$

and exploiting Eq. (2.6) we obtain

$$\mathbb{E}_{\mathbb{Q}}[g_{t+u}^{c*}(\alpha_1, \beta_1) g_{s+u}^c(\alpha_2, \beta_2)] = \mathbb{E}_{\mathbb{Q}}[g_t^{c*}(\alpha_1, \beta_1) g_s^c(\alpha_2, \beta_2)]. \quad (2.64)$$

From this condition, once Eqs. (2.8) and (2.9) are used to rewrite $g_t(\alpha, \beta)$, we obtain:

$$\mathbb{E}_{\mathbb{Q}}[h_{t+u}^{c*}(x_1, p_1) h_{s+u}^c(x_2, p_2)] = \mathbb{E}_{\mathbb{Q}}[h_t^{c*}(x_1, p_1) h_s^c(x_2, p_2)]. \quad (2.65)$$

We will refer to collapse models that satisfy this property as stationary.

2.4 Classification of collapse models

In this section we classify the most well known collapse models. A spontaneous collapse model is completely determined by the complex noise field $h_t(x, p)$ means and correlation functions and by the complex functions $K(\alpha, \beta)$, introduced in Eqs. (2.12), (2.8), respectively. Instead of specifying $K(\alpha, \beta)$ we can also specify the operator \hat{B} as clear by construction (see Eq.(2.11)). In addition, all known collapse models consider a real-valued noise field $h_t(x, p)$. In case the noise does not depend on p , i.e.

$$h_t(x, p) = h_t(x),$$

this leads, as we will see, to non-dissipative models. On the other hand, if one fixes the value of $p = \bar{p}$, i.e.

$$h_t(x, p) \rightarrow \delta(p - \bar{p}) h_t(x, p), \quad (2.66)$$

one obtains, as we will see, the dissipative models in the literature². In either case, we can thus integrate over p in Eq. (2.15) and obtain a simplified noise term:

$$\int dx h_t(x) \hat{B}(x), \quad (2.67)$$

where, in the dissipative case, $h_t(x)$, $\hat{B}(x)$ denote $h_t(x, \bar{p})$, $\hat{B}(x, \bar{p})$, respectively, while in the non-dissipative case, $\hat{B}(x)$ denotes $\int dp \hat{B}(x, p)$.

²From Eq. (2.11) we see that we can set $\bar{p} = 0$ without loss of generality.

	Markovian	Non-Markovian
Non-dissipative	CSL, QMUPL, DP	cCSL, cQMUPL
Dissipative	dCSL, dQMUPL	cdQMUPL

Table 2.1: Classification of collapse models.

All collapse models satisfy conditions (i)-(iv) discussed in Sec. (2.3): probabilistic interpretation, collapse of the state vector, translational covariance and stationary process. On top of these basic properties we can impose two different general properties: (non) Markovianity and (non) dissipation (see Table 2.1).

Markovian models are defined such that

$$\mathbb{E}_{\mathbb{Q}}[h_{\tau}^{c*}(x_1, p_1)h_s^c(x_2, p_2)] = \delta(\tau - s)\mathbb{E}_{\mathbb{Q}}[h_{\tau}^{c*}(x_1, p_1)h_s^c(x_2, p_2)], \quad (2.68)$$

otherwise we call the models non-Markovian.

The definition of dissipative collapse models is more subtle. The first continuous spontaneous collapse models investigated, e.g. CSL, implies a steady increase of temperature:

$$\frac{d}{dt}\text{tr}\left[\frac{\hat{p}^2}{2m}\hat{\rho}_t\right] = \text{const} > 0 \quad (2.69)$$

With dissipative models one usually refers to collapse models that lead to a finite asymptotic energy³. To have a dissipative model we need a map with a unitary contribution that has a \hat{p} dependence. Loosely speaking, we are generalizing the evolution $i\hbar\frac{d}{dt}\hat{\rho} = [\hat{H} + U(\hat{p}), \hat{\rho}]$ to more general maps, where $U(\hat{p})$ is a potential that is taking away energy from the system. This has an interesting implication. In particular, we have seen that maps with a non-trivial \hat{p} dependence break Galilean boost covariance. Thus we have the situation:

$$\text{dissipative model} \implies \text{Galilean boost non-covariant model} \quad (2.70)$$

In Table 2.2 we have classified the most well-known Gaussian spontaneous collapse models. Specifically, we have classified the following Markovian and non-dissipative models: the Diòsi-Penrose (DP) model [30], the continuous spontaneous localization (CSL) model [31, 32] and the quantum mechanics with universal position localization (QMUPL) model [33, 30]. We also classify the dissipative extensions, namely the dissipative CSL (dCSL) [34] and the dissipative QMUPL (dQMUPL) [35], the non-Markovian extensions, namely the colored CSL (cCSL)[19, 20] and the colored QMUPL (cQMUPL) [36]. At present only one non-Markovian and dissipative model exists in the literature, namely the colored and dissipative QMUPL (cdQMUPL) [37].

³This definition is conceptually different from the definition used in open quantum systems [29], where a non-dissipative map is defined as a purely non-unitary modification of the von-Neumann dynamical map.

Model	c	d	$\mathbb{E}_{\mathbb{Q}}[h_t^{c*}(x_1, p_1)h_s^c(x_2, p_2)]$	$-i\hat{B}(x)$
DP	/	/	$\delta(t-s)\delta(x_1-x_2)$	$\int dQ \exp[-\frac{i}{\hbar}Q(\hat{x}-x)] \exp[-r_C^2 Q^2/(2\hbar^2)]$
CSL	/	/	$\delta(t-s)\delta(x_1-x_2)$	$\int dQ \exp[-\frac{i}{\hbar}Q(\hat{x}-x)]/\sqrt{ Q }$
QMUPL	/	/	$\delta(t-s)\delta(x_1-x_2)$	$\hat{x}\delta(x)$
dCSL	/	y	$\delta(t-s)\delta(x_1-x_2)$ $\delta(p_1-\bar{p})\delta(p_2-\bar{p})$	$\int dQ \exp[-\frac{i}{\hbar}Q(\hat{x}-x)]$ $\exp[-r_C^2 ((1+k)Q+2k\hat{p})^2/(2\hbar^2)]$
dQMUPL	/	y	$\delta(t-s)\delta(x_1-x_2)$ $\delta(p_1-\bar{p})\delta(p_2-\bar{p})$	$(\hat{x}+i\mu\hat{p}/\hbar)\delta(x)$
cCSL	y	/	$D(t-s)\delta(x_1-x_2)$	$\int dQ \exp[-\frac{i}{\hbar}Q(\hat{x}-x)] \exp[-r_C^2 Q^2/(2\hbar^2)]$
cQMUPL	y	/	$D(t-s)\delta(x_1-x_2)$	$\hat{x}\delta(x)$
cdQMUPL	y	y	$D(t-s)\delta(x_1-x_2)$ $\delta(p_1-\bar{p})\delta(p_2-\bar{p})$	$(\hat{x}+i\mu\hat{p}/\hbar)\delta(x)$

Table 2.2: Summary of Gaussian collapse models. We omit the normalization factors for the operators \hat{B} . The QMUPL, dQMUPL and cdQMUPL have also a nonzero value of \hat{C} that can be absorbed in the usual Hamiltonian operator \hat{H} (see Eq. (2.28)). c and d denote color and dissipation, respectively.

2.5 Conclusion and discussion

We have constructed a general collapse model from a set of minimal requirements. We have shown how this general model can be used to classify all known collapse models. However, there are still several important unanswered questions. In particular: is the constant energy increase in non-dissipative models a feature or an issue? Why is this intrinsically linked with Galilean boost covariance? The change of measure, from the non-physical measure \mathbb{Q} to the physical measure \mathbb{P} , is a prescription adopted to obtain the Born rule. What is the origin of this prescription?

Chapter 3

CD map and cdCSL model

3.1 Introduction

Several different collapse models have been proposed in the literature [6, 7]: from considerations based on general relativity, namely the Diòsi-Penrose (DP) model [30], to purely phenomenological models, such as the continuous spontaneous localization (CSL) model [31, 32]. In addition, there does not seem to be any guiding principle, within non-relativistic physics, to single out a specific collapse model: general arguments based on symmetries can be made, but the freedom in the construction of collapse models is still large, as the previous chapter shows. Thus a strong argument to single out a specific model, or at least significantly restrict the class of possible collapse models, is highly desirable.

It has been speculated that the origin of the noise in collapse models is related to a background cosmological relic field [34]. Such a relic field may, like for example in the case of the cosmic microwave background (CMB), select a preferred reference frame. In addition, it has also been suggested by Trace dynamics [9], an underlying theory to Quantum mechanics, that Lorentz covariance may only be an approximate symmetry. However, a preferred reference frame has important consequences in the non-relativistic limit: a Lorentz boost non-covariant relativistic model reduces to a Galilei boost non-covariant collapse model (for further discussions see Appendices B, C). This, rather than being a problem, can be a feature, as Galilei boost non-covariant models can be dissipative, as shown in Sec. 2: in particular, dissipation can lead a system to the asymptotic Gibbs state, avoiding the constant gain of energy of Galilei boost covariant (non-dissipative) models [34].

Based on these considerations, we will ask the following question: what is the most general Gaussian map that satisfies (i) probabilistic interpretation, (iii) translational and rotational covariance, (iv) stationary initial conditions and (v) has an asymptotic Gibbs state? (Sec. 3.2). We will refer to the map with these properties as the CD map. We emphasize that this map will not be derived within the specific formalism of spontaneous collapse models: it is a generic dynamics for the statistical operator. We will then construct a spontaneous collapse model type of dynamics, i.e. the dynamics discussed in Sec. 2, such that it satisfies assumptions (i), (iii),(iv),(v) and also the assumptions (ii) collapse of the state vector and (vi) the Gaussian noise is a \mathbb{R} valued field over physical space (\mathbb{R}^3). We will refer to this model as the cdCSL (a colored and dissipative generalization of the CSL model) model (Sec. 3.3): the corresponding dynamical map for the statistical operator will be by construction the CD map (for relativistic extensions see Appendix D).

3.2 CD Map

For simplicity we consider a single particle in the interaction picture, where, to keep the notation simple, we omit the interaction picture notation (I). The generalization to the N particle case is straightforward.

3.2.1 Conditions (i), (iii), (iv)

By imposing conditions (i) probabilistic interpretation and (iii) translational covariance we obtain the map given in Eq. (A.21). Imposing condition (iv) stationary initial conditions we obtain:

$$D_{jk}(\tau + u, s + u) = D_{jk}(\tau, s), \quad (3.1)$$

where u is a time. This condition is a straightforward generalization of the condition in Eq. (2.64), derived in Sec. 2.3.4. We are left to impose two conditions (iii) rotational covariance, which as we will see, will be trivially satisfied, and (v) asymptotic Gibbs state.

3.2.2 Condition (v)

In this section we address the long time behavior of the system. Assuming that the noise correlation times are small compared to the evolution time of the system t , then the dynamics of Eq. (A.21) becomes approximately Markovian for large values of t . We can show this by considering a generic map (a heuristic argument):

$$\mathcal{L}^t[\hat{\rho}_0] = \mathcal{T}[\exp \left[\int_0^t ds \int_0^t d\tau \mathbb{E}_{\mathbb{Q}}[\mathcal{A}_{s,\tau}] \right] \hat{\rho}_0], \quad (3.2)$$

where $\mathcal{A}_{s,\tau}$ is a generic superoperator-valued stochastic process. We make two assumptions: $t \gg \tau_C$ and $\mathbb{E}_{\mathbb{Q}}[\mathcal{A}_{\tau,s}] \simeq 0$ if $|\tau - s| < \tau_C$. Thus we can write

$$\mathcal{L}^t[\hat{\rho}_0] = \mathcal{T}[\exp \left[\int_0^t ds \int_0^t d\tau (\mathbb{E}_{\mathbb{Q}}[\mathcal{A}_{s,\tau}] \delta(s - \tau) + \mathcal{O}_{s,\tau}) \right] \hat{\rho}_0], \quad (3.3)$$

where $\int_0^t ds \int_0^t d\tau \mathcal{O}_{s,\tau}$ is a superoperator of order τ_c/t . We can rewrite this as

$$\mathcal{L}^t[\hat{\rho}_0] = \mathcal{T}[\exp \left[\int_0^t ds \mathbb{E}_{\mathbb{Q}}[\mathcal{A}_{s,s}] \right] \exp \left[\int_0^t ds \int_0^t d\tau \mathcal{O}_{s,\tau} \right] \hat{\rho}_0], \quad (3.4)$$

We now take the time derivative and we obtain:

$$\dot{\hat{\rho}}_t = \mathbb{E}_{\mathbb{Q}}[\mathcal{A}_{t,t}] \hat{\rho}_t + \mathcal{T} \left[\int_0^t ds (\mathcal{O}_{s,t} + \mathcal{O}_{t,s}) \exp \left[\int_0^t ds \mathbb{E}_{\mathbb{Q}}[\mathcal{A}_{s,s}] \right] \exp \left[\int_0^t ds \int_0^t d\tau \mathcal{O}(\tau_c/t) \right] \hat{\rho}_0 \right], \quad (3.5)$$

where the second term is of order τ_c/t . Thus to lowest order in τ_c/t we obtain a Markovian evolution:

$$\dot{\hat{\rho}}_t = \mathbb{E}_{\mathbb{Q}}[\mathcal{A}_{t,t}] \hat{\rho}_t. \quad (3.6)$$

We thus impose

$$D_{jk}(\tau, s) = \delta(\tau - s)D_{jk} \quad (3.7)$$

in Eq. (A.21) which reduces to Eq. (A.36). In addition, imposing the stationary initial condition given by Eq. (3.1), we obtain from Eq. (A.36) the following master equation (in the Schrödinger picture):

$$\frac{d\hat{\rho}_t}{dt} = -\frac{i}{\hbar}[\hat{H}, \hat{\rho}_t] + \sum_l \int dQ \left(e^{\frac{i}{\hbar}Q\hat{x}} \tilde{J}_l(\hat{p}, Q) \hat{\rho}_t \tilde{J}_l^\dagger(\hat{p}, Q) e^{-\frac{i}{\hbar}Q\hat{x}} - \frac{1}{2} \{ \tilde{J}_l^\dagger(\hat{p}, Q) \tilde{J}_l(\hat{p}, Q), \hat{\rho}_t \} \right), \quad (3.8)$$

where

$$\tilde{J}_l(\hat{p}, Q) = J^k(\hat{p}, Q) d_{lk} \quad (3.9)$$

and $D_{jk} = d_{jl}^* d_{lk}$ (a positive definite matrix). We now assume that \sum_l is a sum of only one term, i.e. $D_{jk}(\tau, s)$ in Eq. (A.21) reduces to a positive valued function: we will discuss this assumption briefly below. Thus Eq. (3.8) simplifies to (in the Schrödinger picture):

$$\frac{d\hat{\rho}_t}{dt} = -\frac{i}{\hbar}[\hat{H}, \hat{\rho}_t] + \int dQ \left(e^{\frac{i}{\hbar}Q\hat{x}} \tilde{J}(\hat{p}, Q) \hat{\rho}_t \tilde{J}^\dagger(\hat{p}, Q) e^{-\frac{i}{\hbar}Q\hat{x}} - \frac{1}{2} \{ \tilde{J}^\dagger(\hat{p}, Q) \tilde{J}(\hat{p}, Q), \hat{\rho}_t \} \right). \quad (3.10)$$

For later convenience we also introduce the function f :

$$\tilde{J}(\hat{p}, Q) = N \exp(-f(Q, \hat{p})), \quad (3.11)$$

where N is a normalization constant.

We now consider the Gibbs state:

$$\hat{\rho}_{\text{asm}} = \left(\frac{\beta}{2m\pi} \right)^{3/2} \exp(-\beta\hat{H}), \quad (3.12)$$

where

$$\hat{H} = \frac{\hat{p}^2}{2m} \quad (3.13)$$

and $\beta = 1/(k_B T)$, with k_B the Boltzmann constant and T the temperature. We can now impose that $\hat{\rho}_{\text{asm}}$, defined in Eq. (3.12), is a stationary state of Eq. (3.10). We thus make the ansatz for the operators

$$\tilde{J}(\hat{p}, Q) = N \exp(-(a_1 Q + a_2 \hat{p})^2), \quad (3.14)$$

where a_1, a_2 are real-valued parameters. This choice for the operator is a natural one, given the Gaussianity of the Gibbs state. Using Eqs. (3.14), (3.12), (3.10) we obtain the condition:

$$\int dQ e^{-2(a_1 Q + a_2(\hat{p}-Q))^2} e^{-\beta(\hat{p}-Q)^2/(2m)} = \int dQ e^{-2(a_1 Q + a_2 \hat{p})^2} e^{-\beta \hat{p}^2/(2m)}, \quad (3.15)$$

which implies

$$-2(a_1Q + a_2(\hat{p} - Q))^2 - \beta(\hat{p} - Q)^2/(2m) = -2(a_1(Q + b) + a_2\hat{p})^2 - \beta\hat{p}^2/(2m) \quad (3.16)$$

with $b \in \text{Re}$. Looking at each power in Q , we obtain three conditions:

$$Q^0 : a_1^2 b^2 + 2a_1 a_2 b \hat{p} = 0, \quad (3.17)$$

$$Q^1 : 2a_2^2 \hat{p} + 2a_1^2 b + \frac{\beta}{2m} \hat{p} = 0, \quad (3.18)$$

$$Q^2 : -2a_2^2 + 4a_1 a_2 - \frac{\beta}{2m} = 0. \quad (3.19)$$

From Eq. (3.17) we obtain two solutions:

$$b = -2(a_2/a_1)\hat{p} \quad (3.20)$$

and $b = 0$. However, we do not consider $b = 0$ as it leads to an imaginary a_2 (see Eq. (3.18)), in contradiction with our Ansatz in Eq. (3.14). The remaining two Eqs. (3.18),(3.19) are not independent: we find a_1, a_2 as function of a free parameter, which we denote by r_C . Specifically, we write them, for later convenience, as:

$$a_1 = (1 + k_T)/(\sqrt{2\hbar}/r_C), \quad (3.21)$$

$$a_2 = 2k_T/(\sqrt{2\hbar}/r_C), \quad (3.22)$$

where

$$k_T = \frac{\hbar^2}{8mr_C^2 k_B T}. \quad (3.23)$$

To summarize we have the following operator

$$\tilde{J}(\hat{p}, Q) = \sqrt{\lambda \frac{m^2}{m_0^2} \left(\frac{r_C}{\sqrt{\pi\hbar}} \right)^3} \exp(-(r_C^2/(2\hbar^2))((1 + k_T)/Q + 2k_T\hat{p})^2), \quad (3.24)$$

where the overall normalization, chosen as in [34], is determined by the free parameter λ . In particular, λ can be interpreted as a decoherence rate.

The above calculation thus constrains Eq.(A.21) to (in the interaction picture):

$$\begin{aligned} \mathcal{M}_t = \mathcal{T} \exp \left\{ \int_0^t d\tau \int_0^\tau ds \int dQ D(\tau - s) \right. & \left. ([\tilde{J}_L(\hat{p}, Q) e^{\frac{i}{\hbar} Q \hat{x}_L(s)}] [\tilde{J}_R^\dagger(\hat{p}, Q) e^{-\frac{i}{\hbar} Q \hat{x}_R(\tau)}] \right. \\ & - \theta_{\tau,s} [\tilde{J}_L^\dagger(\hat{p}, Q) e^{-\frac{i}{\hbar} Q \hat{x}_L(\tau)}] [e^{\frac{i}{\hbar} Q \hat{x}_L(s)} \tilde{J}_L(\hat{p}, Q)] \\ & \left. - \theta_{s,\tau} [\tilde{J}_R(\hat{p}, Q) e^{\frac{i}{\hbar} Q \hat{x}_R(s)}] [e^{-\frac{i}{\hbar} Q \hat{x}_R(\tau)} \tilde{J}_R^\dagger(\hat{p}, Q)] \right\}. \end{aligned} \quad (3.25)$$

We first note that condition (iii) rotationally covariance of the map in Eq. (3.25) is satisfied. This map, to which we will refer as the CD map, is completely determined, apart from the

function $D(\tau, s)$, the parameters λ , r_C , T and the boost parameter \mathbf{u} : the map is not Galilei boost covariant (we will discuss this in detail in Sec. 4). The generalization to a matrix $D_{jk}(\tau - s)$ of arbitrary dimension leads to a more tedious calculation: however, from Eq. (3.8) we see that increasing the dimensionality of the matrix $D_{jk}(\tau - s)$ simply increases the number of terms added to the von-Neumann map. Since these terms are all of the same form, we can again assume Gaussian operators and proceed with the above calculation. We leave the analysis of this situation for future research.

In particular, the map in Eq.(3.25) reduces to the cCSL and dCSL map for the statistical operator in the limits $T \rightarrow \infty$, $\tau_C \rightarrow 0$, respectively, where τ_C denotes the correlation time of $D(\tau - s)$.

3.3 cdCSL

We now consider the collapse model dynamics developed in Sec. 2. We impose conditions (i)-(iv): the most general one-particle Gaussian collapse model is given by Eq. (2.15) where the operator \hat{O} is defined in Eq. (2.31) and we set $\hat{C} = 0$ (in the interaction picture, with $\hat{H} = \hat{p}^2/2m$). In addition, we also impose (vi) the Gaussian noise is a field over physical space (\mathbb{R}^3), using Eq. (2.66), in Eq. (2.15), and after a straightforward calculation, we obtain (in the interaction picture):

$$i\hbar \frac{d}{dt} |\psi_t\rangle = \left(\int dx h_t^c(x) \hat{B}_t(x) - \int_0^t d\tau \int dx_1 \int dx_2 \left[\mathbb{E}_{\mathbb{Q}}[h_t^c(x_1) h_\tau^c(x_2)] \hat{B}_t(x_1) - \mathbb{E}_{\mathbb{Q}}[h_t^{c*}(x_1) h_\tau^c(x_2)] \hat{B}_t^\dagger(x_1) \right] \frac{\delta}{\delta h_\tau^c(x_2)} \right) |\psi_t\rangle. \quad (3.26)$$

In particular, from Eq. (2.11) we have:

$$\hat{B}_t(x) = \int d\alpha d\beta K(\alpha, \beta) e^{i\alpha(\hat{x}_t - x) + \beta(\hat{p} - \bar{p})}, \quad (3.27)$$

where \bar{p} is a constant momentum value and $K(\alpha, \beta)$ is a generic complex function constrained by ((iii) rotational covariance)

$$K^*(R\alpha_1, R\beta_1) K(R\alpha_2, R\beta_2) = K^*(\alpha_1, \beta_1) K(\alpha_2, \beta_2), \quad (3.28)$$

where R is a rotation matrix. For later convenience, we rewrite the operator in Eq. (2.11) as:

$$\hat{B}_t(x) = i \int dQ e^{iQ(\hat{x}_t - x)} J(\hat{p}, Q), \quad (3.29)$$

where the imaginary number i is inserted, as we will see, to satisfy condition (ii) collapse of the state vector (see Sec. 2.3.2). The complex Gaussian field $h_t(x)$ defined over physical space (\mathbb{R}^3) has zero mean and correlation functions

$$\mathbb{E}_{\mathbb{Q}}[h_\tau(x_1) h_s(x_2)] = S_{\tau,s}(x_1, x_2), \quad (3.30)$$

$$\mathbb{E}_{\mathbb{Q}}[h_\tau^*(x_1) h_s(x_2)] = D_{\tau,s}(x_1, x_2), \quad (3.31)$$

In addition, we have the following symmetries ((iii) translational covariance and rotational covariance and (iv) stationary initial conditions):

$$D_{\tau,s}(x_1, x_2) = D_{\tau,s}(x_1 - x_2) = D_{\tau,s}(Rx_1, Rx_2) = D_{\tau+u, s+u}(x_1, x_2),$$

where R is a rotation and u is a time (see Sec. 2.3.3). The corresponding dynamical map for the statistical operator is given by Eq. (2.29) and by writing \hat{A}_t as in Eq. (2.10) we obtain:

$$\begin{aligned} \mathcal{L}^t[\hat{\rho}_0] = T[\exp & \left[-\frac{1}{\hbar^2} \int_0^t ds \int_0^t d\tau \int dx_1 \int dx_2 D_{\tau,s}(x_1 - x_2) \right. \\ & \cdot \left. \left(\hat{B}_{\tau,L}^\dagger(x_1) \hat{B}_{s,L}(x_2) \theta_{\tau s} - \hat{B}_{\tau,R}^\dagger(x_1) \hat{B}_{s,L}(x_2) + \hat{B}_{s,R}(x_2) \hat{B}_{\tau,R}^\dagger(x_1) \theta_{s\tau} \right) \right] \hat{\rho}_0], \end{aligned} \quad (3.32)$$

where

$$\hat{\rho}_t = \mathbb{E}_{\mathbb{Q}}[|\psi_t\rangle\langle\psi_t|] \quad (3.33)$$

We now impose, as is the case for all known collapse models, that the noise field is \mathbb{R} valued. In addition, we now make the following specific choices for the correlation functions and for the operator (see Eqs. (3.30), (3.31) and (3.29), respectively):

$$S_{\tau,s}(x_1, x_2) = \delta(x_1 - x_2) D_{\tau,s}, \quad (3.34)$$

$$D_{\tau,s}(x_1 - x_2) = \delta(x_1 - x_2) D_{\tau,s}, \quad (3.35)$$

$$J(\hat{p}, Q) = \sqrt{\lambda \frac{m^2}{m_0^2} \left(\frac{r_C}{\sqrt{\pi} \hbar} \right)^3} \exp(-r_C^2 / (2\hbar^2)) ((1 + k_T)/Q + 2k_T \hat{p})^2, \quad (3.36)$$

where we have $D_{\tau,s} > 0$. In this way the map in Eq. (3.32), using Eq. (3.29) reduces to the CD map in Eq. (3.25). In addition, we construct the Fock operator:

$$\hat{L}(x) = i \int dP \int dP' \hat{a}^\dagger(P') \langle P' | \int dQ e^{iQ(\hat{x}-x)} J(\hat{p}, Q) | P \rangle \hat{a}(P). \quad (3.37)$$

We then insert \hat{L} in place of the one particle operator \hat{B} in Eq. (3.26), and using Eqs. (3.34) and (3.35), we obtain the following stochastic differential equation (in the interaction picture):

$$i\hbar \frac{d}{dt} |\psi_t\rangle = \left(\int dx h_t(x) \hat{L}_t(x) - \int_0^t d\tau \int dx D(t-\tau) \left(\hat{L}_t(x) - \hat{L}_t^\dagger(x) \right) \frac{\partial}{\partial h_\tau(x)} \right) |\psi_t\rangle, \quad (3.38)$$

This equation completely determines the cdCSL model. In particular, this equation reduces to the cCSL and dCSL equations in the limits $T \rightarrow \infty$, $\tau_C \rightarrow 0$, respectively, where τ_C denotes the correlation time of $D(\tau-s)$. We obtain the corresponding map for the statistical operator from Eqs. (3.32), (3.34) and (3.35): we again replace the one particle operator \hat{B} with \hat{L} . Specifically, we obtain the CD map in the second quantized form (in the interaction picture):

$$\begin{aligned} \mathcal{L}^t[\hat{\rho}_0] = T[\exp & \left[-\frac{1}{\hbar^2} \int_0^t ds \int_0^t d\tau D(\tau - s) \int dx (\hat{L}_{\tau,L}^\dagger(x) \hat{L}_{s,L}(x) \theta_{\tau s} \right. \\ & \left. - \hat{L}_{\tau,R}^\dagger(x) \hat{L}_{s,L}(x) + \hat{L}_{s,R}(x) \hat{L}_{\tau,R}^\dagger(x) \theta_{s\tau}) \right] \hat{\rho}_0], \end{aligned} \quad (3.39)$$

3.4 Conclusions

We have obtained the general modification of the von-Neumann map by imposing a minimal set of requirements. In addition, we have constructed the cdCSL collapse model with the noise field selecting a preferred reference frame: the interaction with the stochastic field solves the issue of constant energy production of Galilean boost covariant models.

Here we make a small note about the QMUPL model: the QMUPL model can be derived as the limit of the CSL model [36]. We expect that the cdQMUPL model can be obtained as the limit of the cdCSL model.

Part II

Experimental constraints

Chapter 4

Matter-Wave Interferometry: theory

4.1 Introduction

The interest in exploring, not only theoretically but also experimentally, the foundations of quantum mechanics has significantly increased over the years. After the establishment of quantum non-locality, first with the famous works of J. Bell [38, 1] and subsequently with the experimental confirmation done by the groups of A. Aspect [39, 40, 41], perhaps the most relevant question is if the collapse of the wave function is a physical phenomenon or not.

Recalling what we derived before (see Sec. 3), the CD map is the most general modification of the quantum dynamics satisfying (i) probabilistic interpretation, (iii) translational and rotational covariance, (iv) stationary initial conditions and (v) asymptotic Gibbs state: the map determines the evolution for the statistical operator. On the other hand, the cdCSL collapse model describes the evolution for the state vector such that the evolution for the corresponding statistical operator is given by the CD map and that macroscopic objects are well-localized in physical space (\mathbb{R}^3), i.e. we make the additional assumptions (ii) collapse of the state vector and (vi) the Gaussian noise is a \mathbb{R} valued field over physical space (\mathbb{R}^3).

The CD map is thus a reasonable candidate, to be tested in the laboratory. However, at first sight the CD map might be difficult to test, as it contains, loosely speaking, at least 7 free parameters¹. In this section, we address this point: we will show that the CD map leads to predictions for interferometric experiments, which depend weakly on $D(\tau, s)$, T and \mathbf{u} : interferometric tests can therefore be used to test the CD map for specific values of λ and r_C . This implies that the CD map bounds on (λ, r_C) for interferometric experiments reduce to the CSL map bounds, i.e. non-Markovian and dissipative effects can be neglected for interferometric experiments.

This section is organized in the following way. In Sec. 4.2 we discuss theoretical interference patterns: the interference pattern derived in the density matrix formalism, is not limited only to collapse models, but is valid for a large class of dynamics. In particular, we also discuss under which conditions diffraction experiments can be reduced to a one dimensional problem, since a general dynamics, unlike ordinary quantum mechanics, is not separable in the three spatial dimension, even for the free particle dynamics. In this way we justify the calculation of the interference pattern in the paraxial approximation. In addition, the density matrix formalism outlines the similarities of far-field and near-field interference, by presenting a unified derivation. We also reobtain the results for diffraction experiments

¹We have the parameters λ , r_C , T and \mathbf{u} (3 spatial directions) and the function $D(\tau, s)$, which to first order, can be approximated by a zero mean Gaussian function with standard deviation τ_C .

that were derived in the Wigner function formalism [42, 43, 44]. In Sec. 4.3 we provide a brief summary of the most well known collapse models and the corresponding interference patterns. Specifically, we discuss the Continuous Spontaneous Localization (CSL) model [32, 31], the Ghirardi-Rimini-Weber (GRW) model [8], the Diósi-Penrose (DP) model [30], the Quantum Mechanics with Universal Position Localization (QMUPL) model [30, 33], the colored CSL (cCSL) model [45, 19, 20] and the dissipative CSL (dCSL) model [34]: the latter two maps can be used to discuss the CD map interference patterns. In Sec. (4.4) we discuss the amplification mechanism of collapse models and the localization requirement for macroscopic objects: the CD map bounds for (λ, r_C) again reduce to the CSL map bounds, i.e. non-Markovian and dissipative effects can be neglected for the localization requirement of macroscopic objects (a rough estimate).

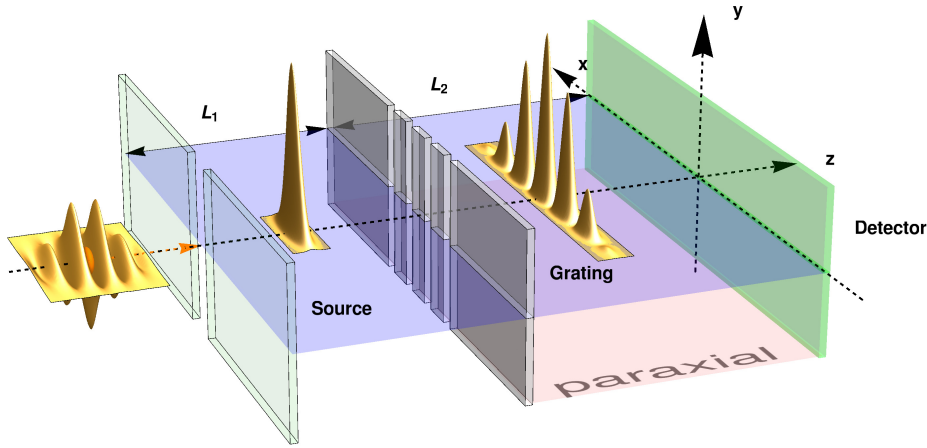


Figure 4.1: The common structure of far-field and near-field diffraction experiments. A molecular beam from an incoherent source propagates along the z axis. Each molecule is emitted from the source, propagates to the grating, where it is diffracted and then recorded by the detector. The molecules individually recorded gradually form an interference pattern. The figure shows a mechanical grating (with $N = 4$ slits), but the analysis applies to more general gratings, e.g. optical gratings. The distance from the source to the grating is L_1 and the distance from the grating to detector is L_2 . Between the grating and the detector we identify the paraxial (Fresnel) regime.

4.2 Derivation of the interference pattern

For all collapse models considered here (see the next Section), the evolution of the free single-particle density matrix has the form:

$$\rho(\mathbf{x}, \mathbf{x}', t) = \frac{1}{(2\pi\hbar)^3} \int d\tilde{\mathbf{k}} \int \tilde{\mathbf{w}} e^{-\frac{i}{\hbar}\tilde{\mathbf{k}}\cdot\tilde{\mathbf{w}}} F(\tilde{\mathbf{k}}, \mathbf{x} - \mathbf{x}', t) \rho^{\text{QM}}(\mathbf{x} + \tilde{\mathbf{w}}, \mathbf{x}' + \tilde{\mathbf{w}}, t), \quad (4.1)$$

where ρ^{QM} is the free standard quantum mechanical density matrix and the function F depends on the type of collapse model.

The quantum mechanical description of matter-wave interferometry is usually treated as a one-dimensional problem. This is justified by the fact that the free Schrödinger dynamics is separable along the three directions of motion. On the contrary, in general the dynamics given by Eq. (4.1) is not separable, not even in the free particle case. We show, however, that due to the specific geometry and experimental parameters of the diffraction experiments here considered, we can effectively separate the collapse dynamics in the three spatial directions, thus considerably simplifying the problem. Along with this, we will investigate the assumptions that are required for the justification of the one dimensional approximation. Actually, it is instructive to first carry out the calculation in the 1D (paraxial) approximation before justifying it.

The derivation of the paraxial interference pattern is the main result of this section. We then apply the paraxial interference formula to the far-field and near-field experimental setups. In order to simplify the comparison with similar results obtained in the literature, we will adopt the notation of [46]. We will also omit the overall normalization factors for the wave functions, density matrices and probability densities. At any step of the calculation, one can obtain a normalized quantity by dividing with an appropriate normalization factor.

4.2.1 Paraxial approximation

We first review the quantum mechanical derivation of the interference pattern in the paraxial (Fresnel) region, as depicted in Fig. 4.1. We label with z_1, z_2, z_3 the positions of source, grating and detector along the optical axis z , respectively. Similarly, we label the horizontal coordinates along the optical elements as x_1, x_2, x_3 , respectively.

In the paraxial diffraction region the evolution of the wave function can be approximated by the free quantum mechanical wave function propagation in one spatial dimension²:

$$\psi(x; t = L/v) = \int_{-\infty}^{+\infty} dx_0 \psi_0(x_0) e^{\frac{ik}{2L}(x-x_0)^2}, \quad (4.2)$$

where k is the wave number of the matter wave, ψ_0 is the initial wave function and ψ is the wave function after it has propagated for a distance L in a time $t = L/v$, where v is the speed of propagation along the optical axis z . One has the usual relation $mv = \hbar k$, where m is the mass of the system (the macromolecule). In the language of density matrices Eq. (4.2) reads:

$$\rho^{\text{QM}}(x, x'; t = L/v) = \int_{-\infty}^{+\infty} dx'_0 \int_{-\infty}^{+\infty} dx_0 \rho_0(x_0, x'_0) e^{\frac{ik}{2L}((x-x_0)^2 - (x'-x'_0)^2)}, \quad (4.3)$$

²This coincides with the Fresnel diffraction integral.

where $\rho_0(x_0, x'_0)$ is the initial density matrix and $\rho^{\text{QM}}(x, x'; t)$ is the density matrix after it has propagated for a distance L in a time $t = L/v$.

The calculation of the interference pattern can be summarized in the following steps.

[**z₁**] We choose the initial wave function at z_1 . Both the far-field and near-field experiments will be modeled by a completely incoherent source at z_1 , meaning that the wave functions associated to different molecules are uncorrelated and spatially localized initially. It is then sufficient to consider a single source at point (x_1, z_1) . At the end, one can integrate over the extension of the source. The corresponding initial wave function is given by

$$\psi_1(\tilde{x}_1) = \delta(x_1 - \tilde{x}_1). \quad (4.4)$$

[**z₁ to z₂**] We propagate the wave function to z_2 according to Eq. (4.2):

$$\psi_2(x_2) = \int_{-\infty}^{+\infty} d\tilde{x}_1 \psi_1(\tilde{x}_1) e^{\frac{ik}{2L_1}(x_2 - \tilde{x}_1)^2}. \quad (4.5)$$

[**z₂**] We now assume that the optical element at position z_2 has a transmission function $t_2(x)$. The wave function immediately after the grating at z_2 is given by $t_2(x_2)\psi_2(x_2)$.

[**z₂ to z₃**] We propagate the wave function from z_2 to z_3 according to Eq. (4.2):

$$\psi_3(x_3) = \int_{-\infty}^{+\infty} dx_2 t_2(x_2) \psi_2(x_2) e^{\frac{ik}{2L_2}(x_3 - x_2)^2}. \quad (4.6)$$

[**z₃**] The detector records the arrival of the molecules along the axis x_3 . The probability distribution is $p_3(x_3) = |\psi_3(x_3)|^2$. After combining the equations of the previous steps we obtain the interference pattern:

$$p_3(x_3) = \int_{-\infty}^{+\infty} dx_2 \int_{-\infty}^{+\infty} dx'_2 t(x_2) t^*(x'_2) e^{-\frac{ik}{2L_2}(x_2 - x'_2)x_3} e^{\frac{ik}{2L_1}(x_2^2 - x'^2_2)} e^{\frac{ik}{2L_2}(x_2'^2 - x_2^2)} e^{-\frac{ik}{L_1}(x_2 - x'_2)x_1}. \quad (4.7)$$

Note that Eq. (4.7) was derived from Eq. (4.2), but it could equally well be derived from the density matrix evolution given by Eq. (4.3).

We now consider what happens if in place of the standard quantum evolution, we have the following density matrix evolution:

$$\rho(x, x'; t) = \frac{1}{2\pi\hbar} \int_{-\infty}^{+\infty} d\tilde{k} \int_{-\infty}^{+\infty} \tilde{w} e^{-\frac{i}{\hbar}\tilde{k}\tilde{w}} F(\tilde{k}, 0, 0; x - x', 0, 0; t) \rho^{\text{QM}}(x + \tilde{w}, x' + \tilde{w}; t). \quad (4.8)$$

We will justify Eq. (4.8) below, when we discuss the separability issue. The calculation of the interference pattern can be again carried out as before.

[**z₁**] We consider a single source at point (x_1, z_1) . The corresponding initial wave function is given by $\psi_1(\tilde{x}_1) = \delta(x_1 - \tilde{x}_1)$ and the corresponding density matrix is given by

$$\rho_1(\tilde{x}_1, \tilde{x}'_1) = \delta(x_1 - \tilde{x}_1) \delta(x_1 - \tilde{x}'_1). \quad (4.9)$$

[**z₁ to z₂**] We propagate the density matrix from the point z_1 to the point z_2 along the optical axis using Eq. (4.8):

$$\rho_2(x_2, x_2) = \frac{1}{2\pi\hbar} \int_{-\infty}^{+\infty} d\tilde{k} \int_{-\infty}^{+\infty} \tilde{w} e^{-\frac{i}{\hbar}\tilde{k}\tilde{w}} F(\tilde{k}, 0, 0; x - x', 0, 0; t) \rho_2^{\text{QM}}(x_2 + \tilde{w}, x_2' + \tilde{w}), \quad (4.10)$$

where according to Eq. (4.3) and Eq. (4.9):

$$\rho_2^{\text{QM}}(x_2, x_2') = e^{\frac{ik}{2L_1}(x_2^2 - x_2'^2)} e^{-\frac{ik}{L_1}(x_2 - x_2')x_1}. \quad (4.11)$$

In Eq. (4.10) the \tilde{w} integration yields a Dirac delta function $\delta(\tilde{k} - \frac{\hbar k}{L_1}(x_2 - x_2'))$ and hence after the \tilde{k} integration we obtain:

$$\rho_2(x_2, x_2') = e^{\frac{ik}{2L_1}(x_2^2 - x_2'^2)} e^{-\frac{ik}{L_1}(x_2 - x_2')x_1} F\left(\frac{\hbar k}{L_1}(x_2 - x_2'), 0, 0; x_2 - x_2', 0, 0; t_1\right). \quad (4.12)$$

[**z₂**] We apply the grating's transmission function $t(x)$ to the density matrix and obtain $t(x_2)\rho_2(x_2, x_2')t^*(x_2')$.

[**z₂ to z₃**] We perform a free propagation according to Eq. (4.8) from z_2 to z_3 :

$$\rho_3(x_3, x_3') = \frac{1}{2\pi\hbar} \int_{-\infty}^{+\infty} d\tilde{k} \int_{-\infty}^{+\infty} \tilde{w} e^{-\frac{i}{\hbar}\tilde{k}\tilde{w}} F(\tilde{k}, 0, 0; x_3 - x_3', 0, 0; t_2) \rho_3^{\text{QM}}(x_3 + \tilde{w}, x_3' + \tilde{w}) \quad (4.13)$$

where

$$\rho_3^{\text{QM}}(x_3, x_3') = \int_{-\infty}^{+\infty} dx_2 \int_{-\infty}^{+\infty} dx_2' t(x_2)t^*(x_2') dx_2' \rho_2(x_2, x_2') e^{\frac{ik}{2L_2}((x_3 - x_2)^2 - (x_3' - x_2')^2)}. \quad (4.14)$$

[**z₃**] The interference pattern is again proportional to the probability density $p(x) = \rho_3(x, x)$. The \tilde{w} integration yields a Dirac delta function $\delta(\tilde{k} + \frac{\hbar k}{L_2}(x_2 - x_2'))$. Hence after the \tilde{k} integration we obtain the interference pattern:

$$p(x) = \int_{-\infty}^{+\infty} dx_2 \int_{-\infty}^{+\infty} dx_2' D(x_2 - x_2') t(x_2)t^*(x_2') \times e^{-i\frac{mv}{\hbar}(x_2 - x_2')(\frac{x_1}{L_1} + \frac{x}{L_2})} e^{i\frac{mv}{\hbar}\frac{L_1 + L_2}{2L_1 L_2}(x_2^2 - x_2'^2)}, \quad (4.15)$$

where

$$D(x_2 - x_2') = F\left(-\frac{\hbar k}{L_2}(x_2 - x_2'), 0, 0; 0, 0, 0; t_2\right) F\left(\frac{\hbar k}{L_1}(x_2 - x_2'), 0, 0; (x_2 - x_2'), 0, 0; t_1\right). \quad (4.16)$$

As we can see, the interference pattern in Eq. (4.15) differs from the pure quantum mechanical interference pattern of Eq. (4.7) by the presence of $D(x_2 - x_2')$.

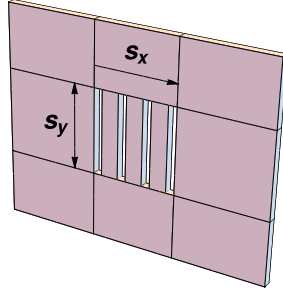


Figure 4.2: The grating has non-zero transmission function limited to a rectangle of size $s_x \times s_y$, e.g. here shown a mechanical grating with $N = 4$ slits with total horizontal extension s_x and slit height s_y . The analysis of this section applies also to other types of gratings, e.g. an optical grating.

4.2.2 Separability

We now perform the full 3D treatment of the problem to justify the 1D approximation. We consider an initial Gaussian wave packet, evolving according to the full dynamics in Eq. (4.1). For the geometry, we refer again to the experimental setup depicted in Fig. 4.1.

We will show under which assumptions the interference pattern is given by Eq. (4.15), thus justifying the above analysis in the 1D (paraxial) approximation. The assumptions are:

- 1 The extension of the macromolecule $\sigma(t)$ is much smaller than the distances L_1, L_2 during the time of flight t :

$$\sigma(t) \ll L_1, L_2. \quad (4.17)$$

This key assumption allows to split the flight of the molecule from the source at time $t = 0$ to the grating at time t_1 , from the motion from the grating at time t_1 to the detector at time $t_1 + t_2$, and to treat the non-free interaction with the grating as instantaneous. This is necessary in order to conveniently introduce a transmission function for the grating $t_{xy}(x, y)$. In particular, we choose $t_{xy}(x, y) = t(x)t_y(y)$, where

$$t(x) = 0 \text{ if } |x| > \frac{s_x}{2}, \quad (4.18)$$

while for $|x| < \frac{s_x}{2}$ it depends on the type of grating and

$$t_y(y) = \begin{cases} 1, & \text{if } |y| \leq \frac{s_y}{2}. \\ 0, & \text{if } |y| > \frac{s_y}{2}. \end{cases} \quad (4.19)$$

where s_x, s_y are described in Fig. 4.2 and $t(x)$ is to be identified with the transmission function used above, when working in the 1D (paraxial) approximation.

- 2 We assume that the molecule extension σ_2 at time t_1 , as it reaches the grating, is much larger than the molecule extension σ_1 , at time $t = 0$, as it leaves the source:

$$\sigma_1 \ll \sigma_2. \quad (4.20)$$

- 3 We require that the grating transmission function satisfies (see Fig. 4.2):

$$s_x \ll \sigma_2, \quad (4.21)$$

$$\sigma_2 \ll s_y. \quad (4.22)$$

Using ordinary quantum mechanics it is easy to give an estimate for the molecule's extension at the grating $\sigma_2 = \frac{\hbar t_1}{m\sigma_1}$, with σ_1 the extension at the source (see analysis below). Using this relation let us check the validity of the above assumptions for the two experiments considered.

For the far-field diffraction experiment [47] we have $L_1 = 0.702\text{m}$, $L_2 = 0.564\text{m}$, $s_x = 3\mu\text{m}$, $s_y = 60\mu\text{m}$ and the molecular speed along the z axis $v \sim 100\text{ms}^{-1}$. The above assumptions are satisfied if the initial molecular extension at the source is contained in the interval $4 \times 10^{-9}\text{m} \lesssim \sigma_1 \lesssim 7 \times 10^{-8}\text{m}$. No one knows the actual value of σ_1 . The range of values here considered make the initial spread much smaller than the extension of the source ($s = 1\mu\text{m}$) as given by the collimator and also provides a justification as to why the source is incoherent.

For the near-field KDTL diffraction experiment [48] we have $L_1 = L_2 = 10.5\text{cm}$, while it is difficult to give estimates for parameters s_x , s_y of the light grating. Anyhow, making the following guess for these parameters: $s_x = 10^{-3}\text{m}$, $s_y = 100 \times 10^{-3}\text{m}$ (and being the molecular speed along the z axis $v \sim 100\text{ms}^{-1}$), the above assumptions are satisfied if the initial molecular extension at the source is contained in the interval $10^{-13}\text{m} \lesssim \sigma_1 \lesssim 10^{-11}\text{m}$. This is to be compared with the slit openings of the source grating $l = 110\text{nm}$. Without more precise estimates for the molecule extension $\sigma(t)$ it is difficult to assess the validity of the above assumptions and hence of the 1D approximation. We stress that we are considering a single molecule emitted from the source. In particular, the single molecule extension $\sigma(t)$ should not be confused with the spatial coherence length of the beam, which is a property of an ensemble of particles emitted from the source.

As in the previous section, the calculation of the interference pattern can be split into several steps.

[z₁] It is convenient to work in a boosted reference frame along the z axis with molecular velocity³ v , i.e. moving alongside the molecule. To simplify the analysis we neglect gravity and we consider an initial Gaussian wave-function centered at $(x_1, 0, 0)$:

$$\psi_1(\tilde{x}_1, \tilde{y}_1, \tilde{z}_1) = e^{-\frac{(x_1 - \tilde{x}_1)^2}{4\sigma_1^2}} e^{-\frac{\tilde{y}_1^2}{4\sigma_1^2}} e^{-\frac{\tilde{z}_1^2}{4\sigma_1^2}}, \quad (4.23)$$

with the corresponding density matrix given by

$$\rho_1(\tilde{x}_1, \tilde{y}_1, \tilde{z}_1; \tilde{x}'_1, \tilde{y}'_1, \tilde{z}'_1) = \psi_1(\tilde{x}_1, \tilde{y}_1, \tilde{z}_1) \psi_1^*(\tilde{x}'_1, \tilde{y}'_1, \tilde{z}'_1). \quad (4.24)$$

[z₁ to z₂] We propagate the density matrix ρ_1 from $t = 0$ to $t = t_1 = L_1/v$ using Eq. (4.1).

We denote the resulting density matrix as $\rho_2(x_2, y_2, z_2; x'_2, y'_2, z'_2)$ (and by $\rho_2^{\text{QM}}(x_2, y_2, z_2; x'_2, y'_2, z'_2)$ the quantum mechanical evolution of ρ_1 at $t = t_1$). In particular, using the separability of ordinary quantum mechanics, the quantum mechanical wave function just before t_1 is given by:

$$\psi_2^{\text{QM}}(x_2, y_2, z_2) = \psi_2^{\text{QM}(1)}(x_2; x_1) \psi_2^{\text{QM}(1)}(y_2; 0) \psi_2^{\text{QM}(1)}(z_2; 0), \quad (4.25)$$

where $\psi_2^{\text{QM}(1)}(x_2; x_1) = \exp\left[-\frac{(x_2 - x_1)^2}{4\sigma_1^2(1 + \frac{i\hbar t_1}{2m\sigma_1^2})}\right]$. Hence the quantum mechanical density matrix is given by:

$$\rho_2^{\text{QM}}(x_2, y_2, z_2; x'_2, y'_2, z'_2; t_1) = \rho_2^{\text{QM}(1)}(x_2, x'_2; x_1) \rho_2^{\text{QM}(1)}(y_2, y'_2; 0) \rho_2^{\text{QM}(1)}(z_2, z'_2; 0), \quad (4.26)$$

³For non boost-invariant dynamics, one has to choose the correct function F depending on the reference frame.

where

$$\begin{aligned} \rho_2^{\text{QM}(1)}(x, x', x_1) = \exp \left[-\frac{1}{\sigma_2^2} \left(x^2 \left(1 - \frac{i\hbar t_1}{2m\sigma_1^2} \right) + x'^2 \left(1 + \frac{i\hbar t_1}{2m\sigma_1^2} \right) \right. \right. \\ \left. \left. - 2xx_1 \left(1 + \frac{i\hbar t_1}{2m\sigma_1^2} \right) - 2x'x_1 \left(1 - \frac{i\hbar t_1}{2m\sigma_1^2} \right) + 2x_1^2 \right) \right]. \end{aligned} \quad (4.27)$$

and $\sigma_2 = \frac{\hbar t_1}{m\sigma_1}$ because of Eq. (4.20), i.e. $\frac{\hbar^2 t_1^2}{4m^2 \sigma_1^4} \gg 1$. To summarize this step of the calculation:

$$\begin{aligned} \rho_2(x_2, y_2, z_2; x'_2, y'_2, z'_2) = \int d\tilde{k}_x \int d\tilde{w}_x \rho_2^{\text{QM}(1)}(x_2 + \tilde{w}_x, x'_2 + \tilde{w}_x; x_1) e^{-\frac{i}{\hbar} \tilde{k}_x \tilde{w}_x} \\ \times \int d\tilde{k}_y \int d\tilde{w}_y \rho_2^{\text{QM}(1)}(y_2 + \tilde{w}_y, y'_2 + \tilde{w}_y; 0) e^{-\frac{i}{\hbar} \tilde{k}_y \tilde{w}_y} \\ \times \int d\tilde{k}_z \int d\tilde{w}_z \rho_2^{\text{QM}(1)}(z_2 + \tilde{w}_z, z'_2 + \tilde{w}_z; 0) e^{-\frac{i}{\hbar} \tilde{k}_z \tilde{w}_z} \\ \times F(\tilde{k}_x, \tilde{k}_y, \tilde{k}_z; x_2 - x'_2, y_2 - y'_2, z_2 - z'_2; t_1) \end{aligned} \quad (4.28)$$

[z2] We apply the transmission function on the x and y axis given by Eqs. (4.18) and (4.19) respectively. Let us first consider the integrals along the x axis. Using Eq. (4.21) we can simplify in Eq. (4.27) (which is contained in Eq. (4.28)):

$$\rho_2^{\text{QM}(1)}(x, x', x_1) t(x) t^*(x') = \exp \left[-\frac{i(-x^2 + x'^2 - 2x_1(x - x')) \frac{\sigma_2}{2\sigma_1}}{\sigma_2^2} \right] t(x) t^*(x'). \quad (4.29)$$

The dependence on \tilde{w}_x , which will be integrated out, is contained in:

$$e^{-\frac{i}{\hbar} \tilde{k}_x \tilde{w}_x} \rho_2^{\text{QM}(1)}(x_2 + \tilde{w}_x, x'_2 + \tilde{w}_x) = \exp \left[\frac{iB(x_2, x'_2) \tilde{w}_x}{\sigma_2^2} \right] \text{Exp} \left[\frac{C(x_2, x'_2)}{\sigma_2^2} \right], \quad (4.30)$$

where

$$B(x_2, x'_2) = \frac{\sigma_2}{\sigma_1} (x_2 - x'_2) - \frac{1}{\hbar} \tilde{k}_x \sigma_2^2 \quad (4.31)$$

$$C(x_2, x'_2) = \frac{i\sigma_2}{2\sigma_1} \left((x_2^2 - x'^2_2) + 2x_1(x_2 - x'_2) \right). \quad (4.32)$$

Hence the \tilde{w}_x integral yields the Dirac delta function $\delta(\tilde{k}_x - (x_2 - x'_2) \frac{m}{\hbar t_1})$, which we use to perform \tilde{k}_x integration. On the y axis, by assumption (4.22), we can replace $t_y(y)$ by 1. To summarize, after performing the x -axis integrations we obtain:

$$\begin{aligned} \rho_2(x_2, y_2, z_2; x'_2, y'_2, z'_2) = e^{\frac{ik}{2L_1}(x_2^2 - x'^2_2)} e^{-\frac{ik}{L_1}(x_2 - x'_2)x_1} \\ \times \int d\tilde{k}_y \int d\tilde{w}_y \rho_2^{\text{QM}(1)}(y_2 + \tilde{w}_y, y'_2 + \tilde{w}_y; 0) e^{-\frac{i}{\hbar} \tilde{k}_y \tilde{w}_y} \\ \times \int d\tilde{k}_z \int d\tilde{w}_z \rho_2^{\text{QM}(1)}(z_2 + \tilde{w}_z, z'_2 + \tilde{w}_z; 0) e^{-\frac{i}{\hbar} \tilde{k}_z \tilde{w}_z} \\ \times F\left(\frac{\hbar k}{L_1}(x_2 - x'_2), \tilde{k}_y, \tilde{k}_z; x_2 - x'_2, y_2 - y'_2, z_2 - z'_2; t_1\right) \end{aligned} \quad (4.33)$$

[**z₂ to z₃**] We apply Eq. (4.1) to $\rho_2(x_2, y_2, z_2; x'_2, y'_2, z'_2)$ for a time $t_2 = \frac{L_2}{v}$:

$$\begin{aligned} \rho_3(x_3, y_3, z_3; x'_3, y'_3, z'_3) &= \int d\tilde{k}_x \int d\tilde{w}_x e^{-\frac{i}{\hbar}\tilde{k}_x\tilde{w}_x} \int d\tilde{k}_y \int d\tilde{w}_y e^{-\frac{i}{\hbar}\tilde{k}_y\tilde{w}_y} \\ &\times \int d\tilde{k}_z \int d\tilde{w}_z e^{-\frac{i}{\hbar}\tilde{k}_z\tilde{w}_z} F(\tilde{k}_x, \tilde{k}_y, \tilde{k}_z; x_3 - x'_3, y_3 - y'_3, z_3 - z'_3; t_2) \\ &\times \rho_3^{\text{QM}}(x_3 + \tilde{w}_x, y_3 + \tilde{w}_y, z_3 + \tilde{w}_z; x'_3 + \tilde{w}_x, y'_3 + \tilde{w}_y, z'_3 + \tilde{w}_z), \end{aligned} \quad (4.34)$$

where

$$\begin{aligned} \rho_3^{\text{QM}}(x_3, y_3, z_3; x'_3, y'_3, z'_3) &= \int_{-\infty}^{+\infty} dx_2 \int_{-\infty}^{+\infty} dx'_2 e^{\frac{ik}{2L_2}((x_3-x_2)^2-(x'_3-x'_2)^2)} \\ &\times \int_{-\infty}^{+\infty} dy_2 \int_{-\infty}^{+\infty} dy'_2 e^{\frac{ik}{2L_2}((y_3-y_2)^2-(y'_3-y'_2)^2)} \\ &\times \int_{-\infty}^{+\infty} dz_2 \int_{-\infty}^{+\infty} dz'_2 e^{\frac{ik}{2L_2}((z_3-z_2)^2-(z'_3-z'_2)^2)} \\ &\times \rho_2(x_2, y_2, z_2; x'_2, y'_2, z'_2) \end{aligned} \quad (4.35)$$

is the free quantum mechanical evolution of $\rho_2(x_2, y_2, z_2; x'_2, y'_2, z'_2)$ for a time t_2 .

[**z₃**] We now set $x = x_3 = x'_3$, $y = y_3 = y'_3$ and $z = z_3 = z'_3$ to obtain the probability density function $p_3(x, y, z) = \rho_3(x, y, z; x, y, z)$, as the molecule interacts with the detector. However, we are only interested in the probability of detecting a particle at a horizontal coordinate x , therefore we consider:

$$p(x) = \int_{-\infty}^{+\infty} dy \int_{-\infty}^{+\infty} dz p_3(x, y, z). \quad (4.36)$$

It is straightforward to perform the integrations along the x axis in Eq. (4.36) at this step of the calculation. In fact, these calculations are completely analogous to those described above (Eqs. (4.9) to (4.16)), when working within the 1D approximation.

Let us now look at the tedious integrations associated with the y axis in Eq. (4.36). In particular, we have from Eq. (4.34):

$$\int dy \int dy_2 \int dy'_2 \rho_2(x_2, y_2, z_2; x'_2, y'_2, z'_2) e^{\frac{ik}{2L_2}(-2(y+\tilde{w}_y)y_2+2(y+\tilde{w}_y)y'_2)} e^{\frac{ik}{2L_2}(y_2^2-y'^2_2)} \quad (4.37)$$

By performing the y integration we obtain a Dirac delta function $\delta(y_2 - y'_2)$ and by performing then also the y'_2 integration, the expression given in Eq. (4.37) reduces to:

$$\int dy_2 \rho_2(x_2, y_2, z_2; x'_2, y_2, z'_2) \quad (4.38)$$

Let us now write the integrations associated with the y axis contained within ρ_2 (see Eqs. (4.33) and (4.27)):

$$\begin{aligned} \int d\tilde{k}_y \int d\tilde{w}_y \int dy_2 \text{Exp} \left[-\frac{2\tilde{w}_y^2 + 2y_2^2 + \tilde{w}_y(4y_2 + \frac{i}{\hbar}\tilde{k}_y\sigma_2^2)}{\sigma_2^2} \right] \\ \times F(\tilde{k}_x, \tilde{k}_y, \tilde{k}_z; x_2 - x'_2, 0, z_2 - z'_2; t_1). \end{aligned} \quad (4.39)$$

By performing the y_2 integration we remove the quadratic term containing \tilde{w}_y :

$$\int d\tilde{k}_y \int d\tilde{w}_y F(\tilde{k}_x, \tilde{k}_y, \tilde{k}_z; x_2 - x'_2, 0, z_2 - z'_2; t_1) \exp\left[-\frac{i}{\hbar}\tilde{w}_y\tilde{k}_y\right]. \quad (4.40)$$

The \tilde{w}_y integration yields a Dirac delta function $\delta(\tilde{k}_y)$ and by then also performing the \tilde{k}_y integration, the expression given in Eq. (4.40) reduces to:

$$F(\tilde{k}_x, 0, \tilde{k}_z; x_2 - x'_2, 0, z_2 - z'_2; t_1). \quad (4.41)$$

In addition, we have just shown that $\rho_3^{QM}(x_3 + \tilde{w}_x, y_3 + \tilde{w}_y, z_3 + \tilde{w}_z; x_3 + \tilde{w}_x, y_3 + \tilde{w}_y, z_3 + \tilde{w}_z)$ defined in Eq. (4.35) does not depend on \tilde{w}_y . Hence we can perform the following integrations:

$$\int d\tilde{w}_y \int d\tilde{k}_y e^{-\frac{i}{\hbar}\tilde{w}_z\tilde{k}_z} F(\tilde{k}_x, \tilde{k}_y, \tilde{k}_z; 0, 0, 0, t_2). \quad (4.42)$$

Since the \tilde{w}_y integration yields a Dirac delta function $\delta(\tilde{k}_y)$ we obtain from the expression given in Eq. (4.42):

$$F(\tilde{k}_x, 0, \tilde{k}_z; 0, 0, 0, t_2). \quad (4.43)$$

We have thus shown that the final probability density is not affected by the dynamics along the y axis. A completely analogous calculation can be performed for the integrations associated with the z axis. Hence we obtain from Eq. (4.36):

$$p(x_3) = \int_{-\infty}^{+\infty} dx_2 \int_{-\infty}^{+\infty} dx'_2 t(x_2)t^*(x'_2)D(x_2 - x'_2) \times e^{-\frac{ik}{L_2}(x_2 - x'_2)x_3} e^{\frac{ik}{2L_1}(x_2^2 - x'^2_2)} e^{\frac{ik}{2L_2}(x_2^2 - x'^2_2)} e^{-\frac{ik}{L_1}(x_2 - x'_2)x_1}, \quad (4.44)$$

where

$$D(x_2 - x'_2) = F\left(-\frac{\hbar k}{L_2}(x_2 - x'_2), 0, 0; 0, 0, 0; t_2\right) F\left(\frac{\hbar k}{L_1}(x_2 - x'_2), 0, 0; (x_2 - x'_2), 0, 0; t_1\right). \quad (4.45)$$

This calculation thus justifies, and gives the limits of applicability, of the 1D treatment discussed before.

4.2.3 Far-field

The experimental setup for the far-field interference experiments is summarized in Fig. 4.3 (left).

The difference with respect to the idealized situation described in the previous section is that instead of a single point source we have an incoherent source of horizontal extension s , centered at $x_1 = 0$. We obtain the interference pattern by integrating Eq. (4.15) over the points x_1 of the source from $-\frac{s}{2}$ to $\frac{s}{2}$:

$$p(x) = \int_{-\infty}^{+\infty} dx_2 \int_{-\infty}^{+\infty} dx'_2 D(x_2 - x'_2) e^{-\frac{ik}{L_2}(x_2 - x'_2)x} \times \text{sinc}\left(\frac{k}{2L_1}(x_2 - x'_2)s\right) e^{ik(x_2^2 - x'^2_2)\left(\frac{1}{2L_1} + \frac{1}{2L_2}\right)}, \quad (4.46)$$

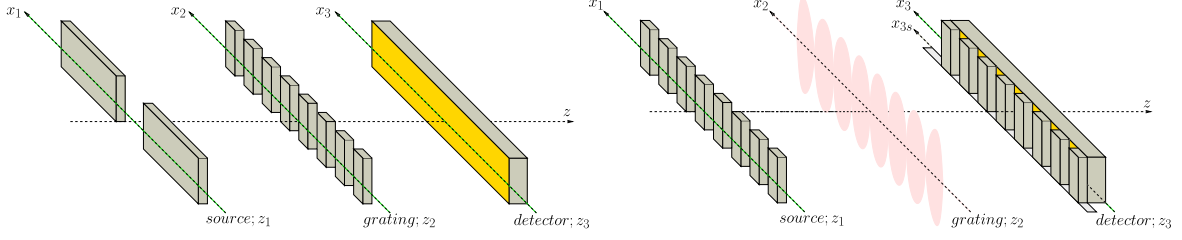


Figure 4.3: Left: Far-field experimental setup. The optical elements are: an incoherent source at z_1 (centered on the optical axis, i.e. around $x_1 = 0$), the diffraction grating at z_2 (here we have shown a mechanical grating with $N = 7$ slits) and the detector at z_3 . For the experiment described in section 5.3 we have the following numerical values. The distance from z_1 to z_2 is $L_1 = 0.702\text{m}$ and the distance from z_2 to z_3 is $L_2 = 0.564\text{m}$. The source extension is taken to be $s = 1\mu\text{m}$. The mechanical grating with $N = 30$ slits is described by the period $d = 100\text{nm}$ and slit width $l = 79\text{nm}$. The van der Waals forces due to the grating are modeled by an effective slit width $l_{eff} = 43\text{nm}$. Right: Talbot Lau near-field experimental setup. In this case the optical elements are: an extended incoherent source at z_1 , a diffraction grating at z_2 (here, an optical grating produced by a standing light wave) and the detector at z_3 . Two additional mechanical gratings block part of the molecules: the mechanical grating located immediately after the source is held fixed, while the mechanical grating immediately before the detector can move along the x_3 axis (we denote the displacement from its initial position by x_{3s}). We assume that all elements have a very large horizontal extension such that one can approximate them with periodic functions. The detector at z_3 records molecules that arrive at all points along the x_3 axis in a certain amount of time. For the experiment described in section 5.3 we have the following numerical values. The distance from z_1 to z_2 and the distance from z_2 to z_3 is $L = L_1 = L_2 = 10.5\text{cm}$. Both mechanical gratings are described by the same period $d = 266\text{nm}$ and slit width $l = 110\text{nm}$. The optical grating is described by the wavelength $\lambda_{laser} = 532\text{nm}$, the laser power $P_{laser} = 1\text{W}$, the optical polarizability $\alpha_{opt} = 410 \times 4\pi\epsilon_0$ and the absorption cross section $\sigma_a = 1.7 \times 10^{-21}\text{m}^2$.

A related study of far-field decoherence effects in the Wigner function formalism is given in [44].

Let us discuss how to evaluate numerically Eq. (4.46). We recognize from the factor $e^{-\frac{ik}{L_2}(x_2-x'_2)x_3}$ a Fourier transform and an inverse Fourier transform. Fourier transforms can be approximated with discrete Fourier transforms using the FFT algorithm. Hence the integrations in Eq. (4.46) can be conveniently evaluated numerically with the row column FFT algorithm.

4.2.4 Talbot Lau near-field

The experimental setup for the KDTL near-field interference experiment is represented in Fig. 4.3 (right). This is essentially the same scheme as presented before (Fig. 4.1) except that now we have two additional gratings at positions z_1, z_3 along the optical axis. We assume that all gratings have a very large horizontal extension such that we can model them by periodic functions. The first grating at z_1 acts as a mask of an infinite incoherent source and similarly the third grating at z_3 acts as a mask of the infinite detection screen. The experiment is performed by moving the masking grating at z_3 along the x_3 axis and recording

the total number of molecules that reach the detector in a certain amount of time. At the end one obtains the number of molecules that reach the detector given a certain displacement x_{3s} of the third grating from its initial position.

In section 5.3 we will describe the KDTL experiment, where the 3 gratings have the same periodicity d and the distance from z_1 to z_2 and from z_2 to z_3 is $L = L_1 = L_2$. Due to the periodicity of the 3 gratings, we adopt the following notation for the Fourier series of the corresponding transmission functions (notation of Ref. [46]):

$$|t_1(x_1)|^2 = \sum_{l=-\infty}^{+\infty} A_l e^{i2\pi l \frac{x_1}{d}}, \quad (4.47)$$

$$t(x_2) = \sum_{j=-\infty}^{+\infty} b_j e^{i2\pi j \frac{x_2}{d}}, \quad (4.48)$$

$$|t_3(x_3)|^2 = \sum_{n=-\infty}^{+\infty} C_n e^{i2\pi n \frac{x_3}{d}}. \quad (4.49)$$

We can now directly proceed with the derivation of the interference pattern starting again from Eq.(4.15):

$$S(x_{3s}) = \int_{-\infty}^{+\infty} \int_{-\infty}^{+\infty} dx_1 dx_3 p(x_3; x_1) |t_1(x_1)|^2 |t_3(x_3 - x_{3s})|^2, \quad (4.50)$$

where with respect to the far-field experiment, there is a further integration over all the detector region, x_{3s} is the horizontal shift of the third grating and $p(x_3; x_1)$ is the interference pattern due to a single source point at x_1 given by Eq. (4.15). In other words, $S(x_{3s})$ gives the number of molecules that reach the infinite detector at z_3 from the infinite source at z_1 in a certain amount of time, given a displacement x_{3s} of the third grating from its initial position. Since this gives formally an infinite value, we have to properly normalize the result. This is done in the following way.

The integrations in Eq. (4.50) over x_1, x_3 yield two delta functions $\delta(\frac{2\pi l}{d} - \frac{k}{L_1}(x_2 - x'_2))$, $\delta(\frac{2\pi n}{d} - \frac{k}{L_2}(x_2 - x'_2))$. We perform the integration over dx'_2 which gives the constraint $x_2 - x'_2 = \frac{2\pi l}{d} \frac{L}{k}$, while the other delta function gives the constrain $l = n$. We now divide by $\delta(0)$ in order to remove the infinite factor due to the delta function giving this first constrain. We are left with the integration over dx_2 which gives a delta function $\delta(\frac{4\pi n}{d} + \frac{2\pi j}{d} - \frac{2\pi j'}{d})$, where j' is the index in the Fourier expansion of $t^*(x'_2)$. This gives the constraint $j' = j + 2n$. We again divide by $\delta(0)$ in order to remove the infinite factor due to the delta function giving this second constrain. We are now left with a finite expression. In order to obtain a notation consistent with that of [46] we relabel n as $-n$ and use the fact that $A_{-n} = A_n^*$, $C_{-n} = C_n^*$. Thus we obtain:

$$S(x_{3s}) = \sum_n A_n^* C_n^* B_n D \left(\frac{2\pi n L}{d} \frac{L}{k} \right) e^{i2\pi n \frac{x_{3s}}{d}}, \quad (4.51)$$

where $B_n = \sum_j b_j b_{j-2n}^* e^{i\frac{\pi^2}{d^2} \frac{L}{k} (n^2 - 2nj)}$. The above equation coincides with the results derived by using the Wigner function formalism [42, 43].

4.3 Summary of Collapse Models and of the interference pattern

4.3.1 Continuous Spontaneous Localization

Here we are referring to the mass-proportional version of the CSL model [49]. The single-particle master equation in 3D is given by [50]:

$$\frac{d}{dt}\hat{\rho}(t) = -\frac{i}{\hbar} [\hat{H}, \hat{\rho}(t)] + \lambda \frac{m^2}{m_0^2} \left(\left(\frac{r_C}{\sqrt{\pi}\hbar} \right)^3 \int d^3\mathbf{Q} e^{-\frac{\mathbf{Q}^2 r_C^2}{\hbar^2}} e^{\frac{i}{\hbar}\mathbf{Q}\cdot\hat{\mathbf{x}}} \hat{\rho}(t) e^{-\frac{i}{\hbar}\mathbf{Q}\cdot\hat{\mathbf{x}}} - \hat{\rho}(t) \right). \quad (4.52)$$

λ gives the frequency of the localization events (a localization rate) for a reference object of mass $m_0 = 1$ amu, while r_C describes how well an object is localized (a localization length). In the free-particle case $\hat{H} = \hat{p}^2/2m$, the equation can be solved exactly. In the coordinate basis, it reads [8]:

$$\rho^{\text{CSL}}(\mathbf{x}, \mathbf{x}', t) = \frac{1}{(2\pi\hbar)^3} \int_{-\infty}^{+\infty} d\tilde{\mathbf{k}} \int_{-\infty}^{+\infty} d\tilde{\mathbf{w}} e^{-\frac{i}{\hbar}\tilde{\mathbf{k}}\cdot\tilde{\mathbf{w}}} F_{\text{CSL}}(\tilde{\mathbf{k}}, \mathbf{x} - \mathbf{x}', t) \rho^{\text{QM}}(\mathbf{x} + \tilde{\mathbf{w}}, \mathbf{x}' + \tilde{\mathbf{w}}, t), \quad (4.53)$$

where $\rho^{\text{QM}}(\mathbf{x}, \mathbf{x}', t)$ is the standard free quantum evolution for the density matrix ($\lambda = 0$) and

$$F_{\text{CSL}}(\tilde{\mathbf{k}}, \mathbf{q}, t) = \exp \left[-\lambda \frac{m^2}{m_0^2} t \left(1 - \frac{1}{t} \int_0^t d\tau e^{-\frac{1}{4r_C^2}(\mathbf{q} - \frac{\tilde{\mathbf{k}}\tau}{m})^2} \right) \right]. \quad (4.54)$$

The interference pattern is given by Eq. (4.15) with the function D defined as follows:

$$D_{\text{CSL}}(x_2 - x'_2) = \exp \left[-\lambda \frac{m^2}{m_0^2} (t_1 + t_2) \left(1 - \frac{\sqrt{\pi}}{2} \frac{\text{erf}\left(\frac{(x_2 - x'_2)}{2r_C}\right)}{\frac{(x_2 - x'_2)}{2r_C}} \right) \right]. \quad (4.55)$$

Note that $D_{\text{CSL}}(x_2 - x'_2)$ was previously derived [42, 43, 44] by using the Wigner function's formalism.

The GRW single-particle master equation has the same mathematical structure as the CSL single-particle master equation. Since our analysis is based entirely on this master equation the above CSL formulae apply also to the GRW model, the only difference being the amplification mechanism discussed in section 4.4.

4.3.2 Diósi-Penrose

The single-particle master equation in 3D for a particle of mass m_0 is given by [30, 50]:

$$\frac{d\hat{\rho}_t}{dt} = -\frac{i}{\hbar} [\hat{H}, \hat{\rho}_t] + \frac{Gm_0^2}{2\pi\hbar^2} \int d\mathbf{Q} \frac{1}{Q^2} e^{-\frac{\mathbf{Q}^2 R_0^2}{\hbar^2}} \left(e^{\frac{i}{\hbar}\mathbf{Q}\cdot\hat{\mathbf{x}}} \hat{\rho}_t e^{-\frac{i}{\hbar}\mathbf{Q}\cdot\hat{\mathbf{x}}} - \hat{\rho}_t \right), \quad (4.56)$$

where R_0 is a regularization parameter, which has to be included in order to avoid divergences at short distances⁴. For a point-like particle⁵ of mass m we have to replace m_0 with m . In

⁴The DP model introduces only one cut-off length phenomenological parameter R_0 , which cures the ultraviolet divergence of the gravitational interaction. The effective collapse rate, analogous to λ , is given by $Gm_0^2/\sqrt{\pi}\hbar R_0$, while R_0 describes how well an object is localized, analogous to r_C .

⁵We thank Prof. Lajos Diósi for signaling this point.

the free-particle case, the equation can be solved exactly, and in the position representation it reads [51]:

$$\rho^{\text{DP}}(\mathbf{x}, \mathbf{x}', t) = \frac{1}{(2\pi\hbar)^3} \int d\tilde{\mathbf{k}} \int \tilde{\mathbf{w}} e^{-\frac{i}{\hbar}\tilde{\mathbf{k}}\cdot\tilde{\mathbf{w}}} F_{\text{DP}}(\tilde{\mathbf{k}}, \mathbf{x} - \mathbf{x}', t) \rho^{\text{QM}}(\mathbf{x} + \mathbf{w}, \mathbf{x}' + \mathbf{w}, t), \quad (4.57)$$

where, again, $\rho^{\text{QM}}(\mathbf{x}, \mathbf{x}', t)$ is the free standard quantum evolution, and

$$F_{\text{DP}}(\tilde{\mathbf{k}}, \mathbf{q}, t) = \exp \left[-\frac{1}{\hbar} \int_0^t d\tau \left(U\left(-\frac{\tilde{\mathbf{k}}\tau}{m} + \mathbf{q}\right) - U(0) \right) \right] \quad (4.58)$$

with $U(\mathbf{x}) = -Gm_0^2 \text{erf}(|\mathbf{x}|/2R_0)/|\mathbf{x}|$.

The interference pattern is given again by Eq. (4.15), with the function D given by:

$$D_{\text{DP}}(x_2 - x'_2) = \exp \left[-\frac{Gm_0^2}{\hbar\sqrt{\pi}R_0} (t_1 + t_2) \left(1 - {}_2F_2 \left(\frac{1}{2}, \frac{1}{2}, \frac{3}{2}, \frac{3}{2}; -\left(\frac{|x_2 - x'_2|}{2R_0} \right)^2 \right) \right) \right], \quad (4.59)$$

where ${}_2F_2\left(\frac{1}{2}, \frac{1}{2}, \frac{3}{2}, \frac{3}{2}; z\right) = \sum_{k=0}^{\infty} \left(\frac{1}{1+2k} \right)^2 \frac{z^k}{k!}$.

It is instructive to compare D_{DP} and D_{CSL} . One can relate the role of λ in the CSL model with $\lambda_{\text{DP}} = \frac{Gm_0^2}{\hbar\sqrt{\pi}R_0}$ in the DP model, and the role of r_C for CSL with R_0 for DP. As Fig. 4.6 shows, when appropriately rescaled, D_{DP} and D_{CSL} have a very similar behavior. In particular, both are equal to 1 for $|x_2 - x'_2| = 0$ and decay more or less in the same way towards the asymptotic value $e^{-\lambda(t_1+t_2)}$ as $|x_2 - x'_2| \rightarrow \infty$.

4.3.3 Dissipative CSL

This is a recently developed new version of the CSL model, which includes dissipative effects, which prevent the energy of the system to increase and eventually diverge. The single-particle master equation in 3D is [34, 51]:

$$\begin{aligned} \frac{d\hat{\rho}_t}{dt} = & -\frac{i}{\hbar} [\hat{H}, \hat{\rho}_t] \\ & + \lambda \frac{m^2}{m_0^2} \left(\left(\frac{r_C(1+k_T)}{\sqrt{\pi}\hbar} \right)^3 \int d\mathbf{Q} e^{\frac{i}{\hbar}\mathbf{Q}\cdot\hat{\mathbf{x}}} e^{-\frac{r_C^2}{2\hbar^2}((1+k_T)\mathbf{Q}+2k_T\hat{\mathbf{p}})^2} \hat{\rho}_t e^{-\frac{r_C^2}{2\hbar^2}((1+k_T)\mathbf{Q}+2k_T\hat{\mathbf{p}})^2} e^{-\frac{i}{\hbar}\mathbf{Q}\cdot\hat{\mathbf{x}}} - \hat{\rho} \right) \end{aligned} \quad (4.60)$$

where $k_T = \frac{\hbar^2}{8mr_C^2 k_B T}$, k_B is Boltzmann constant and T the temperature the system thermalizes to. This is a new parameter of the theory, which together with λ and r_C fully identifies the model. In the limit $k_T \rightarrow 0$ (i.e $T \rightarrow \infty$), one re-obtains standard CSL model.

We simplify the analysis, as in [51, 34], by considering only small values of k_T :

$$k_T \ll 1. \quad (4.61)$$

This assumption identifies a region in the parameter space (T, r_C) , depicted in Fig. 5.1.

In the free particle case the solution reads [34]:

$$\rho^{\text{dCSL}}(\mathbf{x}, \mathbf{x}', t) = \frac{1}{(2\pi\hbar)^3} \int d\tilde{\mathbf{k}} \int \tilde{\mathbf{w}} e^{-\frac{i}{\hbar}\tilde{\mathbf{k}}\cdot\tilde{\mathbf{w}}} F_{\text{dCSL}}(\tilde{\mathbf{k}}, \mathbf{x} - \mathbf{x}', t) \rho^{\text{QM}}(\mathbf{x} + \tilde{\mathbf{w}}, \mathbf{x}' + \tilde{\mathbf{w}}, t), \quad (4.62)$$

where as usual $\rho^{\text{QM}}(\mathbf{x}, \mathbf{x}', t)$ is the free standard quantum evolution, and

$$F_{\text{dCSL}}(\tilde{\mathbf{k}}, \mathbf{q}, t) = \exp \left[-\lambda \frac{m^2}{m_0^2} t \left(1 - \frac{1}{t} \int_0^t d\tau e^{-\frac{\tilde{\mathbf{k}}^2 r_C^2 k_T^2}{\hbar^2} - \frac{(-\frac{\tilde{\mathbf{k}}\tau + \mathbf{q}}{m})^2}{4r_C^2(1+k_T)^2}} \right) \right]. \quad (4.63)$$

The interference pattern is still given by Eq. (4.15), with the function D given by:

$$D_{\text{dCSL}}(x_2 - x'_2) = \exp \left[-\lambda \frac{m^2}{m_0^2} (t_1 + t_2) \right. \\ \left. + \lambda \frac{m^2}{m_0^2} \left(t_1 e^{-\frac{k^2}{L_1^2} (x_2 - x'_2)^2 r_C^2 k_T^2} + t_2 e^{-\frac{k^2}{L_2^2} (x_2 - x'_2)^2 r_C^2 k_T^2} \right) \frac{\sqrt{\pi}}{2} \frac{\text{erf}\left(\frac{(x_2 - x'_2)}{2r_C(1+k_T)}\right)}{\frac{(x_2 - x'_2)}{2r_C(1+k_T)}} \right]. \quad (4.64)$$

We note that this equation reduces to the CSL D function, given in Eq. (4.55), when the following condition is fulfilled:

$$\frac{1}{r_C t} \ll \frac{8k_B T}{\hbar \Delta x}, \quad (4.65)$$

for $t = t_1$ and $t = t_2$. This condition identifies a region in the parameter space (r_C, T) , depicted in Fig. 5.1.

However, the master equation (4.60) is not invariant under boosts. Indeed, the dissipative CSL master equation has the same structure of a quantum linear Boltzmann equation of a particle immersed in a finite temperature bath [52]. Thus the dissipative CSL model contains an additional free parameter, a velocity \mathbf{u} , which is analogous to the relative velocity between bath and particle. In particular, the master equation in the boosted reference frame with boost velocity \mathbf{u} is given by the following equation:

$$\frac{d\hat{\rho}_t}{dt} = -\frac{i}{\hbar} [\hat{H}, \hat{\rho}_t] + \lambda \frac{m^2}{m_0^2} \left(\frac{r_C(1+k_T)}{\sqrt{\pi\hbar}} \right)^3 \\ \times \int d\mathbf{Q} e^{i\mathbf{Q}\cdot\hat{\mathbf{X}}} e^{-\frac{r_C^2}{2\hbar^2} ((1+k_T)\mathbf{Q} + 2k_T(\hat{\mathbf{P}} - m\mathbf{u}))^2} \hat{\rho}_t e^{-\frac{r_C^2}{2\hbar^2} ((1+k_T)\mathbf{Q} + 2k_T(\hat{\mathbf{P}} - m\mathbf{u}))^2} e^{-\frac{i}{\hbar} \mathbf{Q}\cdot\hat{\mathbf{X}}} - \hat{\rho}_t. \quad (4.66)$$

We find the solution of Eq. (4.66) using the characteristic function approach [53]. The solution is given by Eq. (4.62) with the function F_{dCSL} replaced by:

$$F_{\text{dCSL}}^{\text{boosted}}(\tilde{\mathbf{k}}, \mathbf{q}, t; \mathbf{u}) = \exp \left[-\lambda \frac{m^2}{m_0^2} t \left(1 - \frac{1}{t} \int_0^t d\tau e^{-\frac{\tilde{\mathbf{k}}^2 r_C^2 k_T^2}{\hbar^2} - \frac{(-\frac{\tilde{\mathbf{k}}\tau + \mathbf{q}}{m})^2}{4r_C^2(1+k_T)^2}} e^{\frac{i}{\hbar} \frac{2k_T m \mathbf{u}}{1+k_T} \cdot (-\frac{\tilde{\mathbf{k}}\tau + \mathbf{q}}{m})} \right) \right]. \quad (4.67)$$

The interference pattern is given by Eq. (4.15) with the function D replaced by:

$$D_{\text{dCSL}}^{\text{boosted}}(x_2 - x'_2) = \exp \left[-\lambda \frac{m^2}{m_0^2} (t_1 + t_2) \right. \\ \left. + \lambda \frac{m^2}{m_0^2} \left(t_1 e^{-\frac{k^2}{L_1^2} (x_2 - x'_2)^2 r_C^2 k_T^2} + t_2 e^{-\frac{k^2}{L_2^2} (x_2 - x'_2)^2 r_C^2 k_T^2} \right) \right. \\ \left. \times \frac{\int_0^{\frac{(x_2 - x'_2)}{2r_C(1+k_T)}} d\tau e^{-\tau^2} \cos\left(2\tau \frac{2r_C k_T m u_x}{\hbar}\right)}{\frac{(x_2 - x'_2)}{2r_C(1+k_T)}} \right], \quad (4.68)$$

where u_x is the x component of \mathbf{u} . We note that this equation reduces to the CSL D function, given in Eq. (4.55), when in addition to Eq. (4.65), the following condition is fulfilled:

$$\frac{u_x}{r_C^2} \ll \frac{8k_B T}{\hbar \Delta x} \quad (4.69)$$

We note that Eq. (4.68) reduces to Eq. (4.64) as $u_x \rightarrow 0 \text{ms}^{-1}$ and that Eq. (4.64) reduces to Eq. (4.55) as $k_T \rightarrow 0$. This condition identifies a region in the parameter space (r_C, u_x, T) , depicted in Fig. 5.2.

A comparison of $D_{\text{dCSL}}^{\text{boosted}}$ functions evaluated with different temperatures T and different boosts u_x is given in Figs. 4.4, 4.5 respectively. We see from these figures that the dCSL model with large temperatures T and small boosts u_x give the smallest modification with respect to the standard quantum mechanical evolution ($D = 1$) and practically coincide with the CSL model evolution. Hence, given that T and u_x are unknown, the CSL model can be used as a bound for all dCSL models with arbitrary T and \mathbf{u} .

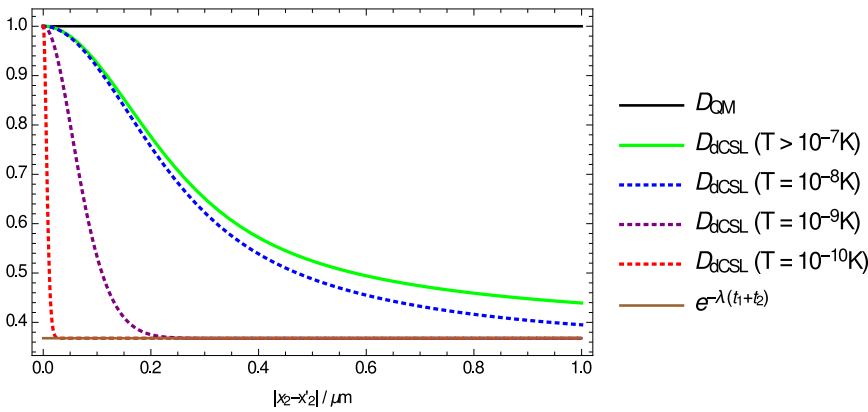


Figure 4.4: Comparison of D_{dCSL} functions for different temperatures T at fixed boost $u_x = 0 \text{ms}^{-1}$. The plot is obtained with $r_C = 10^{-7} \text{m}$, $\lambda = 500 \text{s}^{-1}$, $t_1 = t_2 = 1 \text{ms}$ and $L_1 = L_2 = 0.1 \text{m}$. The black solid line represents the quantum mechanical function ($D = 1$), the green solid line represents the D function for the dCSL models with $T > 10^{-7} \text{K}$ (which includes the CSL model), while the dashed lines represent the dCSL models with temperatures $T = 10^{-8} \text{K}$, $T = 10^{-9} \text{K}$ and $T = 10^{-10} \text{K}$. The solid brown line represents the asymptotic value of the D functions for all the considered collapse models as $|x - x'| \rightarrow +\infty$.

The dGRW single-particle master equation has the same mathematical structure as the dCSL single-particle master equation. Since our analysis is based entirely on this master equation the above dCSL formulae apply also to the dGRW model, the only difference being the amplification mechanism discussed in section 4.4.

4.3.4 Colored CSL

This model presents an additional difficulty with respect to the white noise models discussed in the previous sections. The calculation presented in 4.2 is split into two parts, the free evolution from the source at time τ_1 to the grating at time τ_2 and the free evolution from the grating at time τ_2 to the detector at time τ_3 , whereas at time τ_2 the molecule is subject to a

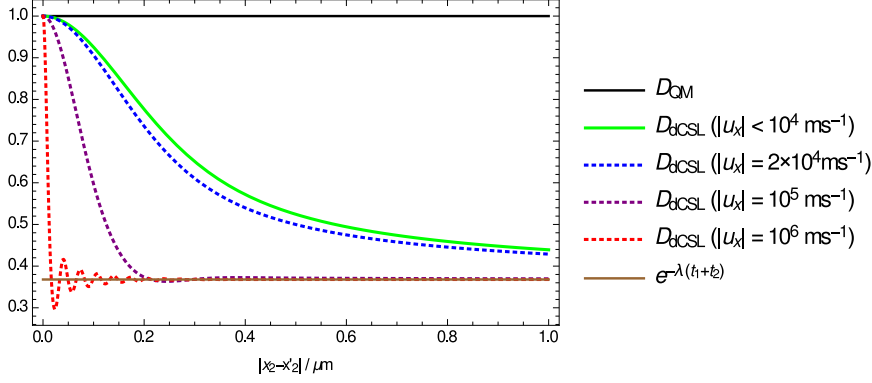


Figure 4.5: Comparison of D_{dCSL} functions for different boost along the x axis u_x at fixed temperature $T = 1K$. The plot is obtained with $r_C = 10^{-7}\text{m}$, $\lambda = 500\text{s}^{-1}$, $t_1 = t_2 = 1\text{ms}$ and $L_1 = L_2 = 0.1\text{m}$. The black solid line represents the quantum mechanical function ($D = 1$), the green solid line represents the D function for the dCSL models with boosts along the x axis $|u_x| < 10^4\text{ms}^{-1}$ (which includes the CSL model), while the dashed lines represent the dCSL models with boost along the x axis $|u_x| = 2 \times 10^4\text{ms}^{-1}$, $|u_x| = 10^5\text{ms}^{-1}$ and $|u_x| = 10^6\text{ms}^{-1}$. The solid brown line represents the asymptotic value of the D functions for all the considered collapse models as $|x - x'| \rightarrow +\infty$.

non free evolution. Let us consider the times $\tau_1 < t_{\text{before}} < \tau_2$ and $\tau_2 < t_{\text{after}} < \tau_3$. The non white noise might correlate the evolution between t_{before} and t_{after} . In order to simplify the analysis we neglect the correlations between these times by assuming a small correlation time $\tau_c \ll \tau_3 - \tau_1$. A similar argument can be put forward for the correlation between times before and after τ_1 . Hence we limit the discussion to non white CSL models with small correlation times. In particular, this assumption justifies the following approximation of the free one particle master equation in 3D [54, 19]:

$$\begin{aligned} \frac{d\hat{\rho}_t}{dt} = & -\frac{i}{\hbar} [\hat{H}, \hat{\rho}_t] \\ & - \lambda \frac{m^2}{m_0^2} \left(\frac{r_C}{\sqrt{\pi\hbar}} \right)^3 \int_0^t ds f(t-s) \int d\mathbf{Q} e^{-\frac{\mathbf{Q}^2 r_C^2}{\hbar^2}} [e^{\frac{i}{\hbar} \hat{\mathbf{x}} \cdot \mathbf{Q}}, [\hat{U}^\dagger(s-t) e^{-\frac{i}{\hbar} \hat{\mathbf{x}} \cdot \mathbf{Q}} \hat{U}(s-t), \hat{\rho}_t]], \end{aligned} \quad (4.70)$$

where $f(t-s)$ is the correlation function and $\hat{U}(t) = e^{-\frac{i}{\hbar} \frac{\hat{\mathbf{p}}^2}{2m} t}$.

We now expand $\hat{U}(\tau)$ to first order: $\hat{U}(\tau) \approx 1 - \frac{i}{\hbar} \frac{\hat{\mathbf{p}}^2}{2m} \tau$, which is justified since τ is limited by the correlation time τ_C of the correlation function $f(s)$ through the time integral in Eq. (4.70). We make the following assumption (we will discuss the validity of this assumption in Sec. 5.2):

$$\frac{1}{\hbar} \frac{\hat{\mathbf{p}}^2}{2m} \tau_C \ll 1. \quad (4.71)$$

Hence by performing the time integration we obtain from Eq. (4.70):

$$\frac{d\hat{\rho}_t}{dt} = L_{\text{CSL}}[\hat{\rho}] + L_{\text{correction}}[\hat{\rho}], \quad (4.72)$$

where

$$L_{\text{CSL}}[\hat{\rho}] = -\frac{i}{\hbar} [\hat{H}, \hat{\rho}_t] + \lambda \frac{m^2}{m_0^2} \left(\left(\frac{r_C}{\sqrt{\pi\hbar}} \right)^3 \int d\mathbf{Q} e^{-\frac{\mathbf{Q}^2 r_C^2}{\hbar^2}} e^{\frac{i}{\hbar} \mathbf{Q} \cdot \hat{\mathbf{x}}} \hat{\rho}(t) e^{-\frac{i}{\hbar} \mathbf{Q} \cdot \hat{\mathbf{x}}} - \hat{\rho}(t) \right) \quad (4.73)$$

is the white noise CSL evolution,

$$L_{\text{correction}}[\hat{\rho}] = \frac{i\bar{\tau}}{2m\hbar} \lambda \frac{m^2}{m_0^2} \left(\frac{r_C}{\sqrt{\pi\hbar}} \right)^3 \int d\mathbf{Q} e^{-\frac{\mathbf{Q}^2 r_C^2}{\hbar^2}} \mathbf{Q} \cdot ([e^{\frac{i}{\hbar} \mathbf{Q} \cdot \hat{\mathbf{x}}} \hat{\rho} e^{-\frac{i}{\hbar} \mathbf{Q} \cdot \hat{\mathbf{x}}}, \hat{\rho}] + e^{\frac{i}{\hbar} \mathbf{Q} \cdot \hat{\mathbf{x}}} [\hat{\rho}, \hat{\rho}] e^{-\frac{i}{\hbar} \mathbf{Q} \cdot \hat{\mathbf{x}}}) \quad (4.74)$$

is the first order correction due to the non white noise and

$$\bar{\tau} = \int_0^t f(s) ds. \quad (4.75)$$

By performing a direct but tedious calculation, it can be shown that Eq. (4.72) is invariant under boost and thus fully Galilean invariant.

Let us now find the solution of Eq. (4.72) by using the characteristic function approach [53]. We multiply Eq. (4.72) by $e^{\frac{i}{\hbar}(\boldsymbol{\nu} \cdot \hat{\mathbf{x}} + \boldsymbol{\mu} \cdot \hat{\mathbf{p}})}$ and take the trace:

$$\frac{\partial}{\partial t} \chi(\boldsymbol{\nu}, \boldsymbol{\mu}, t) = \frac{\boldsymbol{\nu}}{M} \cdot \partial_{\boldsymbol{\mu}} \chi(\boldsymbol{\nu}, \boldsymbol{\mu}, t) + \lambda (\Phi(\boldsymbol{\nu}, \boldsymbol{\mu}) - 1), \quad (4.76)$$

where

$$\Phi(\boldsymbol{\nu}, \boldsymbol{\mu}) = e^{\frac{-\boldsymbol{\mu}^2}{4r_C^2}} \left(1 - \frac{\boldsymbol{\mu} \cdot \boldsymbol{\nu}}{4mr_C^2} \bar{\tau} \right) \quad (4.77)$$

and

$$\chi(\boldsymbol{\nu}, \boldsymbol{\mu}, t) = \text{Tr}[\hat{\rho}_t e^{\frac{i}{\hbar}(\boldsymbol{\nu} \cdot \hat{\mathbf{x}} + \boldsymbol{\mu} \cdot \hat{\mathbf{p}})}]. \quad (4.78)$$

The solution of the characteristic function in Eq. (4.76) is given by:

$$\chi(\boldsymbol{\nu}, \boldsymbol{\mu}, t) = \chi^0(\boldsymbol{\nu}, \boldsymbol{\mu}, t) e^{-\lambda t + \int_0^t \Phi(\boldsymbol{\nu}, \frac{\boldsymbol{\nu}\tau}{m} + \boldsymbol{\mu}) d\tau}, \quad (4.79)$$

where $\chi^0(\boldsymbol{\nu}, \boldsymbol{\mu}, t)$ is the solution of equation $\frac{\partial}{\partial t} \chi^0(\boldsymbol{\nu}, \boldsymbol{\mu}, t) = \frac{1}{m} \boldsymbol{\nu} \cdot \frac{\partial}{\partial \boldsymbol{\mu}} \chi^0(\boldsymbol{\nu}, \boldsymbol{\mu}, t)$. The density matrix can be obtained from the characteristic function using the inversion formula:

$$\rho(\mathbf{x}, \mathbf{x}', t) = \int \frac{d\boldsymbol{\nu}}{(2\pi\hbar)^3} e^{-\frac{i}{2\hbar} \boldsymbol{\nu} \cdot (\mathbf{x} + \mathbf{x}')} \chi(\boldsymbol{\nu}, \mathbf{x} - \mathbf{x}', t). \quad (4.80)$$

Hence the solution of the master equation (4.72) is given by:

$$\rho^{\text{cCSL}}(\mathbf{x}, \mathbf{x}', t) = \frac{1}{(2\pi\hbar)^3} \int d\tilde{\mathbf{k}} \int \tilde{\mathbf{y}} e^{-\frac{i}{\hbar} \tilde{\mathbf{k}} \cdot \tilde{\mathbf{y}}} F_{\text{cCSL}}(\tilde{\mathbf{k}}, \mathbf{x} - \mathbf{x}', t) \rho^{QM}(\mathbf{x} + \mathbf{y}, \mathbf{x}' + \mathbf{y}, t), \quad (4.81)$$

where

$$F_{\text{cCSL}}(\tilde{\mathbf{k}}, \mathbf{q}, t) = F_{\text{CSL}}(\tilde{\mathbf{k}}, \mathbf{q}, t) \exp \left[\frac{\lambda \bar{\tau}}{2} \left(e^{-\frac{(\mathbf{q} - \frac{\tilde{\mathbf{k}} t}{m})^2}{4r_C^2}} - e^{-\frac{\mathbf{q}^2}{4r_C^2}} \right) \right]. \quad (4.82)$$

For further details about the characteristic function approach see Ref. [53, 51]. The interference pattern is given by Eq. (4.15) with the function D replaced by $D_{\text{cCSL}} = D_{\text{CSL}}$ given in Eq. (4.55). Although F_{CSL} and F_{cCSL} in general differ, i.e. CSL and cCSL have different free evolutions, we have the curious situation that the non Markovian effects in diffraction experiments cancel exactly, i.e. the CSL and cCSL interference patterns coincide.

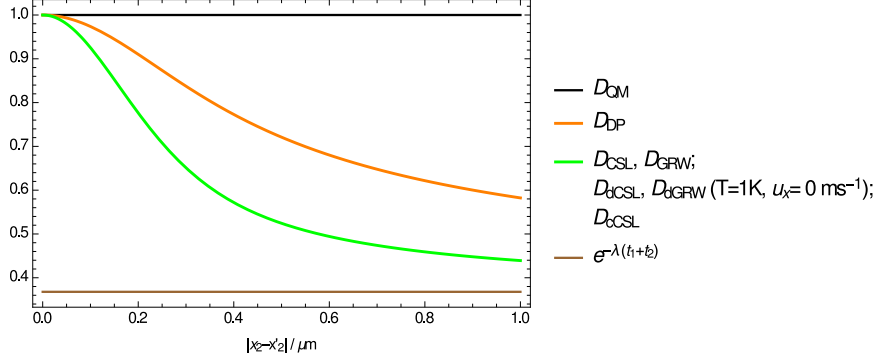


Figure 4.6: Comparison of D functions for the considered collapse models. The plot is obtained with $r_C = 10^{-7}m$, $\lambda = 500s^{-1}$, $t_1 = t_2 = 1ms$, $L_1 = L_2 = 0.1m$, $R_0 = 10^{-7}m$, $\lambda_{DP} = \lambda = 500s^{-1}$, where the rescaled λ , λ_{DP} are such that $\lambda(t_1 + t_2) = 1$. The black solid line represents the quantum mechanical function ($D = 1$), the orange solid line represents the D function for the DP model, the green solid line represents that of the CSL, GRW, dCSL, dGRW and cCSL models (for temperatures $T > 10^{-7}K$ and boost along the x axis $u_x < 10^4ms^{-1}$). The solid brown line represents the asymptotic value of the D functions for all the considered collapse models as $|x - x'| \rightarrow +\infty$.

4.3.5 Quantum mechanics with universal position localization

Here we are referring to the mass-proportional version of the QMUPL model [30, 33]. The single-particle master equation in 3D is given by [50]:

$$\frac{d\hat{\rho}}{dt} = -\frac{i}{\hbar} \left[\frac{\hat{\mathbf{P}}^2}{2m}, \rho_t \right] - \frac{\eta}{2} \frac{m}{m_0} \left[\hat{\mathbf{X}}, [\hat{\mathbf{X}}, \hat{\rho}] \right] \quad (4.83)$$

The solution to this master equation can be obtained with the help of the characteristic function:

$$\rho^{\text{QMUPL}}(\mathbf{x}, \mathbf{x}', t) = \frac{1}{(2\pi\hbar)^3} \frac{1}{(2\pi\hbar)^3} \int_{-\infty}^{+\infty} d\tilde{\mathbf{k}} \int_{-\infty}^{+\infty} d\tilde{\mathbf{w}} e^{-\frac{i}{\hbar} \tilde{\mathbf{k}} \cdot \tilde{\mathbf{w}}} F_{\text{QMUPL}}(\tilde{\mathbf{k}}, \mathbf{x} - \mathbf{x}', t) \rho^{\text{QM}}(\mathbf{x} + \tilde{\mathbf{w}}, \mathbf{x}' + \tilde{\mathbf{w}}, t), \quad (4.84)$$

where $\rho^{\text{QM}}(\mathbf{x}, \mathbf{x}', t)$ denotes the usual free quantum mechanical evolution ($\eta = 0$) and

$$F_{\text{QMUPL}}(\tilde{\mathbf{k}}, \mathbf{q}, t) = \exp \left[+\frac{\eta}{2} \frac{m}{m_0} \left[\mathbf{q}^2 - \frac{\mathbf{q} \cdot \tilde{\mathbf{k}} t}{m} + \frac{\tilde{\mathbf{k}}^2 t^2}{m^2 3} \right] \right]. \quad (4.85)$$

The interference pattern is given by Eq. (4.15) with the function D defined as follows:

$$D_{\text{QMUPL}}(x_2 - x'_2) = \exp \left[-\frac{\eta}{3} \frac{m}{m_0} (t_1 + t_2) (x_2 - x'_2)^2 \right]. \quad (4.86)$$

The function $D_{\text{QMUPL}}(q)$ completely encodes the modification to the quantum mechanical interference pattern ($\eta = 0$).

4.4 Center-of-mass motion for a rigid object and the amplification mechanism

Matter-wave experiments use large molecules and create spatial superpositions of their center-of-mass motion. In this section, starting from the many-particle collapse dynamics, we will derive a closed equation for the center of mass, under the rigid-body approximation. We will show and quantify the amplification mechanism: the larger the system, the faster the collapse of the center-of-mass wave function.

We will start by considering the CSL model. Under suitable assumptions, discussed at the end of this section, the analysis applies also to the dCSL, cCSL with small correlation time, and to the DP model. We will discuss three approximations for the geometry of a planar molecule, namely Adler's formula [55], the homogeneous disk approximation and the 2D lattice structure approximation [56].

The N -particle CSL master equation reads:

$$\frac{d}{dt}\hat{\rho}(t) = -\frac{i}{\hbar} [\hat{H}, \hat{\rho}(t)] + \lambda \frac{m^2}{m_0^2} \left(\frac{r_C}{\sqrt{\pi\hbar}} \right)^3 \sum_{j,l}^N \int d\mathbf{Q} e^{-\frac{\mathbf{Q}^2 r_C^2}{\hbar^2}} \left(e^{\frac{i}{\hbar} \mathbf{Q} \cdot \hat{\mathbf{x}}_j} \hat{\rho}(t) e^{-\frac{i}{\hbar} \mathbf{Q} \cdot \hat{\mathbf{x}}_l} - \hat{\rho}(t) \right), \quad (4.87)$$

where m is the mass of a single particle and $\hat{\mathbf{x}}_i$ is the position operator of particle i . By performing a trace over the relative coordinates, we obtain the master equation for the reduced density matrix $\hat{\rho}_{\text{CM}}(t)$ describing the center-of-mass motion:

$$\begin{aligned} \frac{d}{dt}\hat{\rho}_{\text{CM}}(t) &= -\frac{i}{\hbar} [\hat{H}, \hat{\rho}_{\text{CM}}(t)] \\ &+ \lambda \left(\frac{r_C}{\sqrt{\pi\hbar}} \right)^3 \frac{m^2}{m_0^2} \int d\mathbf{Q} R(\mathbf{Q}) e^{-\frac{\mathbf{Q}^2 r_C^2}{\hbar^2}} \left(e^{\frac{i}{\hbar} \mathbf{Q} \cdot \hat{\mathbf{X}}} \hat{\rho}_{\text{CM}}(t) e^{-\frac{i}{\hbar} \mathbf{Q} \cdot \hat{\mathbf{X}}} - \hat{\rho}_{\text{CM}}(t) \right), \end{aligned} \quad (4.88)$$

where $\hat{\mathbf{X}} = \sum_{i=1}^N \hat{\mathbf{x}}_i / N$ is the center of mass position operator and

$$R(\mathbf{Q}) = \int d\mathbf{r}_1 \dots d\mathbf{r}_N \sum_{j=1, l=1}^N e^{\frac{i}{\hbar} \mathbf{Q} \cdot (\mathbf{r}_j - \mathbf{r}_l)} \quad (4.89)$$

encodes the distribution of atoms in space around the center of mass. By considering a rigid body and neglecting rotations around the center of mass, we can remove the integrations over the relative coordinates[32]:

$$R(\mathbf{Q}) = \sum_{j=1, l=1}^N e^{\frac{i}{\hbar} \mathbf{Q} \cdot (\mathbf{r}_j - \mathbf{r}_l)}. \quad (4.90)$$

The next step is to replace $R(\mathbf{Q})$ with a function independent of the position of the particles, so that Eq. (4.88) reduces to a single-particle master equation like Eq. (4.52), with λ replaced by an enhanced factor Λ , which depends on the total number of particle and their geometrical distribution. Hence we want to show that under suitable approximations:

$$\lambda \frac{m^2}{m_0^2} \int d\mathbf{Q} R(\mathbf{Q}) e^{-\frac{\mathbf{Q}^2 r_C^2}{\hbar^2}} e^{\frac{i}{\hbar} \mathbf{Q} \cdot \hat{\mathbf{X}}} \hat{\rho}_{\text{CM}}(t) e^{-\frac{i}{\hbar} \mathbf{Q} \cdot \hat{\mathbf{X}}} \rightarrow \Lambda \int d\mathbf{Q} e^{-\frac{\mathbf{Q}^2 r_C^2}{\hbar^2}} e^{\frac{i}{\hbar} \mathbf{Q} \cdot \hat{\mathbf{X}}} \hat{\rho}_{\text{CM}}(t) e^{-\frac{i}{\hbar} \mathbf{Q} \cdot \hat{\mathbf{X}}}, \quad (4.91)$$

$$-\lambda \frac{m^2}{m_0^2} \left(\frac{r_C}{\sqrt{\pi\hbar}} \right)^3 \int d\mathbf{Q} R(\mathbf{Q}) e^{-\frac{\mathbf{Q}^2 r_C^2}{\hbar^2}} \hat{\rho}_{\text{CM}}(t) \rightarrow -\Lambda \hat{\rho}_{\text{CM}}(t). \quad (4.92)$$

We now review the three possible methods of approximation mentioned above.

4.4.1 Adler's formula

Consider first the situation when the molecule is enclosed in a radius $r_s \ll r_C$ (see Fig. 4.7). According to Eq. (4.88) the weight $\exp(-\mathbf{Q}^2 r_C^2 / \hbar^2)$ selects those values of $|\mathbf{Q}|$ such that $|\mathbf{Q}| < \hbar / r_C$. Hence we have that $|\frac{1}{\hbar} \mathbf{Q} \cdot (\mathbf{r}_j - \mathbf{r}_l)| < |\frac{(\mathbf{r}_j - \mathbf{r}_l)|}{r_C}| \approx 0$, and we can write:

$$R(\mathbf{Q}) \approx \sum_{j=1, l=1}^N 1 = N^2. \quad (4.93)$$

On the opposite side, let us consider the situation when the distance between nearest neighbor atoms r_a is much bigger than r_C , i.e. $r_C \ll r_a$. We group the terms $e^{-\mathbf{Q}^2 r_C^2 / \hbar^2} (e^{i \mathbf{Q} \cdot (\mathbf{r}_j - \mathbf{r}_l)} + e^{-i \mathbf{Q} \cdot (\mathbf{r}_j - \mathbf{r}_l)})$, which can be rewritten as: $2e^{-\mathbf{Q}^2 r_C^2 / \hbar^2} \cos(\mathbf{Q} \cdot (\mathbf{r}_j - \mathbf{r}_l) / \hbar)$. Let us rewrite: $\mathbf{Q} \cdot (\mathbf{r}_j - \mathbf{r}_l) = |\mathbf{Q}| |\mathbf{r}_j - \mathbf{r}_l| \cos(\theta)$. Except for the cases when $\cos(\theta) \approx 0$, if $j \neq l$ the condition $r_C \ll r_a$ implies that the oscillations of $\cos(|\mathbf{Q}| |\mathbf{r}_j - \mathbf{r}_l| \cos(\theta) / \hbar)$ make the \mathbf{Q} integrals negligible. Therefore, the dominant contribution in Eq. (4.90) comes from $j = l$ terms, and we can write:

$$R(\mathbf{Q}) \approx \sum_{j=1}^N 1 = N. \quad (4.94)$$

The conclusion is that, when N particles in the system are distant less than r_C , we have a quadratic scaling ($\sim N^2$) of Λ for the center of mass motion. On the other hand, when the mutual distance between the N particles is larger than r_C , then Λ for the center of mass motion increases linearly with N .

We also need to consider the intermediate case, where a more careful analysis is needed. In this situation, the behavior is expected to interpolate between the linear and quadratic scaling. We model the macro-molecules used in the experiments by atoms uniformly distributed over a thin disk, as depicted in Fig. 4.7. We neglect the electrons, as their mass is small compared to the nucleon mass and we describe the atomic nuclei as single particles of average mass $m_a = \frac{m}{n_a}$ (average atomic mass), where n_a is the total number of atoms. We limit the discussion to values of r_C larger than the nucleon size $\sim 10^{-15} \text{m}$.

The mean area covered by a single atom is πr_a^2 , where we take the mean atomic radius to be $r_a = 10^{-10} \text{m}$. The number of atoms contained within a circle of radius r_C is:

$$n(r_C) = \begin{cases} 1, & \text{if } r_C < r_a. \\ \frac{\pi r_C^2}{\pi r_a^2}, & \text{if } r_a \leq r_C \leq r_s. \\ n_a & \text{if } r_s < r_C. \end{cases} \quad (4.95)$$

These will contribute quadratically to the collapse rate. The molecule can be covered by $n_a/n(r_C)$ circles of radius r_C and atoms belonging to different circles contribute linearly to the collapse rate. Thus we model the collapse rate for the center of mass of the molecule according to the formula:

$$\Lambda = \frac{n_a}{n(r_C)} \left(\frac{m_a n(r_C)}{m_0} \right)^2 \lambda. \quad (4.96)$$

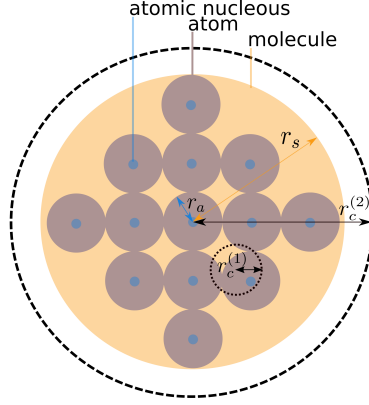


Figure 4.7: Macro-molecule thin disk approximation with uniformly distributed atoms. The blue circles represent atomic nuclei, the purple circles the atoms of radius r_a and the orange circle of radius r_s denotes the area spanned by the molecule. We assume for simplicity, that the purple circles denoting atoms completely fill the orange circle denoting the molecule, so that empty spaces can be neglected. When $r_C > r_s$, the whole molecule is contained within a circle of radius r_C , and the quadratic scaling law applies (e.g. $r_C = r_C^{(2)}$). When $r_C < r_a$, only one nucleus is contained within a circle of radius r_C , and the linear scaling law applies (e.g. for $r_C = r_C^{(1)}$). When $r_a < r_C < r_s$, we interpolate the two limiting cases with the scaling law (4.96).

This is the formula we will use in following sections. We will describe the center of mass motion as that of a single particle via Eq. (4.1), and in all formulas derived starting from it, $\lambda \left(\frac{m}{m_0}\right)^2$ is replaced by Λ . Of course, in the limiting case when the molecular radius r_s is smaller than r_C , the above scaling reduces to the purely quadratic scaling law, while when the atomic radius r_a is larger than r_C it reduces to the purely linear scaling law. We now discuss two further approximation schemes which will confirm the validity of Eq. (4.96).

4.4.2 Homogeneous thin disk approximation

As a different way to tackle the problem, let us consider the molecule as a thin homogeneous disk of radius r_s and thickness d . In this continuous limit, we can approximate:

$$\sum_{j=1}^N e^{i\mathbf{Q}\cdot\mathbf{r}_j} \longrightarrow \int d\mathbf{x} \rho_{\text{rel}}(\mathbf{x}) e^{i\mathbf{Q}\cdot\mathbf{x}} = \tilde{\rho}_{\text{rel}}(\mathbf{Q}), \quad (4.97)$$

where $\rho_{\text{rel}}(\mathbf{x})$ is the matter distribution around the center of mass, and $\tilde{\rho}_{\text{rel}}(\mathbf{Q})$ its Fourier transform. Then Eq. (4.90) reduces to:

$$R(\mathbf{Q}) = |\tilde{\rho}_{\text{rel}}(\mathbf{Q})|^2. \quad (4.98)$$

In particular, by labeling the axis of rotational symmetry of the disk as the z axis and its orthogonal plane (x - y plane) with the label o , we find that

$$\tilde{\rho}_{\text{rel}}(\mathbf{Q}) = \frac{2\hbar}{Q_o R} J_1\left(\frac{Q_o R}{\hbar}\right) \text{sinc}\left(\frac{Q_z d}{2\hbar}\right), \quad (4.99)$$

where Q_z, Q_o are the z axis and the x - y plane components of \mathbf{Q} , respectively and J_1 denotes the Bessel function of the first kind. We now insert $\tilde{\rho}_{\text{rel}}(\mathbf{Q})$ into Eqs. (4.91) and (4.92) and take the limit $d \rightarrow 0$ (very thin disk approximation). To perform the approximation in Eq. (4.91) and Eq. (4.92), we work in the position basis, i.e. we apply $\langle x, y, z |, |x', y', z' \rangle$ from the left and right, respectively. In addition, we assume that the superposition is on distances much greater than the size of the system, i.e. $\Delta x = x - x'$ is either $|\Delta x| \gg r_s$ or $\Delta x = 0$ and similarly for the y axis. It is then easy to obtain the rescaling of the parameter λ :

$$\Lambda = \frac{4\lambda m^2 r_C^2 \left(1 - e^{-\frac{r_s^2}{4r_C^2}}\right)}{m_0^2 r_s^2}. \quad (4.100)$$

4.4.3 2D Lattice disk

As a different approximation, we consider a 2-D lattice, as depicted in Fig. 4.7, of point-like nuclei (small blue circles) forming a thin disk of radius r_s (orange circle). The axis of rotational symmetry of the disk is z , the nuclei sit on the x - y plane and their position is denoted as (n_x, n_y) . The index n_x runs from $n_{\text{min}} = -\lfloor \frac{r_s}{a} \rfloor$ to $n_{\text{max}} = \lfloor \frac{r_s}{a} \rfloor$, where we take $a = 10^{-10}$ m to be the lattice constant and $\lfloor \cdot \rfloor$ indicates the floor rounded value. Hence the n_y index runs from $-\left\lfloor \sqrt{\frac{r_s^2}{a^2} - n_x^2} \right\rfloor$ to $\left\lfloor \sqrt{\frac{r_s^2}{a^2} - n_x^2} \right\rfloor$ in accordance with the circular shape of the molecule $n_x^2 + n_y^2 \leq \left(\frac{r_s}{r_a}\right)^2$. In other words, we consider the following $R(\mathbf{Q})$ function (4.90):

$$R(\mathbf{Q}) = \sum_{\substack{n_x^2 + n_y^2 \leq n_{\text{max}}^2 \\ n_x'^2 + n_y'^2 \leq n_{\text{max}}^2}} e^{\frac{i}{\hbar} a(n_x - n_x')Q_x + \frac{i}{\hbar} a(n_y - n_y')Q_y} \quad (4.101)$$

where the primed and unprimed variables label the first and second sum, respectively.

Let us first deal with the rescaling in Eq. (4.92). We perform the $d\mathbf{Q}$ integration and we get the rescaled parameter Λ :

$$\Lambda = \lambda \sum_{\substack{n_x^2 + n_y^2 \leq n_{\text{max}}^2 \\ n_x'^2 + n_y'^2 \leq n_{\text{max}}^2}} \exp\left(-\frac{a^2 (\Delta n_x)^2}{4r_C^2} - \frac{a^2 (\Delta n_y)^2}{4r_C^2}\right). \quad (4.102)$$

where $\Delta n_x = n_x - n_x'$ and $\Delta n_y = n_y - n_y'$.

Next, we consider the rescaling in Eq. (4.91). To ease the analysis, we work in the position basis, i.e. we apply $\langle x, y, z |, |x', y', z' \rangle$ from the left and right, respectively. We consider a single term in Eq. (4.101) and perform the $d\mathbf{Q}$ integration in Eq. (4.91), we get:

$$\lambda \exp\left(-\frac{(a\Delta n_x + \Delta x)^2}{4r_C^2} - \frac{(a\Delta n_y + \Delta y)^2}{4r_C^2} - \frac{\Delta z^2}{4r_C^2}\right), \quad (4.103)$$

where $\Delta x, \Delta y, \Delta z$ are $x - x', y - y', z - z'$ respectively. Let us again assume that the superposition varies on distances much greater than the size of the system, i.e. Δx is either

$|\Delta\mathbf{x}| \gg a\Delta n$ or $\Delta\mathbf{x} = 0$. Hence we can approximate $(a\Delta n + \Delta\mathbf{x})^2 \approx (a\Delta n)^2 + (\Delta\mathbf{x})^2$. A similar argument can be carried also for the y axis variables. Thus, combining Eq. (4.102) and Eq. (4.103) we finally obtain:

$$\Lambda \exp\left(-\frac{\Delta x^2 + \Delta y^2 + \Delta z^2}{4r_C^2}\right) - \Lambda, \quad (4.104)$$

which implies that the center of mass density matrix satisfies the one particle CSL master equation with the rescaled parameter Λ .

4.4.4 Comparison and other collapse models

The three approximations discussed here above are compared in Fig. 4.8.

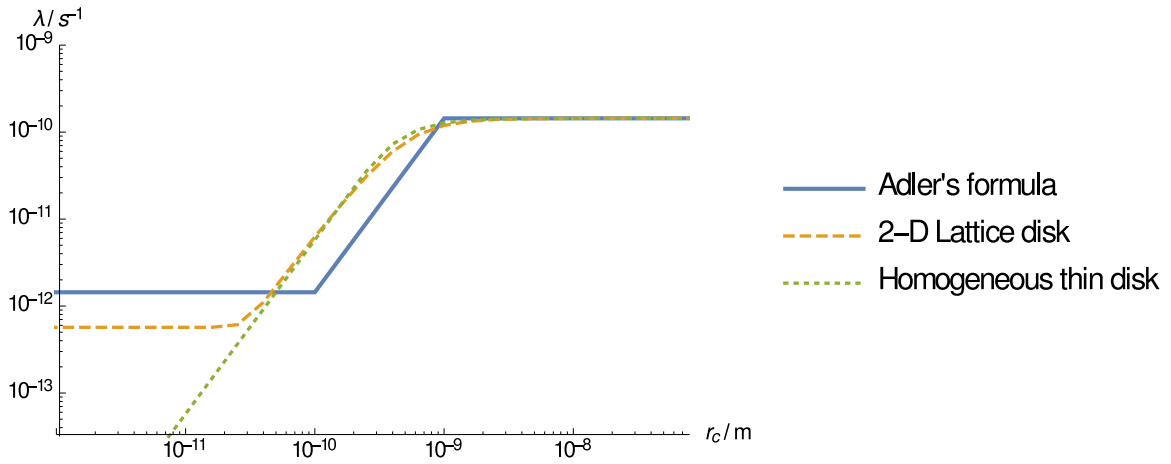


Figure 4.8: Amplification of the parameter Λ as a function of r_C for three different approximations: Adler's formula (solid blue line), homogeneous disk approximation (dotted green line), 2D lattice approximation (dashed orange line). We see, that Adler's formula agrees very well with the more sophisticated 2D lattice model approximation, while the homogenous disk approximation breaks down at distances below the atomic radius ($r_a = 10^{-10}\text{m}$). The plot is obtained for $N = 100$ atoms with atomic (nuclei) mass $12m_0 = 12\text{amu}$.

In particular, we see that Adler's heuristic formula is in good agreement with the 2D lattice model amplification mechanism. We also see that the homogeneous thin disk approximation begins to break down for r_C values smaller than the atomic radius r_a .

We also stress the key assumption used in the derivation of the amplification mechanism: $r_s \ll r_{sup}$, where r_s is the size of the system (e.g. molecular radius) and r_{sup} is the size of the macroscopic superposition. Only using this assumption, we were able to effectively describe the center of mass motion master equation (4.88) by the single particle master equation (4.52) with the rescaled parameter Λ . When $r_s \gtrsim r_{sup}$ we have a weaker suppression of macroscopic superpositions.

The dCSL and cCSL (with small correlation time) many particle master equations have a similar structure as that of the CSL model. Hence, as in part argued in Refs. [34],[19], the

amplification mechanism is analogous to the CSL amplification mechanism. For the dCSL, one has to also consider the parameter k_T , which limits the validity of the approximations.

The previous analysis is also applicable to the DP model, as it can be easily shown by considering the many particle DP master equation. As previously stated, in the DP model, R_0 can be identified with r_C and λ can be identified with $\frac{Gm_0^2}{\hbar\sqrt{\pi R_0}}$. As in the CSL model λ rescales to $\Lambda(r_C)$, in the DP model $\frac{Gm_0^2}{\hbar\sqrt{\pi R_0}}$ rescales to $\lambda_{DP} = \frac{Gm_0^2}{\hbar\sqrt{\pi R_0}} \frac{\Lambda(R_0)}{\lambda}$.

In Fig. (4.4.4) we show how Λ varies as a function of the total number of atoms N according to Eq. (4.96), where the atoms form a thin disk lattice structure, as described in Fig. 4.7,

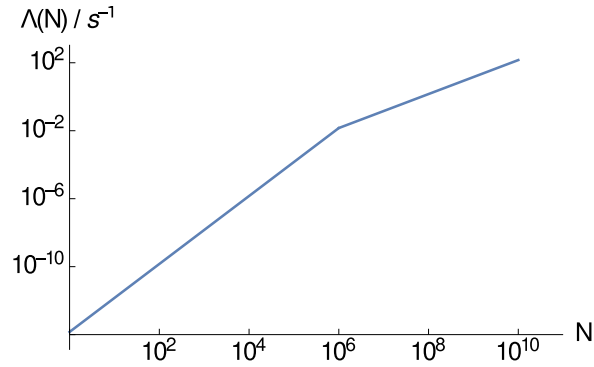


Figure 4.9: The plot shows the amplification of the effective collapse rate Λ according to Eq. (4.96) for the thin disk model described in the text. The plot is obtained with $\lambda = 10^{-16}\text{s}^{-1}$, $r_C = 10^{-7}\text{m}$, atomic radius $r_a = 10\text{m}$ and atomic mass $m_a = 12m_0 = 12\text{amu}$. We notice that at $N = 10^6$ the amplification mechanism changes behavior as the total size of the system r_s becomes equal to r_C .

The GRW and dGRW models have a simple linear scaling of Λ with the mass of the system by construction.

4.4.5 Localization requirement of macroscopic objects

In the next chapter we will derive the upper bounds on the collapse parameters, with reference to the KDTL experiment, but there are also lower bounds, as the collapse cannot be too weak, otherwise the model loses its usefulness. The basic requirement for any collapse model is the rapid suppression of macroscopic superpositions. We make the following reasonable, although arbitrary, minimal request: a macroscopic superposition of an object, visible by the naked eye (with spatial resolution r), should decay within a short time, set by the temporal resolution t of the eye. This implies for example that a macroscopic superposition for a single-layered Graphene disk of radius r localizes with an effective rate t^{-1} .

The quantitative analysis is carried out in the following way. We neglect the free quantum mechanical evolution, while retaining the modification due to the collapse dynamics, i.e. we neglect $\hat{H} = \hat{p}^2/2m$. This is a reasonable assumption since the free quantum mechanical evolution is negligible for macroscopic objects on the time scale during which the wave function localizes. We have solved the resulting dynamics for each of the collapse models

using the characteristic function approach [53]. For each of the considered collapse models the corresponding characteristic function equation is given by:

$$\frac{\partial}{\partial t} \chi(\boldsymbol{\nu}, \boldsymbol{\mu}, t) = \Lambda (\Phi(\boldsymbol{\nu}, \boldsymbol{\mu}) - 1), \quad (4.105)$$

where Φ depends on the model. We can easily obtain the solution to this equation:

$$\chi(\boldsymbol{\nu}, \boldsymbol{\mu}, t) = \chi(\boldsymbol{\nu}, \boldsymbol{\mu}, 0) \exp(-\Lambda t(1 - \Phi(\boldsymbol{\nu}, \boldsymbol{\mu}))), \quad (4.106)$$

Using the inversion formula given by Eq. (4.80) we obtain the corresponding density matrix:

$$\rho(\mathbf{x}, \mathbf{x}', t) = \frac{1}{(2\pi\hbar)^3} \int d\tilde{\mathbf{k}} \int d\tilde{\mathbf{w}} e^{-\frac{i}{\hbar}\tilde{\mathbf{k}}\cdot\tilde{\mathbf{y}}} \exp\left(-\Lambda t(1 - \Phi(\tilde{\mathbf{k}}, \mathbf{x} - \mathbf{x}'))\right) \rho(\mathbf{x} + \mathbf{w}, \mathbf{x}' + \mathbf{w}, 0), \quad (4.107)$$

where $\rho(\mathbf{x} + \mathbf{w}, \mathbf{x}' + \mathbf{w}, 0)$ is the initial density matrix.

Formally, we can also obtain the solution of the collapse dynamics (without the free quantum mechanical term) from the full solution (with the free quantum mechanical term) by taking the limit $m \rightarrow \infty$ kg in the expressions originating from the free quantum mechanical evolution, while keeping finite m in the other expressions.

We now list the solutions for the considered collapse models using the notation of section 4.3. For the CSL we obtain:

$$\rho_{\text{CSL}}(\mathbf{x}, \mathbf{x}', t) = \rho(\mathbf{x}, \mathbf{x}', 0) \exp\left(-\Lambda t \left(1 - e^{-\frac{(\mathbf{x}-\mathbf{x}')^2}{4r_C^2}}\right)\right). \quad (4.108)$$

The same formula applies also for the cCSL model with small correlation times τ_C .

For the QMUPL we obtain:

$$\rho_{\text{QMUPL}}(\mathbf{x}, \mathbf{x}', t) = \rho(\mathbf{x}, \mathbf{x}', 0) \exp\left(-\eta \frac{m}{m_0} t (\mathbf{x} - \mathbf{x}')^2\right). \quad (4.109)$$

For the DP we obtain:

$$\rho_{\text{DP}}(\mathbf{x}, \mathbf{x}', t) = \rho(\mathbf{x}, \mathbf{x}', 0) \exp\left(-\frac{t}{\hbar} (U(\mathbf{x} - \mathbf{x}') - U(0))\right) \quad (4.110)$$

For the dCSL we obtain:

$$\rho_{\text{dCSL}}(\mathbf{x}, \mathbf{x}', t) = \frac{1}{(2\pi\hbar)^3} \int d\tilde{\mathbf{w}} \rho(\mathbf{x} + \tilde{\mathbf{w}}, \mathbf{x}' + \tilde{\mathbf{w}}, 0) \int d\tilde{\mathbf{k}} e^{-\frac{i}{\hbar}\tilde{\mathbf{k}}\cdot\tilde{\mathbf{w}}} \exp\left(-\Lambda t \left(1 - e^{-\frac{\tilde{\mathbf{k}}^2 r_C^2 k_T^2}{\hbar^2}} e^{-\frac{(\mathbf{x}-\mathbf{x}')^2}{4r_C^2(1+k_T)^2}} e^{\frac{i}{\hbar} \frac{2k_T m \mathbf{u}}{(1+k_T)} \cdot (\mathbf{x}-\mathbf{x}')}\right)\right), \quad (4.111)$$

where in the limit $k_T \rightarrow 0$ we obtain the CSL solution given by Eq. (4.108). While for the CSL, cCSL and DP models we were able to perform the $\tilde{\mathbf{k}}$ and $\tilde{\mathbf{w}}$ integrations, for the dCSL the two integrations in general cannot be performed analytically. Hence for the dCSL we do not have in general a simple exponential decay of the off-diagonal elements. However, we can still investigate the dCSL decay of the off-diagonal elements by considering a particular initial state and performing a numerical simulation. In particular, we have considered a superposition state of two Gaussians centered at points $(r/2, 0, 0)$ and $(-r/2, 0, 0)$:

$$\psi(\mathbf{x}, 0) = \left(\exp\left[-\frac{(x - r/2)^2}{4\sigma^2}\right] + \exp\left[-\frac{(x + r/2)^2}{4\sigma^2}\right] \right) \exp\left[-\frac{y^2}{4\sigma^2}\right] \exp\left[-\frac{z^2}{4\sigma^2}\right] \quad (4.112)$$

with r the spatial resolution of the eye and $\sigma = 10^{-5}\text{m}$.

For the considered collapse models we can thus write the localization requirement for macroscopic objects as an inequality:

$$\left| \frac{\rho(\mathbf{x}, \mathbf{x}', t)}{\rho(\mathbf{x}, \mathbf{x}', 0)} \right| < \exp(-1), \quad (4.113)$$

where we set $\mathbf{x} = (r/2, 0, 0)$, $\mathbf{x}' = (-r/2, 0, 0)$ and t and r are the eye temporal and spatial resolutions, respectively. The constant $\exp(-1) \sim 0.37$ is chosen arbitrarily, reflecting that for most collapse models the decay of the off-diagonal elements is exponential. This inequality will be used to obtain bounds on collapse parameters.

The same analysis applies also for the GRW and dGRW models, the only difference being the amplification mechanism discussed in section 4.4.

Chapter 5

Matter-Wave Interferometry: experiments

5.1 Introduction

Bounds on collapse models parameters were first investigated in [55] and an overview is given in [57]. Tests of the CSL model with matter-wave interferometry experiments were first investigated in [55, 58], in particular, the OTIMA experiment [42]. In this section, we complete and improve the previous results. The bounds on the parameters (λ, r_C) can be conveniently studied in the parameter space [59, 60] shown in Fig. 5.5, while the bounds on the DP parameter R_0 and QMUPL parameter η are shown in Figs. 5.7 and 5.6 respectively. We obtain bounds for all the collapse models introduced in Sec. 4.3: from the localization requirement of macroscopic objects and from matter-wave interferometry. In addition, as argued in Sec. 4, the bounds we obtain on the CSL model, both from interferometric experiments and from the localization requirement of macroscopic objects, are also bounds on the CD map (within the limits of validity).

This section is organized in the following way. In section 5.2 we discuss the limits of validity of the CD bounds for the parameters (λ, r_C) . We compare the theoretical interference patterns with the experimental data from the 2012 far-field matter-wave interferometry experiment [47] and the 2013 Kapitza Dirac Talbot Lau (KDTL) near-field matter-wave interferometry experiment [48], both performed by Arndt's group in Vienna, in section 5.3. In section 5.4, we combine all the bounds for the CSL, dCSL and cCSL models in a single parameter diagram, which is also the parameter diagram for the CD map. In addition, we discuss the bounds on the parameters of the DP and QMUPL models.

5.2 Limits of validity of the CD bounds

In this section we discuss the limits of validity of the bounds on the CD map parameters (λ, r_C) for a wide range of values of the other parameters. There is a natural reason for choosing (λ, r_C) among the free parameters. These are the two parameters that characterize the Galilean boost covariant (non-dissipative) and Markovian limits:

$$\begin{aligned} T &\rightarrow \infty, \\ D(s) &\rightarrow \delta(s), \end{aligned}$$

respectively. In other words, the freedom in T , \mathbf{u} and $D(s)$ characterizes dissipative and non-Markovian effects, respectively. We consider the boost parameter to satisfy $|\mathbf{u}| < c$, where $c \approx 10^8 \text{ms}^{-1}$ is the speed of light: each component has to be smaller or equal to $u = |\mathbf{u}|$. In addition, when we are close to the Markovian limit the function $D(s)$ is non-negligible only on a small interval: we denote the cut-off value, i.e. the correlation time, by τ_C . In conclusion, we will now discuss the limits of validity of the CD map parameters (λ, r_C) for a wide range of values of the parameters (T, u, τ_C) .

We will discuss separately the limits of validity when only dissipative effects are present (the CD map reduces to the dCSL map in Sec. 4.3.3) and when only non-Markovian effects are present (the CD map reduces to the cCSL map in Sec. 4.3.4). We estimate these limits for experimental situations where the spatial and temporal extension of the superpositions is limited to distances $\Delta x \lesssim 10^{-5} \text{m}$ and duration $t \lesssim 10^{-2} \text{s}$, respectively.

We first discuss the limits of validity of dissipative effects parametrized by T, u . We have three conditions: the condition given by Eq. (4.61) is depicted together with the condition given in Eq. (4.65) in Fig. 5.1, while the condition given by Eq. (4.69) is depicted in Fig. 5.2.

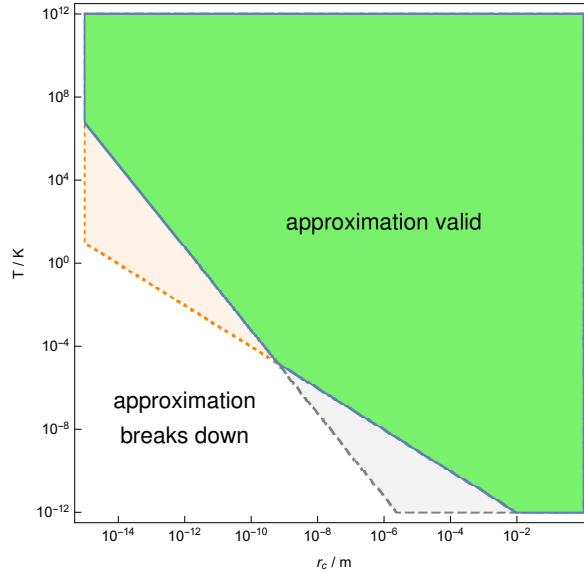


Figure 5.1: Graphical depiction of the conditions given in Eqs. (4.61), (4.65). The condition given by Eq. (4.61) is satisfied in the orange and green regions, while the condition given in Eq. (4.65) is satisfied in the gray and green regions: both conditions are satisfied in the green region.

We next discuss the limits of validity of non-Markovian effects parametrized by τ_C . We have only the condition given by Eq. (4.71). We can make a rough estimate for the maximum value of τ_C by replacing the operator with the expectation value in Eq.(4.71): $\langle \hat{\mathbf{p}}^2/2m \rangle \tau_C / \hbar \ll 1$, We consider the temperature of the system to be $T \approx 10^2 - 10^3 \text{K}$. Thus based on the equipartition theorem we replace $\langle \hat{\mathbf{p}}^2/2m \rangle$ by $k_B T$ which gives the condition $\tau_c \lesssim 10^{-13} \text{s}$. This gives us a corresponding minimum ultraviolet frequency cut-off $\Omega \gg 13 \text{GHz}$ for the Fourier transform of the correlation function.

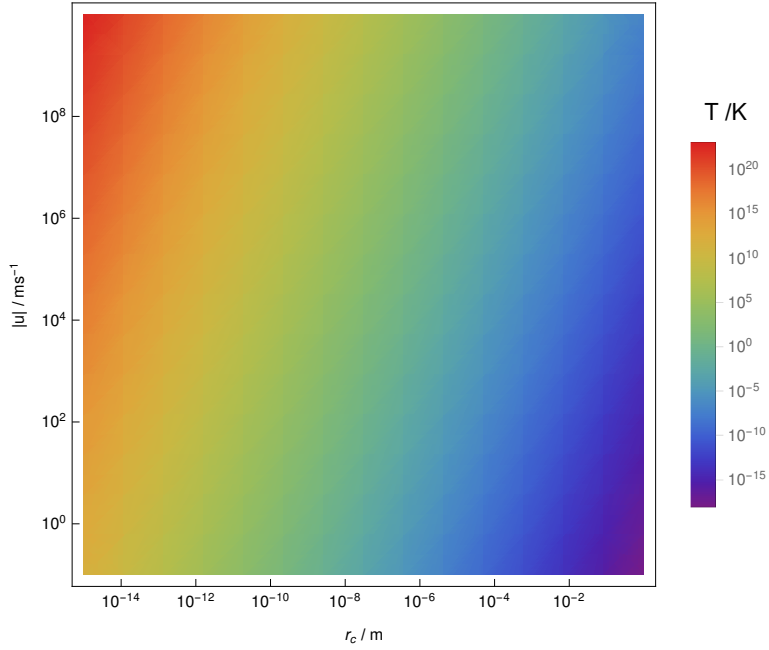


Figure 5.2: Graphical depiction of the condition given in Eq. (4.69). The color indicates the minimum temperature, for a given value of r_C and u , such that the condition given in Eq. (4.69) is satisfied.

5.3 Experimental data analysis

We are now ready to apply the above results to the experiments [47] and [48]. For concreteness, we illustrate the procedure with the CSL model. The same procedure is applicable for each collapse model described in Sec. 4.3.

In these experiments one has a source of molecules that have different velocities v along the optical axis z . Hence the real far-field interference pattern is given by:

$$\int_0^{+\infty} p_f(v)p(x;v)dv, \quad (5.1)$$

where p is given by Eq. (4.46) and $p_f(v)$ is the macromolecule velocity profile. Similarly the real near-field interference pattern is given by

$$\int_0^{+\infty} p_n(v)S(x_{3s};v)dv, \quad (5.2)$$

where S is given by Eq. (4.51) and $p_n(v)$ is the macromolecule velocity profile.

To make a quantitative comparison with experimental data, we consider a grid of pairs (λ, r_C) and for each pair we perform a χ^2 minimization procedure for the predicted CSL pattern according to Eqs. (5.1) and (5.2). In this way, we obtain a parameter diagram with an exclusion zone of pairs (λ, r_C) that are incompatible with experimental data.

A note of caution is at order. We have initially attempted to fit the experimental data by adopting the Poisson experimental error \sqrt{I} for each value I recorded by the detector since error bars were not reported in the papers. With this choice we were unable to obtain reasonable values of χ^2 even for the standard quantum mechanical predictions. This is probably

due, at least in part, to the approximations of the models used and to unknown sources of error in the experiment. In order to circumvent this problem and to obtain reasonable values of χ^2 , we used an enlarged Poisson experimental error $a\sqrt{I}$, where a is a constant. In order for the standard quantum mechanical fits to have reasonable χ^2 values, we take $a = 4.5$ for both experiments, but different values of a (within the same magnitude) do not change the final result.

5.3.1 Far-field

We first analyze the interference experiment with Phthalocyanine $C_{32}H_{18}N_8$ molecules reported in [61], with the data taken from Ref. [47]. The experimental setup is shown in Fig. 4.3. The velocity profile was estimated according to Ref. [47]. One has to be careful in considering the van der Waals forces between the molecules and the grating. This is modeled by considering an effective slit width smaller than the real one as described in [61]. The effective value is $l_{eff} = 43nm$. The finite spatial resolution of the detector $4\mu m$ was also taken into account.

As an example, in Fig. 5.3 we plot a comparison between the experimental interference pattern, the quantum mechanical fit and the CSL fit, for some arbitrarily chosen pair of parameters λ, r_C .

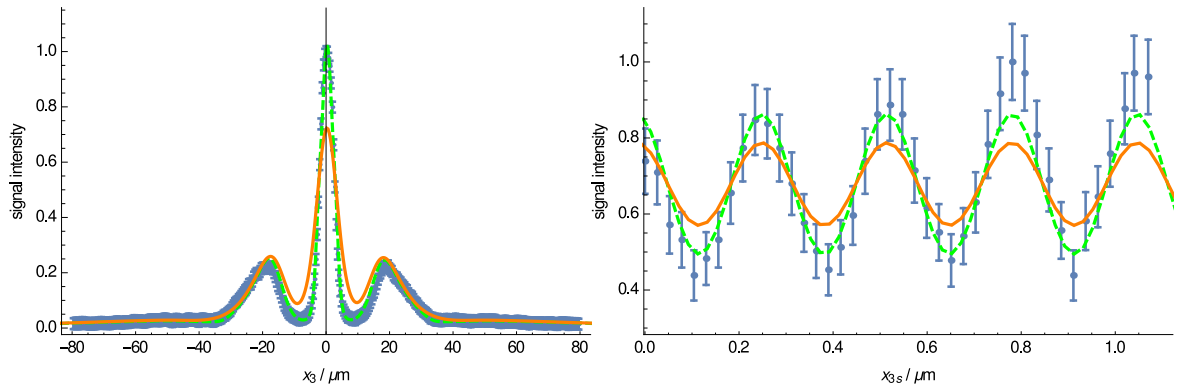


Figure 5.3: Left: Far-field experiment [47]: $\lambda \approx 3.8 \cdot 10^{-3} s^{-1}$ and $r_C = 10^{-7} m$. Right: KDTL near-field experiment [48]: $\lambda \approx 0.98 \cdot 10^{-5} s^{-1}$, $r_C = 10^{-7} m$, laser power $P_{laser} = 1W$. The orange dashed line represents the quantum mechanical fit, the solid orange line represents the CSL fit for an arbitrarily chosen (large) parameter λ and the conventional r_C value and the blue points and blue error bars represent the experimental data. The y axis values are rescaled such that the maximum value is equal to unity.

More importantly, we repeated the simulation for different pairs of parameters λ, r_C as described before, obtaining the CSL parameter diagram shown in Fig. 5.4.

5.3.2 Near-field KDTL

We now consider the experiment with $L_{12} = C_{284}H_{190}F_{320}N_4S_{12}$ molecules reported in [48]. The experimental setup is shown in Fig. 4.3. The Fourier coefficients defined in Eqs. (4.47)

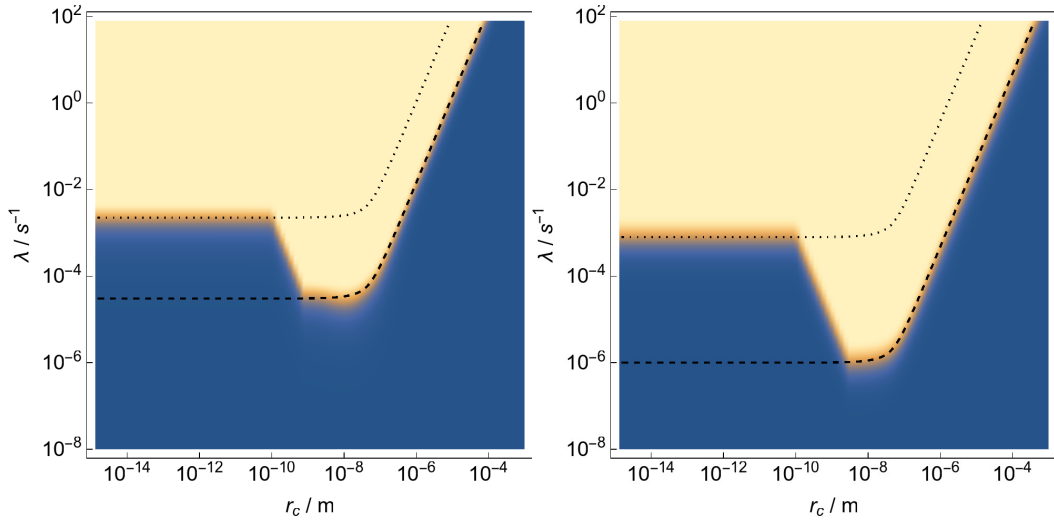


Figure 5.4: Left: CSL parameter diagram for the far-field experiment [47]. Right: CSL parameter diagram for the KDTL near-field experiment [48]. Each λ, r_C pair is colored by the corresponding χ^2 value obtained from the χ^2 minimization procedure. The yellow color indicates pairs that can be excluded by our analysis, while the blue color indicates pairs that cannot be excluded. The dashed and dotted lines represent the boundary of the exclusion zone according to the quadratic scaling law and to the linear scaling law, respectively. The values of the CSL parameters suggested in [8] and [55] are $\lambda = 10^{-16}\text{s}^{-1}$, $r_C = 10^{-7}\text{m}$ and $\lambda = 10^{-9}\text{s}^{-1}$, $r_C = 10^{-7}\text{m}$, respectively.

and (4.49) for the transmission functions of the mechanical gratings can be calculated analytically: $A_n = C_n = \frac{2l}{d} \text{sinc}(\frac{l}{d}n)$. The velocity profile was approximated by a Gaussian centered around $v = 85\text{m s}^{-1}$ with spread $\Delta v_{FWHM} = 30\text{m s}^{-1}$ [48].

As an example, in Fig. 5.3 we plot a comparison between the experimental interference pattern, the quantum mechanical fit and the CSL fit, for an arbitrarily chosen pair of parameters λ, r_C . We repeated the simulation for different pairs of parameters λ, r_C as previously described. We obtain the parameter diagram shown in Fig. 5.4.

5.3.3 Comparison of near and far field experiments.

Fig. 5.4 shows the exclusion zone of the CSL parameters λ, r_C for the far and near field experiments here considered. As we can see, they are similar: the near-field experiment sets a bound which is roughly two orders of magnitude stronger than the far-field experiment. This can be understood by the following argument. Let us fix r_C and focus our attention to the CSL model. The only remaining parameter is λ .

We expect that deviations from standard quantum mechanics become important as λt increases. For the far-field experiment we have a typical flight time $t \approx 5\text{ms}$ and molecular mass $m \approx 500\text{amu}$. For the near-field experiment we have a typical flight time $t \approx 2\text{ms}$ and molecular mass $m \approx 10000\text{amu}$. Hence the ratio of bounds on λ from the two experiments is approximately:

$$\frac{\lambda t|_{KDTL}}{\lambda t|_{far}} = \frac{(10000\text{amu})^2 2\text{ms}}{(500\text{amu})^2 5\text{ms}} \approx 100. \quad (5.3)$$

This rough estimate provides a simple explanation why the KDTL near-field experiment gives bounds which are 2 order of magnitude stronger than the bounds obtained from the far-field experiment.

5.4 Parameter space bounds

Let us now combine the results of the previous sections to determine the region of the parameter space, which can be ruled out for the CD map: these are also the bounds for the CSL, cCSL and dCSL models. Specifically, the limits of validity of the cCSL and dCSL maps, as discussed in Sec. 5.2, give the limits of validity for the parameter space λ, r_C for the CD map.

The bounds on the CD map are shown in Fig. 5.5 with reference to the KDTL experiment which sets the strongest bound among the two experiments here considered. The figure also shows the bounds coming from requiring that macroscopic objects are always well localized. This bound puts the original value proposed by GRW right on the border of the exclusion zone (the shaded region).

The dCSL bounds from interferometry and the macroscopic localization requirement change only slightly until we consider very low temperatures or very high boosts. In addition, as already stressed before, the smallest modification of the quantum mechanical interference pattern is given by the dCSL model with infinite temperature and no boost, i.e. the CSL model. Hence, since we do not know the temperature and speed of the noise, the most conservative interferometric bounds for all dCSL models coincide with the CSL bounds. On the other hand, the macroscopic localization requirement is not to be taken too rigidly, as it relies on an arbitrary notion of a macroscopic object. We also remark, as discussed in Sec. 4, that for very small values of r_C , the bounds for dCSL models with very low temperature may become invalid, as the approximations used begin to break down (see Figs. 5.1, 5.2).

The cCSL bounds from interferometry experiments are valid for noises with a frequency cut-off $\Omega \gg 10^{13} Hz$. For comparison, bounds from X-ray experiments [62], refer to the cCSL model with a frequency cut-off $\Omega \gg 10^{18} Hz$. For completeness, we have also shown the bounds from the LISA experiment [63], which are valid for the CSL model.

The fact that the CD, CSL, dCSL and cCSL bounds in Fig. 5.5 coincide is due to the fact the time scale of dissipative and non-Markovian effects: much longer and much shorter than the experimental times, respectively. This result, shows that interferometric experiments provide bounds that are insensitive to dissipative or non-Markovian extensions of the original models. Interferometric experiments can thus provide a test for the CD map.

The bounds for the GRW and dGRW models can be obtained from the bounds of the CSL and dCSL models, respectively, by changing the amplification factor Λ (see Sec. 4).

The bounds on the QMUPL model parameter η are shown in Fig. 5.6. We can obtain some reference values for the parameter η in the following way: the QMUPL model can be obtained as the limit of the CSL model, specifically, we have $\eta = \lambda/(2r_C^2)$. Using the values suggested in [8] we obtain ($\lambda = 10^{-16} s^{-1}$, $r_C = 10^{-7} m$):

$$\eta_{GRW} = 10^{-2} s^{-1} m^{-2} \quad (5.4)$$

We will refer to these value as the Ghirardi values. In [55] we have two different choices: $\lambda = 10^{-8 \pm 2} s^{-1}$ ($\lambda = 10^{-6 \pm 2} s^{-1}$) and $r_C = 10^{-7} m$ ($r_C = 10^{-6} m$). These give the following value:

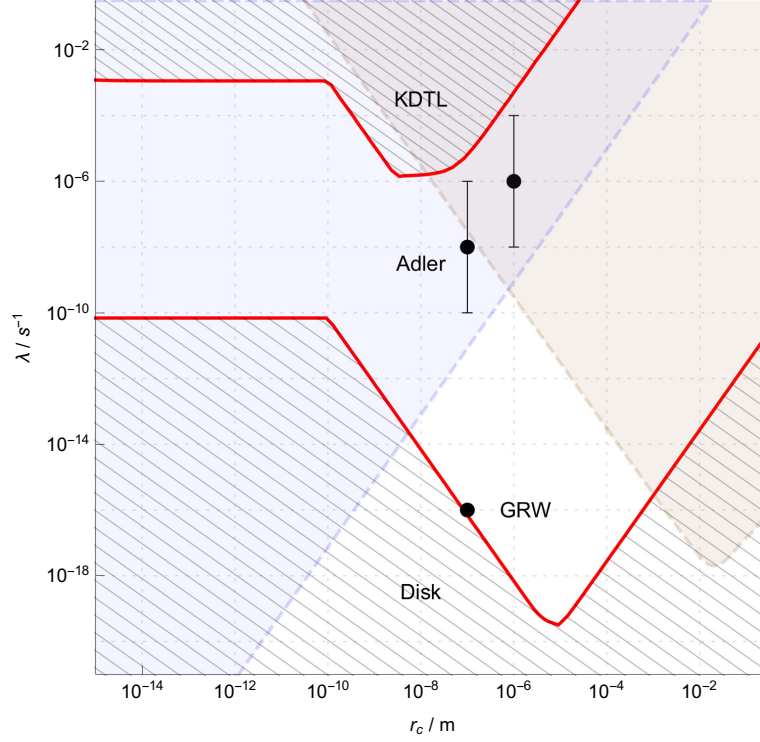


Figure 5.5: Parameter diagram for the CD, CSL, dCSL and cCSL map. The shaded exclusion zone bordered by the red solid lines applies for the CD, CSL, cCSL and dCSL maps. The limits of validity are discussed in Sec. 5.2: the frequency cutoff is $\Omega \gtrsim 10^{13} Hz$ and T, u are discussed in Figs. 5.1, 5.2). On the bottom of the diagram, it denotes the parameter subspace excluded by the requirement that a single-layered Graphene disk of radius $r = 0.01 mm$ is localized within $t = 10 ms$. On the top it denotes the parameter subspace excluded by the KDTL macromolecule interferometry experiment [48]. For comparison we have included the bounds from X-ray experiments [62], valid for the CSL model and the cCSL model with frequency cutoff $\Omega \gg 10^{18} Hz$, and the bounds from the LISA experiment [63], valid for the CSL model: the exclusion zones are denoted by the blue and brown colors, respectively. We have also included for reference, the values $(\lambda = 10^{-16} s^{-1}, r_C = 10^{-7} m)$, $(\lambda = 10^{-8} s^{-1}, r_C = 10^{-7} m)$ proposed by GRW [8] and Adler [55], respectively.

$$\eta_{\text{Adler}} = 10^{5 \pm 2} s^{-1} m^{-2} \quad (5.5)$$

We will refer to this value as the Adler value.

The bounds on the DP are shown in Fig.5.7. The KDTL bounds fall below the regime of applicability of the DP model ($R_0 > 10^{-15} m$). In fact, the effective collapse rate of the DP model $\lambda_{DP} = \frac{Gm_0^2}{\hbar\sqrt{\pi}R_0}$ is very small above $10^{-15} m$, e.g. for $R_0 = 10^{-15} m$ we have $\lambda_{DP} \approx 10^{-15} s^{-1}$, while for $R_0 = 10^{-7} m$ we have $\lambda_{DP} \approx 10^{-23} s^{-1}$: the total effective collapse rate $\Lambda_{DP} = A\lambda_{DP}$, where A is the amplification factor of the macro-molecule, is still orders of magnitude below the CSL bounds $\lambda \approx 10^{-3} s^{-1}$ ($\lambda \approx 10^{-6} s^{-1}$) for $r_C = 10^{-15} m$ ($r_C = 10^{-7} m$), respectively. On the other hand, the requirement that macroscopic objects are always well localized provide very strong bounds. If we require that a single layered

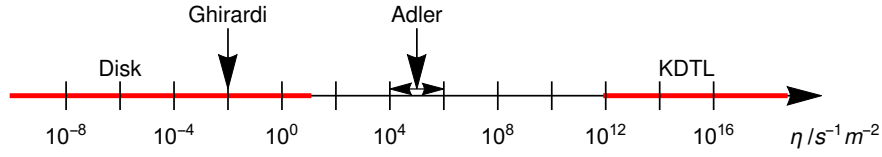


Figure 5.6: Bounds on the parameter η from matter-wave interferometry (denoted by KDTL) and from the request of suppression of macroscopic superpositions (denoted by Disk). The excluded values are denoted by red lines.

Graphene disk of radius $r = 0.01\text{mm}$ is to be localized within $t = 10\text{ms}$, as we have done for the CSL family of models, we can already exclude all R_0 values. However, even if we consider a larger value, for example $r = 1\text{mm}$, as in Fig. 5.7, the values $R_0 = 10^{-15}\text{m}$, $R_0 = 10^{-7}\text{m}$ proposed by Diósi [64] and Ghirardi [50], respectively, are still excluded.

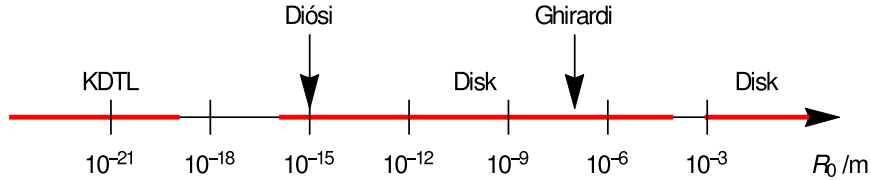


Figure 5.7: Parameter diagram for the DP model parameter R_0 . The excluded intervals are denoted by red lines: the lines labeled by “Disk” are obtained from the requirement that a single-layered Graphene disk of radius $r = 1\text{mm}$ is localized within $t = 10\text{ms}$, while the line labeled by “KDTL” is obtained from the KDTL interferometry experiment [48]. We have also included for reference, the values $R_0 = 10^{-15}\text{m}$ and $R_0 = 10^{-7}\text{m}$ proposed by Diósi [64] and Ghirardi [50], respectively.

In conclusion, interferometry experiments provide the most direct test for the collapse models. In particular, the bounds obtained for the most well-known non-dissipative, Markovian models are bounds also for more general, dissipative or non-Markovian generalizations. This is in stark contrast with other indirect experiments, which test only particular collapse models. In addition, we have seen that a single-layered Graphene disk provides very stringent bounds for the collapse parameters.

We thank Prof. Markus Arndt for the data and the setup parameters of the experiment in [47] and for useful discussions.

Chapter 6

Conclusion

We have discussed theoretical (Part I) and experimental (Part II) constraints on the collapse mechanism. In part I we have, starting from a set of minimal requirements, obtained a single dynamical map parametrized by the localization rate λ , the characteristic localization rate r_C , the temperature T and the temporal correlation function $f(s)$, namely the CD map: in addition, we have constructed the cdCSL model, a colored and dissipative extension of the CSL model. Here we remark that the derivation of the CD map is based only on a small set of assumptions: the CD map applies to all (non-unitary) modifications of the von Neumann map, i.e. it is not limited to collapse models. In part II we have discussed interferometry experiments with macro-molecules, which provide a direct test of the superposition principle in the mesoscopic regime. In particular, we have shown that the bounds on the CD map parameters λ , r_C are robust, i.e. the bounds, for reasonable values of T and $f(s)$, depend weakly on T and $f(s)$.

However, the analysis of non-relativistic modifications of the von Neumann map has lead us to a Galilei non-covariant map. This raises an important question: if the map is not Galilean covariant, what can we say about relativistic extensions, in particular, what can we say about Lorentz covariance of classicalization maps? We discuss these points in the appendices: we consider a relativistic theory, based on the F-W transformation, where particle/antiparticle interaction are suppressed (Appendix B), we discuss the role of particle/antiparticle interactions for classicalization maps (Appendix C) and give relativistic extensions of the CD map and of the cdCSL model, namely the rCD map and rcdCSL model, respectively (Appendix D).

We conclude, based on the analysis of this thesis, with the following question: what is the relation between relativity, classicalization maps and system - environment interactions?

Chapter 7

Acknowledgments

I would like to thank my supervisor Prof. Angelo Bassi for his guidance and for the warm welcome in his research group. I would also like to thank my co-workers, in particular, for the many interesting discussions about the physical world. I also want to express my immense gratitude to my family, for their encouragement and support.

Appendices

Appendix A

Galilean covariant Gaussian maps

A.1 Introduction

The evolution of the statistical operator is constrained by the basic request of trace-preservation (TP) and complete positivity (CP). In addition, if one imposes the request of Markovianity, one obtains the well-known structure of the Lindblad generator [65, 66]. Other types of constraints are obtained by imposing the covariance under space-time transformations. In particular, for a Markovian evolution, imposing the covariance under translations and Galilean boosts one obtains the well-known structure of the Holevo generator [67, 68, 69, 70].

Recently, the Lindblad generator has been generalized to a non-Markovian Gaussian dynamics [29]. In particular, it has been shown that the most general, completely positive (CP) Gaussian map (in interaction picture) has the following structure (Einstein summation convention):

$$\mathcal{M}_t = \mathcal{T} \exp \left\{ \int_0^t d\tau \int_0^t ds D_{jk}(\tau, s) \left(\hat{A}_{sL}^k \hat{A}_{\tau R}^j - \theta_{\tau, s} \hat{A}_{\tau L}^j \hat{A}_{sL}^k - \theta_{s, \tau} \hat{A}_{sR}^k \hat{A}_{\tau R}^j \right) \right\} \quad (\text{A.1})$$

where the subscript L (R) denotes the operator acting on the statistical operator ρ from the left (right), e.g. $\hat{A}_L^k \hat{A}_R^j \rho = \hat{A}^k \rho \hat{A}^j$, \mathcal{T} denotes the time-ordering operator acting separately on left and right operators, $D_{jk}(\tau, s)$ is the j, k element of a complex valued positive semi-definite matrix and \hat{A}^k are hermitian self-adjoint operators. We will impose on this structure the additional request of covariance under specific space-time transformations. In particular, we will characterize translational and Galilean covariant maps. In this way we will obtain a generalization of the Holevo generators to non-Markovian Gaussian maps.

A.2 Map

It is convenient for our purpose to decompose the operators in Eq. (A.1) by using Weyl's decomposition [21]:

$$\hat{A}_t = \int d\alpha \int d\beta g_t(\alpha, \beta) e^{i(\alpha \hat{x} + \beta \hat{p})}, \quad (\text{A.2})$$

where $g_t(\alpha, \beta)$ is a complex function of the real parameters α and β .

It is then straightforward to show that

$$\mathcal{M}_t = \mathcal{T} \exp \left\{ \int_0^t d\tau \int_0^t ds \int d\alpha_1 \int d\beta_2 \int d\alpha_2 \int d\beta_2 \mathcal{D}(\alpha_1, \beta_1, \alpha_2, \beta_2, \tau, s) \right. \\ \left. \begin{aligned} & (e^{i(\alpha_1 \hat{x}_L(s) + \beta_1 \hat{p}_L)} e^{-i(\alpha_2 \hat{x}_R(\tau) + \beta_2 \hat{p}_R)} \\ & - \theta_{\tau, s} e^{-i(\alpha_1 \hat{x}_L(\tau) + \beta_1 \hat{p}_L)} e^{i(\alpha_2 \hat{x}_L(s) + \beta_2 \hat{p}_L)} \\ & - \theta_{s, \tau} e^{i(\alpha_1 \hat{x}_R(s) + \beta_1 \hat{p}_R)} e^{-i(\alpha_2 \hat{x}_R(\tau) + \beta_2 \hat{p}_R)}) \end{aligned} \right\}, \quad (\text{A.3})$$

where $\hat{x}_L(s)$ is the interaction picture operator and

$$\mathcal{D}(\alpha_1, \beta_1, \alpha_2, \beta_2, \tau, s) = D_{jk}(\tau, s) g_\tau^{j*}(\alpha_1, \beta_1) g_s^k(\alpha_2, \beta_2) \quad (\text{A.4})$$

is a kernel that satisfies the following symmetry property¹:

$$\mathcal{D}(\alpha_1, \beta_1, \alpha_2, \beta_2, \tau, s) = \mathcal{D}^*(\alpha_2, \beta_2, \alpha_1, \beta_1, s, \tau) \quad (\text{A.5})$$

A.3 Covariance

We start from the single particle Hilbert space \mathcal{H} (the generalization to the N -particle Hilbert space is straightforward). We consider the generators of the centrally extended unitary representation of the Galilei group (\mathcal{G}) on \mathcal{H} in the interaction picture, with $H = \hat{p}^2/2m$. In particular, the generators of translations, rotations and boosts are

$$\hat{P} = \hat{p}, \quad (\text{A.6})$$

$$\hat{J} = \hat{x} \times \hat{p}, \quad (\text{A.7})$$

$$\hat{K} = m\hat{x}, \quad (\text{A.8})$$

respectively. A generic dynamical map is covariant under the Galilei group transformation if [71, 72]:

$$\mathcal{M}_t = \mathcal{G}^{-1} \circ \mathcal{M}_t \circ \mathcal{G} \quad (\text{A.9})$$

where the Galilei group is represented as:

$$\mathcal{G}[\cdot] = \hat{U}^\dagger \cdot \hat{U} \quad (\text{A.10})$$

and \hat{U} denotes a unitary transformation generated by the operators given in Eqs. (A.6), (A.7) and (A.8). Exploiting Eq. (A.10), and the fact that we are considering a unitary

¹By construction we have $D_{kj}(s, \tau)^* = D_{jk}(\tau, s)$ [29].

representation, we can rewrite Eq. (A.9) in the more explicit form:

$$\begin{aligned}
& \mathcal{T} \exp \left\{ \int_0^t d\tau \int_0^t ds \int d\alpha_1 \int d\beta_2 \int d\alpha_2 \int d\beta_2 \mathcal{D}(\alpha_1, \beta_1, \alpha_2, \beta_2, \tau, s) \right. \\
& \quad \left(e^{i(\alpha_1 \hat{x}_L(s) + \beta_1 \hat{p}_L)} e^{-i(\alpha_2 \hat{x}_R(\tau) + \beta_2 \hat{p}_R)} \right. \\
& \quad \left. - \theta_{\tau, s} e^{-i(\alpha_1 \hat{x}_L(\tau) + \beta_1 \hat{p}_L)} e^{i(\alpha_2 \hat{x}_L(s) + \beta_2 \hat{p}_L)} \right. \\
& \quad \left. - \theta_{s, \tau} e^{i(\alpha_1 \hat{x}_R(s) + \beta_1 \hat{p}_R)} e^{-i(\alpha_2 \hat{x}_R(\tau) + \beta_2 \hat{p}_R)} \right) \Big\} = \\
& \mathcal{T} \exp \left\{ \int_0^t d\tau \int_0^t ds \int d\alpha_1 \int d\beta_2 \int d\alpha_2 \int d\beta_2 \mathcal{D}(\alpha_1, \beta_1, \alpha_2, \beta_2, \tau, s) \right. \\
& \quad \left(e^{i(\alpha_1 \mathcal{G}[\hat{x}_L(s)] + \beta_1 \mathcal{G}[\hat{p}_L])} e^{-i(\alpha_2 \mathcal{G}[\hat{x}_R(\tau)] + \beta_2 \mathcal{G}[\hat{p}_R])} \right. \\
& \quad \left. - \theta_{\tau, s} e^{-i(\alpha_1 \mathcal{G}[\hat{x}_L(\tau)] + \beta_1 \mathcal{G}[\hat{p}_L])} e^{i(\alpha_2 \mathcal{G}[\hat{x}_L(s)] + \beta_2 \mathcal{G}[\hat{p}_L])} \right. \\
& \quad \left. - \theta_{s, \tau} e^{i(\alpha_1 \mathcal{G}[\hat{x}_R(s)] + \beta_1 \mathcal{G}[\hat{p}_R])} e^{-i(\alpha_2 \mathcal{G}[\hat{x}_R(\tau)] + \beta_2 \mathcal{G}[\hat{p}_R])} \right) \Big\}, \tag{A.11}
\end{aligned}$$

It is straightforward to show that the above equation is satisfied if only if the following conditions are simultaneously satisfied:

$$\begin{aligned}
& \int_0^t d\tau \int_0^t ds \int d\alpha_1 \int d\beta_2 \int d\alpha_2 \int d\beta_2 \mathcal{D}(\alpha_1, \beta_1, \alpha_2, \beta_2, \tau, s) \\
& \quad \left[e^{i(\alpha_1 \mathcal{G}[\hat{x}_L(s)] + \beta_1 \mathcal{G}[\hat{p}_L])} e^{-i(\alpha_2 \mathcal{G}[\hat{x}_R(\tau)] + \beta_2 \mathcal{G}[\hat{p}_R])} - e^{i(\alpha_1 \hat{x}_L(s) + \beta_1 \hat{p}_L)} e^{-i(\alpha_2 \hat{x}_R(\tau) + \beta_2 \hat{p}_R)} \right] = 0 \tag{A.12}
\end{aligned}$$

$$\begin{aligned}
& \int_0^t d\tau \int_0^t ds \int d\alpha_1 \int d\beta_2 \int d\alpha_2 \int d\beta_2 \mathcal{D}(\alpha_1, \beta_1, \alpha_2, \beta_2, \tau, s) \\
& \quad \theta_{\tau, s} \left(e^{-i(\alpha_1 \mathcal{G}[\hat{x}_L(\tau)] + \beta_1 \mathcal{G}[\hat{p}_L])} e^{i(\alpha_2 \mathcal{G}[\hat{x}_L(s)] + \beta_2 \mathcal{G}[\hat{p}_L])} - e^{-i(\alpha_1 \hat{x}_L(\tau) + \beta_1 \hat{p}_L)} e^{i(\alpha_2 \hat{x}_L(s) + \beta_2 \hat{p}_L)} \right) = 0 \tag{A.13}
\end{aligned}$$

$$\begin{aligned}
& \int_0^t d\tau \int_0^t ds \int d\alpha_1 \int d\beta_2 \int d\alpha_2 \int d\beta_2 \mathcal{D}(\alpha_1, \beta_1, \alpha_2, \beta_2, \tau, s) \\
& \quad \theta_{s, \tau} \left(e^{i(\alpha_1 \mathcal{G}[\hat{x}_R(s)] + \beta_1 \mathcal{G}[\hat{p}_R])} e^{-i(\alpha_2 \mathcal{G}[\hat{x}_R(\tau)] + \beta_2 \mathcal{G}[\hat{p}_R])} - e^{i(\alpha_1 \hat{x}_R(s) + \beta_1 \hat{p}_R)} e^{-i(\alpha_2 \hat{x}_R(\tau) + \beta_2 \hat{p}_R)} \right) = 0 \tag{A.14}
\end{aligned}$$

These equations give general constraints on the structure of the dynamical map under the request of Galilei covariance. In particular, as we will see in the following section, the request of translation (boost) covariance completely characterizes the structure of the dynamical map.

A.3.1 Translation-covariance

Restricting to the case where \mathcal{G} describes the group of translations we have that

$$\mathcal{G}[\hat{x}(s)] = \hat{x}(s) + a, \tag{A.15}$$

$$\mathcal{G}[\hat{p}] = \hat{p}, \tag{A.16}$$

where a is the translation vector. Using Eqs. (A.15), (A.16) we obtain from Eq. (A.12):

$$\int_0^t d\tau \int_0^t ds \int d\alpha_1 \int d\beta_2 \int d\alpha_2 \int d\beta_2 \mathcal{D}(\alpha_1, \beta_1, \alpha_2, \beta_2, \tau, s) e^{i(\alpha_1 \hat{x}_L(s) + \beta_1 \hat{p}_L)} e^{-i(\alpha_2 \hat{x}_R(\tau) + \beta_2 \hat{p}_R)} (1 - e^{i(\alpha_1 - \alpha_2)a}) = 0 \quad (\text{A.17})$$

Since this relation must be satisfied $\forall a$, it follows that Eq. (A.17) is satisfied only if, under the integral $\int d\alpha_1 d\alpha_2$, the following equality holds

$$\mathcal{D}(\alpha_1, \beta_1, \alpha_2, \beta_2, \tau, s) = \delta(\alpha_1 - \alpha_2) \mathcal{D}_T(\alpha_1, \beta_1, \alpha_2, \beta_2, \tau, s), \quad (\text{A.18})$$

where \mathcal{D}_T is a complex valued function. It is now easy to verify that the condition given by Eq. (A.18) is enough to guarantee the validity of Eq. (A.13) and Eq. (A.14). Using Eqs. (A.18), (A.4) and the standard commutation relation, we can rewrite the first exponent of Eq. (A.3) as

$$\begin{aligned} & \int_0^t d\tau \int_0^t ds \int d\alpha_1 \int d\beta_2 \int d\alpha_2 \int d\beta_2 \mathcal{D}(\alpha_1, \beta_1, \alpha_2, \beta_2, \tau, s) e^{i(\alpha_1 \hat{x}_L(s) + \beta_1 \hat{p}_L)} e^{-i(\alpha_2 \hat{x}_R(\tau) + \beta_2 \hat{p}_R)} \\ &= \int_0^t d\tau \int_0^t ds \int d\alpha D_{jk}(s, \tau) J_{s,L}^k(\hat{p}, \alpha) e^{i\alpha \hat{x}_L(s)} J_{\tau,R}^{j\dagger}(\hat{p}, \alpha) e^{-i\alpha \hat{x}_R(\tau)}, \end{aligned} \quad (\text{A.19})$$

where

$$J_{\tau}^k(\hat{p}, \alpha) = \int d\beta g_{\tau}^k(\alpha, \beta) e^{i\beta(\hat{p} - \alpha/2)} \quad (\text{A.20})$$

are arbitrary operator valued functions. Performing an analogous calculation for the remaining two terms we can rewrite Eq. (A.3) as

$$\begin{aligned} \mathcal{M}_t = \mathcal{T} \exp \left\{ \int_0^t d\tau \int_0^t ds \int d\alpha D_{jk}(\tau, s) \left([J_{s,L}^k(\hat{p}, \alpha) e^{i\alpha \hat{x}_L(s)}] [J_{\tau,R}^{j\dagger}(\hat{p}, \alpha) e^{-i\alpha \hat{x}_R(\tau)}] \right. \right. \\ \left. \left. - \theta_{\tau,s} [J_{\tau,L}^{j\dagger}(\hat{p}, \alpha) e^{-i\alpha \hat{x}_L(\tau)}] [e^{i\alpha \hat{x}_L(s)} J_{s,L}^k(\hat{p}, \alpha)] - \theta_{s,\tau} [J_{s,R}^k(\hat{p}, \alpha) e^{i\alpha \hat{x}_R(s)}] [e^{-i\alpha \hat{x}_R(\tau)} J_{\tau,R}^{j\dagger}(\hat{p}, \alpha)] \right) \right\} \end{aligned} \quad (\text{A.21})$$

This equation completely characterizes the translation covariant completely positive Gaussian maps.

A.3.2 Boost-covariance

Restricting to the case where \mathcal{G} describes the group of boost we have that:

$$\mathcal{G}[\hat{x}(s)] = \hat{x}(s) + vt, \quad (\text{A.22})$$

$$\mathcal{G}[\hat{p}] = \hat{p} + mv, \quad (\text{A.23})$$

where v is the boost vector. In order to find the structure of the boost covariant dynamical map \mathcal{M}_t we perform an analogous calculation as in Sec. A.3.1. We obtain the following equality:

$$\mathcal{D}(\alpha_1, \beta_1, \alpha_2, \beta_2, \tau, s) = \delta(\alpha_1 s - \alpha_2 \tau + \beta_1 m - \beta_2 m) \mathcal{D}_B(\alpha_1, \beta_1, \alpha_2, \beta_2, \tau, s) \quad (\text{A.24})$$

where \mathcal{D}_B is a complex valued function. Using Eq. (A.24) we can then eventually rewrite Eq. (A.3) as:

$$\begin{aligned} \mathcal{M}_t = \mathcal{T} \exp \left\{ \int_0^t d\tau \int_0^t ds \int d\beta D_{jk}(\tau, s) \left([J_{sL}^k(\hat{x}(s), \beta) e^{i\beta\hat{p}_L}] [J_{\tau R}^{j\dagger}(\hat{x}(\tau), \beta) e^{-i\beta\hat{p}_R}] \right. \right. \\ \left. \left. - \theta_{\tau, s} [J_{\tau L}^{j\dagger}(\hat{x}(\tau), \beta) e^{-i\beta\hat{p}_L}] [e^{i\beta\hat{p}_L} J_{sL}^k(\hat{x}(s), \beta)] - \theta_{s, \tau} [J_{sR}^k(\hat{x}(s), \beta) e^{i\beta\hat{p}_R}] [e^{-i\beta\hat{p}_R} J_{\tau R}^{j\dagger}(\hat{x}(\tau), \beta)] \right) \right\}, \end{aligned} \quad (\text{A.25})$$

where $J_s^k(\hat{x}(s), \beta)$ are arbitrary operator valued functions. This equation completely characterizes boost covariant completely positive Gaussian maps.

A.3.3 Translation-boost Covariance

We consider now translation and boost covariant maps. The dynamical map \mathcal{M}_t must satisfy both condition (A.18) and (A.24), *i.e.*

$$\mathcal{D}(\alpha_1, \beta_1, \alpha_2, \beta_2, \tau, s) = \delta(\alpha_1 - \alpha_2) \delta(\alpha_1 s - \alpha_2 \tau + \beta_1 m - \beta_2 m) \mathcal{D}_{TB}(\alpha_1, \beta_1, \alpha_2, \beta_2, \tau, s), \quad (\text{A.26})$$

where \mathcal{D}_{TB} is a complex valued function. Replacing Eq. (A.26) in Eq. (A.3) one eventually obtains

$$\begin{aligned} \mathcal{M}_t = \mathcal{T} \exp \left\{ \int_0^t d\tau \int_0^t ds \int d\alpha \int d\beta \mathcal{F}(\alpha, \beta, \tau, s) \left(e^{i(\alpha\hat{x}_L(s) + \beta\hat{p}_L)} e^{-i(\alpha\hat{x}_R(\tau) + \beta\hat{p}_R)} \right. \right. \\ \left. \left. - \theta_{\tau, s} e^{-i(\alpha\hat{x}_L(\tau) + \beta\hat{p}_L)} e^{i(\alpha\hat{x}_L(s) + \beta\hat{p}_L)} - \theta_{s, \tau} e^{-i(\alpha\hat{x}_R(s) + \beta\hat{p}_R)} e^{i(\alpha\hat{x}_R(\tau) + \beta\hat{p}_R)} \right) \right\}, \end{aligned} \quad (\text{A.27})$$

where $\mathcal{F}(\alpha, \beta, \tau, s)$ is an arbitrary complex valued function. This equation completely characterizes translation and boost covariant completely positive Gaussian maps.

A.3.4 Rotation Covariance

For completeness we also analyze rotation covariance:

$$\mathcal{G}[\hat{x}(s)] = R\hat{x}(s), \quad (\text{A.28})$$

$$\mathcal{G}[\hat{p}] = R\hat{p}, \quad (\text{A.29})$$

where R denotes the rotation matrix. We define R^{-1} as the dual map of R associated to the scalar product between the operator vectors \hat{x} , \hat{p} and the real vectors α , β . Using Eqs. (A.28), (A.29) can now rewrite Eq. (A.12) as:

$$\begin{aligned} \int_0^t d\tau \int_0^t ds \int d\alpha_1 \int d\beta_2 \int d\alpha_2 \int d\beta_2 \mathcal{D}(\alpha_1, \beta_1, \alpha_2, \beta_2, \tau, s) \\ \left[e^{i(R^{-1}[\alpha_1]\hat{x}_L(s) + R^{-1}[\beta_1]\hat{p}_L)} e^{-i(R^{-1}[\alpha_2]\hat{x}_R(\tau) + R^{-1}[\beta_2]\hat{p}_R)} - e^{i(\alpha_1\hat{x}_L(s) + \beta_1\hat{p}_L)} e^{-i(\alpha_2\hat{x}_R(\tau) + \beta_2\hat{p}_R)} \right] = 0 \end{aligned} \quad (\text{A.30})$$

Recalling that the integral measure $d\alpha_j d\beta_j$ is invariant under rotations one can perform the change of variables $\alpha_j \rightarrow R\alpha_j$, $\beta_j \rightarrow R\beta_j$ to obtain

$$\begin{aligned} \int_0^t d\tau \int_0^t ds \int d\alpha_1 \int d\beta_2 \int d\alpha_2 \int d\beta_2 e^{i(\alpha_1\hat{x}_L(s) + \beta_1\hat{p}_L)} e^{-i(\alpha_2\hat{x}_R(\tau) + \beta_2 R\hat{p}_R)} \\ [\mathcal{D}(R\alpha_1, R\beta_1, R\alpha_2, R\beta_2, \tau, s) - \mathcal{D}(\alpha_1, \beta_1, \alpha_2, \beta_2, \tau, s)] = 0. \end{aligned} \quad (\text{A.31})$$

It is now easy to verify that the above equation constrains \mathcal{D} to be invariant under rotations, *i.e.*

$$\mathcal{D}(R\alpha_1, R\beta_1, R\alpha_2, R\beta_2, \tau, s) = \mathcal{D}(\alpha_1, \beta_1, \alpha_2, \beta_2, \tau, s) \quad (\text{A.32})$$

and that the rotation invariance of \mathcal{D} is enough to guarantee the validity of Eq. (A.13) and Eq. (A.14).

A.3.5 Markovian limits

The general completely positive Gaussian translational (boost) covariant maps reduce in the Markovian limit to the well known characterization of Markovian completely positive Gaussian translational (boost) covariant maps. In particular, we reobtain the Holevo structures for the generators of the covariant quantum dynamical semi-group. This can be seen by setting the correlation function to be delta correlated in time, *i.e.*

$$\mathcal{D}(\alpha_1, \beta_1, \alpha_2, \beta_2, s, \tau) = \delta(s - \tau) \mathcal{D}_M(\alpha_1, \beta_1, \alpha_2, \beta_2, s), \quad (\text{A.33})$$

where \mathcal{D}_M is a complex valued function. In particular, Eq. (A.3) reduces to

$$\begin{aligned} \mathcal{M}_t = \mathcal{T} \exp \left\{ \int_0^t d\tau \int d\alpha_1 \int d\beta_2 \int d\alpha_2 \int d\beta_2 \mathcal{D}_M(\alpha_1, \beta_1, \alpha_2, \beta_2, \tau) \right. \\ \left. \left(e^{i(\alpha_1 \hat{x}_L(\tau) + \beta_1 \hat{p}_L)} e^{-i(\alpha_2 \hat{x}_R(\tau) + \beta_2 \hat{p}_R)} \right. \right. \\ \left. \left. - \frac{1}{2} e^{-i(\alpha_1 \hat{x}_L(\tau) + \beta_1 \hat{p}_L)} e^{i(\alpha_2 \hat{x}_L(\tau) + \beta_2 \hat{p}_L)} \right. \right. \\ \left. \left. - \frac{1}{2} e^{i(\alpha_1 \hat{x}_R(\tau) + \beta_1 \hat{p}_R)} e^{-i(\alpha_2 \hat{x}_R(\tau) + \beta_2 \hat{p}_R)} \right) \right\}, \quad (\text{A.34}) \end{aligned}$$

It is straightforward to obtain the generator \mathcal{L}_t of the map \mathcal{M}_t :

$$\mathcal{L}_t = (\partial_t \mathcal{M}_t) \mathcal{M}_t^{-1} \quad (\text{A.35})$$

In particular, the generator of translation covariant maps is given by (in Schrödinger picture)

$$\begin{aligned} \mathcal{L}_t = \int d\alpha D_{jk}(t) \left(J_{tL}^k(\hat{p}, \alpha) e^{i\alpha \hat{x}_L} J_{tR}^{j\dagger}(\hat{p}, \alpha) e^{-i\alpha \hat{x}_R} \right. \\ \left. - \frac{1}{2} J_{tL}^{j\dagger}(\hat{p}, \alpha) J_{tL}^k(\hat{p}, \alpha) - \frac{1}{2} J_{tR}^k(\hat{p}, \alpha) J_{tR}^{j\dagger}(\hat{p}, \alpha) \right), \quad (\text{A.36}) \end{aligned}$$

the generator for the boost-covariant maps is given by (in Schrödinger picture)

$$\begin{aligned} \mathcal{L}_t = \int d\beta D_{jk}(t) \left(J_{tL}^k(\hat{x}, \beta) e^{i\beta \hat{p}_L} J_{tR}^{j\dagger}(\hat{x}, \beta) e^{-i\beta \hat{p}_R} \right. \\ \left. - \frac{1}{2} J_{tL}^{j\dagger}(\hat{x}, \beta) J_{tL}^k(\hat{x}, \beta) - \frac{1}{2} J_{tR}^k(\hat{x}, \beta) J_{tR}^{j\dagger}(\hat{x}, \beta) \right) \quad (\text{A.37}) \end{aligned}$$

and the generator for the boosts and translation covariant maps is given by (in Schrödinger picture)

$$\mathcal{L}_t = \int d\alpha \int d\beta \mathcal{F}_M(\alpha, \beta, t) \left(e^{i(\alpha \hat{x}_L + \beta \hat{p}_L)} e^{-i(\alpha \hat{x}_R + \beta \hat{p}_R)} - 1 \right), \quad (\text{A.38})$$

where \mathcal{F}_M is a complex valued function. Eqs. (A.36), (A.37) and (A.38) correspond to the Holevo results for covariance under translation, boost and boost-translation, respectively.

A.4 Discussion and conclusions

We analyzed the non-Markovian Gaussian dynamics under the request of covariance under translation, rotation and boost. We generalized the fundamental features of the well-known translation and boost covariant Lindblad master equation for non-Markovian Gaussian dynamics.

Appendix B

Canonical quantum mechanics

B.1 Canonical quantum mechanics

Foldy's canonical quantum-mechanical framework [73, 74, 75, 76] is a theory of particles, valid when particle/antiparticle interactions are negligible. This is a reasonable choice, as particle/antiparticle phenomena are not expected to play a significant role in the mesoscopic and macroscopic regimes. In this framework, loosely speaking, we have the kinematics of non-relativistic quantum mechanics with a relativistic dynamics. The properties, in particular the causality of the theory, have been investigated in [75], while some important cases, such as the free particle evolution, have been investigated in [76]. This theory can be motivated by the Foldy-Wouthuysen transformation [77]: a perturbative method to separate the particle and anti-particle sector to a given order in $\mathcal{O}(1/c^2)$. In particular, the non-relativistic limit within this theory is straightforward, and as often claimed, it is the only way to obtain a meaningful non-relativistic limit.

In this section we summarize the framework discussed in [74]. Latin indices denote the three spatial axis, i.e. i, j from 1 to 3, while Greek indices denotes the particle number, i.e. μ, ν from 1 to N .

B.1.1 Canonical Poincaré covariant quantum mechanics

We impose the canonical commutation relations:

$$[\hat{x}_\mu^i, \hat{x}_\nu^j] = [\hat{p}_\mu^i, \hat{p}_\nu^j] = [\hat{s}_\mu^i, \hat{x}_\nu^j] = [\hat{s}_\mu^i, \hat{p}_\nu^j] = 0 \quad (\text{B.1})$$

$$[\hat{x}_\mu^i, \hat{p}_\nu^j] = i\delta_{\mu\nu}\delta_{ij} \quad (\text{B.2})$$

$$[\hat{s}_\mu^i, \hat{s}_\nu^j] = i\delta_{\mu\nu}\epsilon_{ijk}\hat{s}_\nu^k \quad (\text{B.3})$$

where $\hat{r}_\mu, \hat{p}_\mu, \hat{s}_\mu$ are the position, momentum and spin operators of particle μ , respectively. We then construct the following operators

$$\mathcal{P} = \sum_{\mu} \hat{p}_{\mu}, \quad (\text{B.4})$$

$$\mathcal{J} = \sum_{\mu} (\hat{x}_{\mu} \times \hat{p}_{\mu} + \hat{s}_{\mu}), \quad (\text{B.5})$$

$$\mathcal{K} = \sum_{\mu} (\hat{K}_{\mu} + \beta \hat{V}), \quad (\text{B.6})$$

$$\mathcal{H} = \sum_{\mu} (\hat{H}_{\mu} + \beta \hat{U}), \quad (\text{B.7})$$

where

$$\hat{K}_{\mu} = (1/(2c^2))(\hat{x}_{\mu} \hat{H}_{\mu} + \hat{H}_{\mu} \hat{x}_{\mu}) - \frac{\hat{s}_{\mu} \times \hat{p}_{\mu}}{m_{\mu} c^2 + \hat{H}_{\mu}} - t \hat{p}_{\mu}, \quad (\text{B.8})$$

$$\hat{H}_{\mu} = (\hat{p}_{\mu}^2 c^2 + m_{\mu}^2 c^4)^{1/2}. \quad (\text{B.9})$$

The operators defined in Eqs. (B.4),(B.5),(B.6),(B.7) form an algebra isomorphic to the Poincaré algebra:

$$[\mathcal{P}_i, \mathcal{P}_j] = 0, \quad (\text{B.10})$$

$$[\mathcal{P}_i, \mathcal{H}] = 0, \quad (\text{B.11})$$

$$[\mathcal{J}_i, \mathcal{H}] = 0, \quad (\text{B.12})$$

$$[\mathcal{J}_i, \mathcal{J}_j] = i \epsilon_{ijk} \mathcal{J}_k, \quad (\text{B.13})$$

$$[\mathcal{J}_i, \mathcal{P}_j] = i \epsilon_{ijk} \mathcal{P}_k, \quad (\text{B.14})$$

$$[\mathcal{J}_i, \mathcal{K}_j] = i \epsilon_{ijk} \mathcal{K}_k, \quad (\text{B.15})$$

$$[\mathcal{K}_i, \mathcal{H}] = i \mathcal{P}_i, \quad (\text{B.16})$$

$$[\mathcal{K}_i, \mathcal{K}_j] = -i \epsilon_{ijk} \mathcal{J}_k / c^2, \quad (\text{B.17})$$

$$[\mathcal{K}_i, \mathcal{P}_j] = i \delta_{ij} \mathcal{H} / c^2. \quad (\text{B.18})$$

In particular, we can identify \mathcal{P} , \mathcal{J} , \mathcal{K} , \mathcal{H} with the generators of translations, rotations, boosts and time-evolution, respectively.

The time-evolution for the state vector is given by the Schrödinger-Foldy equation:

$$i \frac{d}{dt} |\psi\rangle = \mathcal{H} |\psi\rangle. \quad (\text{B.19})$$

and the corresponding evolution map for the statistical operator is given by

$$\rho_{t_2} = \mathcal{M}^{(P)}(t_2, t_1) [\rho_{t_1}], \quad (\text{B.20})$$

where ρ_{t_j} denotes the statistical operator at time t_j and the map $\mathcal{M}^{(P)}(t_2, t_1)$, derived from Eq. (B.19), is given by:

$$\mathcal{M}^{(P)}(t_2, t_1) [\cdot] = \exp(-i \mathcal{H}(t_2 - t_1)) [\cdot] \exp(i \mathcal{H}(t_2 - t_1)). \quad (\text{B.21})$$

In Eqs. (B.6), (B.7) we have introduced an internal potential \hat{U} and the corresponding “interaction boost” \hat{V} . From the commutation relations given by Eqs. (B.11), (B.12) we get the following constraints for \hat{U} :

$$[\hat{U}, \mathcal{P}] = [\hat{U}, \mathcal{J}] = 0. \quad (\text{B.22})$$

From Eq. (B.18) we see that a nonzero \hat{U} implies the existence of a nonzero \hat{V} :

$$[\hat{V}_i, \mathcal{P}_j] = i\delta_{ij}\hat{U}/c^2, \quad (\text{B.23})$$

In addition, Eqs. (B.15), (B.17) give the additional constrains on \hat{V} :

$$[\mathcal{J}_i, \hat{V}_j] = i\epsilon_{ijk}\hat{V}_k, \quad (\text{B.24})$$

$$[\hat{V}_i, \sum_{\mu} \hat{K}_{\mu}^j] - [\hat{V}_j, \sum_{\mu} \hat{K}_{\mu}^i] + \beta[\hat{V}_i, \hat{V}_j] = 0, \quad (\text{B.25})$$

respectively.

B.1.2 The non-relativistic limit

We can obtain the non-relativistic limit, namely the canonical Galilean covariant quantum mechanics, by setting $c \rightarrow \infty$ and removing the rest-energy term mc^2 , i.e. the Inönü-Wigner contraction [78]. In particular, from the generators given by Eqs. (B.4),(B.5),(B.6),(B.7) we obtain:

$$\mathcal{P} = \sum_{\mu} \hat{p}_{\mu}, \quad (\text{B.26})$$

$$\mathcal{J} = \sum_{\mu} (\hat{x}_{\mu} \times \hat{p}_{\mu} + \hat{s}_{\mu}), \quad (\text{B.27})$$

$$\mathcal{K} = \sum_{\mu} \hat{K}_{\mu} + \beta\hat{V}^{(0)}, \quad (\text{B.28})$$

$$\mathcal{H} = \sum_{\mu} \hat{H}_{\mu} + \beta\hat{U}^{(0)}, \quad (\text{B.29})$$

where

$$\hat{K}_{\mu} = m\hat{x}_{\mu} - t\hat{p}_{\mu}, \quad (\text{B.30})$$

$$\hat{H}_{\mu} = \hat{p}_{\mu}^2/2m. \quad (\text{B.31})$$

These generators form an algebra isomorphic to the Galilei algebra. $\hat{U}^{(0)}$, $\hat{V}^{(0)}$ are the non-relativistic part of the interaction potential and interaction boost \hat{U} , \hat{V} , respectively. However, as shown in [73], we can always, by a change of representation, set $\hat{V}^{(0)} = 0$ in full generality.

The algebra is given by the commutators in Eqs. (B.10)-(B.16), while in place of the commutators given by Eqs. (B.17), (B.18) we have

$$[\mathcal{K}_i, \mathcal{K}_j] = 0, \tag{B.32}$$

$$[\mathcal{K}_i, \mathcal{P}_j] = i\delta_{ij}m, \tag{B.33}$$

respectively. In addition, Eq. (B.19) reduces to the usual Schrödinger map and the map for the statistical operator given by Eq. (B.21) reduces to the usual non-relativistic von Neumann map.

Appendix C

Relativity and classicalization maps

C.1 Introduction

Combining relativity and quantum mechanics was, and in part still is, a difficult problem. However, the two theories, when successfully combined, lead to important and highly non-trivial results. In this section, we investigate the two frameworks within the theory of relativistic open quantum systems. In particular, we look at the problem of constructing translational and Lorentz boost covariant dynamical maps: we argue that such a modification cannot be constructed when particle/antiparticle interaction is suppressed. This is in stark contrast with fully relativistic dynamical maps, where particle/antiparticle interaction is not suppressed [79]. The discussion of relativistic maps, where particle/antiparticle interaction is suppressed, will bridge the gap between the fully relativistic maps and the non-relativistic maps. In addition, we will discuss two implications for non-relativistic quantum mechanics: for the intrinsic non-unitary modifications of the dynamics and for the measures of macroscopicity.

We will work in the framework of canonical Poincaré covariant quantum mechanics introduced in Appendix B. In Sec. (C.2.5) we present the main result: there exist only trivial translational and Lorentz covariant relativistic maps. We will prove this explicitly at order $1/c^2$ and argue that the same result applies also for higher order relativistic corrections. In Sec. (C.3) we briefly discuss the implications for non-unitary modification of canonical quantum mechanics and for the measure of macroscopicity.

C.2 Covariance of relativistic maps

We first discuss Weyl-Wigner type decompositions of generic maps in Sec C.2.1. We define covariance of (non) relativistic maps in Sec. C.2.2. We then first consider non-relativistic translations and boosts in Sec. C.2.3. In Sec. C.2.4 we present the main result: at order $1/c^2$ there are only trivial translational and Lorentz covariant relativistic maps. In Sec. C.2.5 we give some physical insight into this result and argue that the same applies also for higher order relativistic corrections. In this appendix we explicitly indicate scalar products (with \cdot), to emphasize the role of three spatial dimensions in the 1+3 Minkowski spacetime in the calculations.

C.2.1 Map decompositions

We consider first, for simplicity of presentation, a single particle with spin $s = 0$. It is convenient to switch to the interaction picture

$$|\psi^{(I)}_t\rangle = e^{i\mathcal{H}t}|\psi_t\rangle, \quad (\text{C.1})$$

$$\hat{A}^{(I)}(t) = e^{i\mathcal{H}t}\hat{A}e^{-i\mathcal{H}t}, \quad (\text{C.2})$$

where \mathcal{H} is given by Eq.(B.7) or Eq.(B.29) depending on the symmetry group.

A generic operator $\hat{A}^{(I)}(t)$ can be written in Weyl - Wigner decomposition [21]:

$$\hat{A}^{(I)}(t) = \int d\alpha \int d\beta g(\alpha, \beta, t) e^{i(\alpha \cdot \hat{x} + \beta \cdot \hat{p})}, \quad (\text{C.3})$$

where \hat{x} , \hat{p} on the right hand-side are the usual Schrödinger picture operators. However, this decomposition is not unique. We now introduce an alternative decomposition, which, as we will see, is more convenient for discussing relativistic covariance. To this end we consider a unitary transformation $\xi = \exp(-i\phi)$. We now write:

$$\hat{A}^{(I)}(t) = \xi \left[\xi^\dagger \hat{A}^{(I)}(t) \xi \right] \xi^\dagger, \quad (\text{C.4})$$

where $\xi^\dagger \hat{A}^{(I)}(t) \xi$, a completely general operator, can be decomposed using Eq. (C.3). Thus, using Eqs. (C.3) for $\xi^\dagger \hat{A}^{(I)}(t) \xi$ in Eq. (C.4) we obtain the alternative general decomposition:

$$\hat{A}^{(I)}(t) = \int d\alpha \int d\beta g(\alpha, \beta, t) e^{i(\alpha \cdot \hat{\chi} + \beta \cdot \hat{\pi})}, \quad (\text{C.5})$$

where

$$\hat{\chi} = \xi \hat{x} \xi^\dagger, \quad (\text{C.6})$$

$$\hat{\pi} = \xi \hat{p} \xi^\dagger. \quad (\text{C.7})$$

We will refer to this decomposition as the generalized Weyl Wigner decomposition: for $\xi = \mathbb{I}$ we reobtain the usual Weyl Wigner decomposition.

Let us now consider a generic map (in interaction picture) $\mathcal{M}_{t_2, t_1}^{(I)}[\cdot]$ in place of the map given by Eq. (B.21). We can always write a generic map as:

$$\mathcal{M}^{(I)}(t_2, t_1)[\cdot] = \sum_i \hat{A}_i(t_2, t_1)[\cdot] \hat{B}_i(t_2, t_1), \quad (\text{C.8})$$

where \hat{A}_i , \hat{B}_i are generic operators. We now use the generalized Weyl Wigner decomposition of operators defined in Eq. (C.5) and obtain the following decomposition of a generic map:

$$\begin{aligned} \mathcal{M}^{(I)}(t_2, t_1)[\cdot] &= \int d\alpha_L \int d\beta_L \int d\alpha_R \int d\beta_R g(t_2, t_1, \alpha_L, \beta_L, \alpha_R, \beta_R) \\ &\times e^{i(\alpha_L \cdot \hat{\chi} + \beta_L \cdot \hat{\pi})}[\cdot] e^{-i(\alpha_R \cdot \hat{\chi} + \beta_R \cdot \hat{\pi})}, \end{aligned} \quad (\text{C.9})$$

where \hat{x} , \hat{p} on the right hand-side are the usual Schrödinger picture operators.

C.2.2 Covariance

The map \mathcal{M} transforms covariantly when

$$\mathcal{M}^{(I)}(t_2, t_1) = \mathcal{G}^{-1} \circ \mathcal{M}^{(I)}(t_2, t_1) \circ \mathcal{G}, \quad (\text{C.10})$$

where

$$\mathcal{G}[\cdot] = \mathcal{U}^{(I)\dagger} \cdot \mathcal{U}^{(I)}$$

and $\mathcal{U}^{(I)}$ is an element of the unitary representation of the symmetry group in interaction picture. Combining Eqs. (C.9), (C.10) we obtain the covariance condition:

$$\begin{aligned} & \int d\alpha_L \int d\beta_L \int d\alpha_R \int d\beta_R g(t_2, t_1, \alpha_L, \beta_L, \alpha_R, \beta_R) \\ & \times \left(e^{i(\alpha_L \mathcal{U}^{(I)\dagger} \hat{\chi} \mathcal{U}^{(I)} + \beta_L \mathcal{U}^{(I)\dagger} \hat{\pi} \mathcal{U}^{(I)})} [\cdot] e^{-i(\alpha_R \mathcal{U}^{(I)\dagger} \hat{\chi} \mathcal{U}^{(I)} + \beta_R \mathcal{U}^{(I)\dagger} \hat{\pi} \mathcal{U}^{(I)})} \right. \\ & \quad \left. - e^{i(\alpha_L \cdot \hat{\chi} + \beta_L \cdot \hat{\pi})} [\cdot] e^{-i(\alpha_R \cdot \hat{\chi} + \beta_R \cdot \hat{\pi})} \right) = 0, \end{aligned} \quad (\text{C.11})$$

Specifically, in the following sections we will consider the unitary operators representing translations and boosts (in interaction picture):

$$\mathcal{U}_{\mathcal{P}}^{(I)} = \exp(i\mathcal{P}^{(I)} a), \quad (\text{C.12})$$

$$\mathcal{U}_{\mathcal{K}}^{(I)} = \exp(i\mathcal{K}^{(I)} \eta), \quad (\text{C.13})$$

where \mathcal{P} , \mathcal{K} are defined in Eqs. (B.4), (B.6), respectively. a is a translation vector and $\eta = c \tanh^{-1}(v/c)$ is the rapidity, which for infinitesimal transformations, reduces to the infinitesimal velocity v .

In the following sections, we will consider infinitesimal transformations. Specifically, the unitary transformations in Eqs. (C.12), (C.13) reduce to:

$$\mathcal{U}_{\mathcal{P}}^{(I)} \cdot \mathcal{U}_{\mathcal{P}}^{(I)\dagger} \approx \cdot + i[\mathcal{P}^{(I)} a, \cdot], \quad (\text{C.14})$$

$$\mathcal{U}_{\mathcal{K}}^{(I)} \cdot \mathcal{U}_{\mathcal{K}}^{(I)\dagger} \approx \cdot + i[\mathcal{K}^{(I)} v, \cdot], \quad (\text{C.15})$$

respectively. Thus a necessary condition for the covariance condition in Eq. (C.11) to be true is given by:

$$[G \cdot \theta, \alpha \cdot \hat{\chi} + \beta \cdot \hat{\pi}] = \lambda \mathbb{I}, \quad (\text{C.16})$$

where α , β are \mathbb{R} numbers, λ is a \mathbb{C} number, G denotes $\mathcal{P}^{(I)}$ or $\mathcal{K}^{(I)}$, while θ denotes a or v , respectively. In this way the operators in the exponents, acting on the statistical operators from the left and right in Eq. (C.11), reduce to

$$(\alpha_L \cdot \mathcal{U}^{(I)\dagger} \hat{\chi} \mathcal{U}^{(I)} + \beta_L \cdot \mathcal{U}^{(I)\dagger} \hat{\pi} \mathcal{U}^{(I)}) = (\alpha_L \cdot \hat{\chi} + \beta_L \cdot \hat{\pi}) + i\lambda_L \mathbb{I}, \quad (\text{C.17})$$

$$(\alpha_R \cdot \mathcal{U}^{(I)\dagger} \hat{\chi} \mathcal{U}^{(I)} + \beta_R \cdot \mathcal{U}^{(I)\dagger} \hat{\pi} \mathcal{U}^{(I)}) = (\alpha_R \cdot \hat{\chi} + \beta_R \cdot \hat{\pi}) + i\lambda_R \mathbb{I}, \quad (\text{C.18})$$

respectively. If we are now able to set $\lambda_L = \lambda_R$, by imposing a constraint on $g(t_2, t_1, \alpha_L, \beta_L, \alpha_R, \beta_R)$, then the covariance condition in Eq. (C.11) is satisfied.

C.2.3 Non-relativistic translations and boosts

To gain some familiarity with the formalism we first consider non-relativistic maps and the non-relativistic generators of translations and boosts given in Eqs. (B.26), (B.28), respectively. We write them in the interaction picture:

$$\mathcal{P}^{(I)} = \hat{p}, \quad (\text{C.19})$$

$$\mathcal{K}^{(I)} = m\hat{x}. \quad (\text{C.20})$$

We now consider the necessary condition for the covariance given by Eq. (C.16). Specifically, for translations and boosts we obtain the following two conditions:

$$[\hat{p} \cdot a, \alpha \cdot \hat{\chi} + \beta \cdot \hat{\pi}] = \lambda \mathbb{I}, \quad (\text{C.21})$$

$$[m\hat{x} \cdot v, \alpha \cdot \hat{\chi} + \beta \cdot \hat{\pi}] = \tilde{\lambda} \mathbb{I}, \quad (\text{C.22})$$

respectively, where $\lambda, \tilde{\lambda}$ are \mathbb{C} numbers. These two conditions are satisfied by considering $\xi = \mathbb{I}$ in Eqs. (C.6),(C.7):

$$\hat{\chi} = \hat{x}, \quad (\text{C.23})$$

$$\hat{\pi} = \hat{p}. \quad (\text{C.24})$$

Specifically, with this particular ξ , from Eqs. (C.21),(C.22) we obtain:

$$\lambda = \alpha \cdot a,$$

$$\tilde{\lambda} = \beta \cdot v,$$

respectively. We can now set $\lambda_L = \lambda_R$ and $\tilde{\lambda}_L = \tilde{\lambda}_R$, where $\lambda_L = \alpha_L \cdot a$, $\lambda_R = \alpha_R \cdot a$, $\tilde{\lambda}_L = \beta_L \cdot v$ and $\tilde{\lambda}_R = \beta_R \cdot v$, by imposing the following symmetry:

$$g(t_2, t_1, \alpha_L, \beta_L, \alpha_R, \beta_R) = \delta(\alpha_L - \alpha_R) \delta(\beta_L - \beta_R) g(t_2, t_1, \alpha_L, \beta_L, \alpha_R, \beta_R), \quad (\text{C.25})$$

Thus the request of translation and Galilean boost covariance only restricts the class of possible modifications of the dynamics, but does not exclude a priori all modifications (for Gaussian maps see [17]).

C.2.4 Relativistic translations and boosts

We now consider the generators of translations and boosts given in Eqs. (B.4), (B.6), respectively. Specifically, the generators in the interaction picture up to (including) order $1/c^2$ reduce to:

$$\mathcal{P}^{(I)} = \hat{p}, \quad (\text{C.26})$$

$$\mathcal{K}^{(I)} = m\hat{x} + \frac{1}{2c^2} \left\{ \hat{x}, \frac{\hat{p}^2}{2m} \right\}. \quad (\text{C.27})$$

We now consider the necessary condition for covariance given by Eq. (C.16). Specifically, for translations and boosts we obtain the following two conditions:

$$[\hat{p} \cdot a, \alpha \cdot \hat{\chi} + \beta \cdot \hat{\pi}] = \lambda \mathbb{I}, \quad (\text{C.28})$$

$$[m\hat{x} \cdot v + \frac{1}{2c^2} \{\hat{x} \cdot v, \frac{\hat{p}^2}{2m}\}, \alpha \cdot \hat{\chi} + \beta \cdot \hat{\pi}] = \tilde{\lambda} \mathbb{I}, \quad (\text{C.29})$$

respectively, where $\lambda, \tilde{\lambda}$ are \mathbb{C} numbers. From Eq. (C.28) we obtain the condition

$$\alpha \cdot \hat{\chi} + \beta \cdot \hat{\pi} = f(\hat{p}) + b \cdot \hat{x} \quad (\text{C.30})$$

where $f(\cdot)$ is an operator valued function and b a \mathbb{C} number. We now use Eq. (C.30) in Eq. (C.29) to obtain:

$$[m\hat{x} \cdot v + \frac{1}{2c^2} \{\hat{x} \cdot v, \frac{\hat{p}^2}{2m}\}, f(\hat{p}) + b \cdot \hat{x}] = \tilde{\lambda} \mathbb{I}, \quad (\text{C.31})$$

which, after some algebra, reduces to:

$$i \left(\frac{1}{c^2} \frac{\hat{p}^2}{2m} + m \right) (v \cdot \partial_{\hat{p}}) f(\hat{p}) - \frac{i}{2c^2} \{\hat{x} \cdot v, \frac{\hat{p} \cdot b}{m}\} = \tilde{\lambda} \mathbb{I}. \quad (\text{C.32})$$

From the first term we obtain the condition that $f(\hat{p}) = C$ is a \mathbb{C} number. From the second term we obtain the condition that $\hat{p} \perp b$, which implies in Eq. (C.30) that $b \cdot \hat{x} = 0$. Thus we obtain that Eq. (C.30) reduces to

$$\alpha \cdot \hat{\chi} + \beta \cdot \hat{\pi} = C \quad (\text{C.33})$$

This equation, in case $\hat{\chi}$ and $\hat{\pi}$ are non-trivial, i.e. are not 0 or \mathbb{I} , can be satisfied only by setting $C = 0$ together with $\alpha = 0$ and $\beta = 0$.

The analysis of the previous paragraph applies both for the operators acting on the statistical operator from the left and from the right. We can set $\alpha_L = \alpha_R = 0$ and $\beta_L = \beta_R = 0$ by imposing the following constraint:

$$g(t_2, t_1, \alpha_L, \beta_L, \alpha_R, \beta_R) = \delta(\alpha_L) \delta(\alpha_R) \delta(\beta_L) \delta(\beta_R) g(t_2, t_1, \alpha_L, \beta_L, \alpha_R, \beta_R) \quad (\text{C.34})$$

In other words, we can only have trivial relativistic translation and Lorentz boost covariant maps, i.e. proportional to 0 or \mathbb{I} . On the other hand, if $\hat{\chi}$ or $\hat{\pi}$ are trivial, we still reach the same conclusion. The same should be true also for higher order relativistic corrections: we leave a rigorous analysis for future research.

Let us now consider a particle with spin $s \neq 0$. In place of the map given in Eq. (C.9) we have a $(2s+1)$ -dimensional matrix map. Based on the results above, the $(2s+1)$ -dimensional matrix map cannot depend on \hat{x} and \hat{p} . A similar extension also applies to the n particle case.

In the next section we give some physical insight into this result and argue that the analysis of this section extends to higher order relativistic corrections.

C.2.5 Physical insight

We consider a system S immersed in an environment E and the corresponding statistical operator ρ defined on the Hilbert space $\mathcal{H}^{(S)} \otimes \mathcal{H}^{(E)}$. We assume, for simplicity of presentation, that the system is composed of a single particle and that the environment is composed by $N-1$ particles. In addition, we assume that the N particles are interacting, with the interaction described by \hat{U} , constrained by Eq. (B.22). Thus, as discussed above, it is possible to write a representation of the Poincaré group with the generators given by Eqs. (B.4), (B.5), (B.6), (B.7): in particular, the evolution map \mathcal{M} is given by Eq. (B.21). We now ask the question: is the map given by Eq. (B.21) covariant under a boost of only the system S ? In the following we assume that Eq. (B.21) is covariant under a translation of only the system S : the key issue, as we have seen in the previous section, is related to Lorentz boosts.

Let us first consider the non-relativistic limit: the generators reduce to the expressions in Eqs. (B.26),(B.27),(B.28),(B.29). By construction, the map \mathcal{M} is Galilei boost covariant, where the boost generator is \mathcal{K} . As discussed above, by an appropriate choice of representation we can set $\hat{V}^{(0)} = 0$ and thus we have

$$\mathcal{K} = \sum_{\mu} \hat{K}_{\mu}. \quad (\text{C.35})$$

Thus, since $[\hat{K}_{\mu}^i, \mathcal{K}^j] = 0$, it follows immediately that it is also covariant under a Galilean boost of the system S .

On the other hand, in the relativistic case, if we have $[\hat{K}_{\mu}^k, \hat{V}^l] \neq 0$ we cannot set $\hat{V} = 0$ by a change of representation as in the non-relativistic case. In addition, from Eq. (B.25) we see that we cannot have $[\hat{K}_{\mu}^k, \hat{V}^l] = 0$, when we have interaction, i.e. $\beta \neq 0$. This argument can be avoided only if we restrict to one spatial dimension, i.e. to a pathological $1+1$ space-time, where the Poincaré algebra contains only the generators of translation in space, evolution in time and boost (without rotations): because the generator of rotations is absent, the constraint given by Eq. (B.25) is trivially satisfied, i.e. it reduces to $0 = 0$, and thus we are allowed to set $\hat{V} = 0$ even in the relativistic case. We thus conclude, for a system of interacting particles in the $1+3$ Minkowski space-time, that we always have $[\hat{K}_{\mu}^i, \mathcal{K}^j] \neq 0$, and thus the dynamics is not covariant under a boost of only the system S : the evolution for the system S cannot be described by a Lorentz covariant map.

We now give some physical insight into this result. In particular, we give a heuristic answer to the following question: why, differently from the non relativistic case, is the relativistic N particle boost \mathcal{K} not a sum of single particle boosts? We argue that this can be explained already looking at the classical relativistic system of N particles with the interaction mediated by a classical field, e.g. charged particles interacting through the electromagnetic field [80]. The field degrees of freedom can be integrated away and thus we obtain a Lagrangian (Hamiltonian) depending only on the particle degrees of freedom, which after quantization can be identified with quantum mechanical operators.

In the non-relativistic case, the interaction becomes instantaneous, and thus the resulting Lagrangian depends only on the positions and velocities of the particles. Based on this analysis, we do not expect anything different from Eq. (C.35). On the other hand, in the relativistic case, considering relativistic corrections due to retardation effects, the resulting Lagrangian will depend also on higher time derivatives of position. Thus, loosely speaking, retardation effects can be associated to a volume around the particle position (higher time derivatives), and the free particle Lorentz boost fails to account for this volume. In other

words, the particle and the volume around the particle, originating from the field degrees of freedom, should be boosted together. Thus, based on this heuristic argument, in the relativistic case it is reasonable to expect Eq. (B.6) in place of Eq. (C.35) for the boost generator (see Fig. C.1).

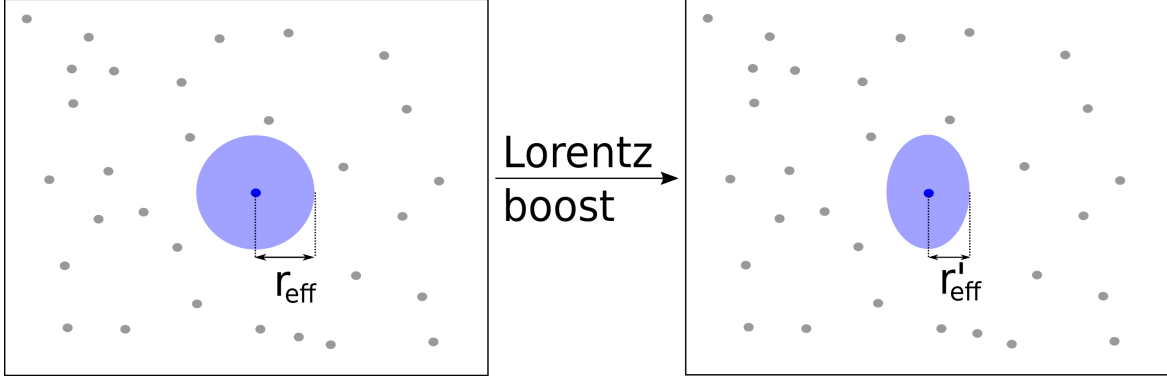


Figure C.1: Depiction of a classical relativistic system (left) and of the Lorentz boosted system (right). The one-particle system S is denoted by the small blue circle, while the environment particles E are depicted by small gray circles. Because of the retardation effects, arising from the finite speed of light, one must consider not only the position of the system particle, but also an effective volume around the particle, denoted by the blue colored region, to correctly boost the system S within the environment E . In particular, the “interaction volume” gets deformed after a Lorentz boost: the sphere gets contracted along the boost axis, i.e. $r'_{eff} < r_{eff}$. This classical relativistic effect prevents the construction of Lorentz covariant maps in a quantum mechanical framework, where particle/antiparticle interactions are suppressed.

C.3 Implications

In this section we look at the implications of the result derived in the previous section.

C.3.1 Non-unitary modification of canonical quantum mechanics

The most well-known examples of non-unitary modifications of the Schrödinger dynamics lead to dynamical maps that also describe decoherence [7, 6]: these maps can be obtained, within the theory of open quantum systems, by tracing away the environment degrees of freedom (both for non-relativistic and fully relativistic modifications). We thus look, based on the result of the previous Sec. C.2.5, at the implications for relativistic modifications of the Schrödinger dynamics, where particle/antiparticle interactions are suppressed, and address the implications for non-relativistic modifications.

The impossibility of a Lorentz covariant modification of the canonical quantum mechanics has an interesting implication for non-relativistic non-unitary modifications of the Schrödinger dynamics: the constraint of exact Galilean covariance can be abandoned. Thus non-relativistic quantum-mechanical modifications are constrained by only an approximately Galilean boost covariance as, within experimental errors, both the microscopic and macroscopic objects obey approximately Galilei covariant laws. An example of such a modification

is given by the dissipative (dCSL) extension [34] of the continuous spontaneous localization (CSL) collapse model [32]: the exact Galilean covariance is broken by a preferred reference frame of a classical noise field. In addition, such models, with only approximate Galilei boost covariance, are motivated by Trace Dynamics [9]. In this theory canonical quantum mechanics is recovered after a coarse graining: in particular, Lorentz covariance is recovered only approximately.

A remark is in order. Relativistic canonical quantum mechanics is only an approximate theory: the approximations involved could potentially be the cause of the impossibility result of this section. Thus, as with all no-go results, the implications have to be carefully considered. In particular, we have shown the impossibility of a relativistic Lorentz covariant quantum theory only within the framework of canonical quantum mechanics, where particle/antiparticle interactions are suppressed. The result of this section could thus be understood as an argument that particle/antiparticle interactions are an essential part of non-unitary modifications of the Schrödinger dynamics: this is the case of recently proposed relativistic spontaneous collapse models [81] (and references therein).

C.3.2 Macroscopicity measure

Recently a measure of macroscopicity μ based on Galilean covariance has been introduced [82]: it is a quantitative measure of the degree of macroscopicity achieved in an experiment. In particular, the macroscopicity measure is constructed from Galilei covariant modifications of the von-Neumann map:

$$\mathcal{M} = \mathcal{M}^{(vN)} + \frac{1}{\tau} \mathcal{M}^{(GM)}, \quad (\text{C.36})$$

where $\mathcal{M}^{(vN)}$ is the von Neumann map discussed in Sec. B.1.2, $\mathcal{M}^{(GM)}$ denotes a Markovian Galilei covariant modification and τ is a characteristic time that quantifies the suppression of linear superpositions. The degree of macroscopicity obtained in a given experiment is defined as:

$$\mu = \log_{10}(\tau_e/1s), \quad (\text{C.37})$$

where τ_e is the greatest excluded time τ of the modification $\mathcal{M}^{(GM)}$.

The assumption of Markovianity and Galilean covariance is a reasonable one, as both microscopic and macroscopic objects, in the non-relativistic regime, are described by Markovian Galilei covariant theories, namely, Quantum and Classical mechanics, respectively. However, as discussed in [58], a relativistic macroscopicity measure is still an open problem. We now address this problem.

Based on the impossibility result of a Lorentz covariant canonical Quantum mechanics, it is reasonable to consider the map:

$$\mathcal{M}^{(aGM)} = \mathcal{M}^{(vN)} + \mathcal{M}^{(GM)} + \mathcal{M}^{(nGM)}, \quad (\text{C.38})$$

where $\mathcal{M}^{(nGM)}$ is a term that breaks Galilei boost covariance. Thus the map $\mathcal{M}^{(aGM)}$ is only approximately Galilean covariant. Although for most experiments the term $\mathcal{M}^{(nGM)}$ is negligible, it might become important for certain experimental predictions.

A similar discussion also applies to non-Markovian effects. The map $\mathcal{M}^{(GM)}$ is a Markovian modification of the von-Neumann map $\mathcal{M}^{(vN)}$. This is again a reasonable assumption as both microscopic and macroscopic objects, in the non-relativistic regime, are described

by approximately Markovian theories, namely, Quantum and Classical mechanics, respectively. However, certain experimental predictions might be sensitive to a non-Markovian modification.

Thus, combining non-Galilei covariant and non-Markovian terms, it might be reasonable to consider the map given by Eq. (C.38), where $\mathcal{M}^{(nGM)}$ is a term that breaks Galilei covariance and is also non-Markovian: $\mathcal{M}^{(aGM)}$ is thus only approximately Galilean boost covariant and only approximately Markovian. We leave for future research the implications for the macroscopicity measure μ in specific experiments.

C.4 Conclusions

We have shown the impossibility of constructing a Lorentz covariant canonical Quantum mechanics. We have briefly discussed the implications. These results may be of relevance for the theoretical development of non-unitary models as well as for definition of macroscopicity. In particular, experiments that probe the lowest order relativistic corrections, i.e. to order $\mathcal{O}(1/c^2)$, could become reality in the near future and could thus provide a test for the ideas of this section.

Appendix D

Relativistic corrections

D.1 Introduction

In this appendix we discuss relativistic extensions of the collapse dynamics introduced in Sec. 3, namely the relativistic CD (rCD) map and the relativistic cdCSL (rcdCSL) model. Specifically, we will obtain, within Foldy's canonical quantum-mechanical framework introduced in Appendix B, explicit $1/c^2$ corrections to the CD map and for the cdCSL model. In addition, we will discuss the procedure to obtain higher order corrections, i.e. to order $1/c^{2n}$ with n a positive integer.

In Sec. D.2 we generalize the CD map to first order in $\mathcal{O}(1/c^2)$. In Sec. D.2 we generalize the cdCSL model to first order in $\mathcal{O}(1/c^2)$. In Sec. D.3 we will discuss the relation of the rcdCSL model with the relativistic CSL proposed in [83].

D.2 Dynamical map

We consider the Gibbs state:

$$\hat{\rho}_{\text{asm}} = \left(\frac{\beta}{2m\pi} \right)^{3/2} \exp(-\beta\hat{H}), \quad (\text{D.1})$$

where

$$\hat{H} = \sqrt{(\hat{p}c)^2 + m^2c^4} \quad (\text{D.2})$$

and $\beta = 1/k_B T$, with k_B the Boltzmann constant. For later convenience we introduce the notation

$$\hat{H} = \hat{H}_{NR} + \hat{H}_{RC}, \quad (\text{D.3})$$

where $\hat{H}_{NR} = mc^2 + \hat{p}^2/2m$ is the non-relativistic Hamiltonian and \hat{H}_{RC} denotes relativistic corrections. Specifically, to order $1/c^2$ we have:

$$\hat{H}_{RC} = -\frac{1}{c^2} \left[\frac{\hat{p}^4}{8m^3} \right]. \quad (\text{D.4})$$

We thus make the ansatz for the operators

$$\tilde{J}(\hat{p}, Q) = \left[\tilde{J}(\hat{p}, Q) \right]_{NR} \exp(-R(\hat{p}, Q)), \quad (\text{D.5})$$

where $\left[\tilde{J}(\hat{p}, Q) \right]_{NR}$ is the non-relativistic operator given in Eq. (3.24) and $R(\hat{p}, Q)$ is an operator valued function to be determined. Specifically, to order $1/c^2$ we make the ansatz:

$$R(\hat{p}, Q) = \frac{1}{c^2} [a_3 \hat{p}^4] \quad (\text{D.6})$$

We now essentially repeat the same procedure as for the non-relativistic calculation in Sec. 3. We impose, to order $1/c^2$, the asymptotic Gibbs state D.1 in Eq.(3.10), where $\tilde{J}(\hat{p}, Q)$ is given in Eq. (D.5):

$$\begin{aligned} & \int dQ \left[\tilde{J}(\hat{p} - Q, Q) \right]_{NR}^2 \hat{\rho}_{NR}(\hat{p} - Q) e^{-R(\hat{p}-Q, Q)} e^{-\beta \hat{H}_{RC}(\hat{p}-Q)} \\ &= \int dQ \left[\tilde{J}(\hat{p}, Q) \right]_{NR}^2 \hat{\rho}_{NR}(\hat{p}) e^{-R(\hat{p}, Q)} e^{-\beta \hat{H}_{RC}(\hat{p})}, \end{aligned} \quad (\text{D.7})$$

where $\hat{\rho}_{NR}$ denotes the non-relativistic part of the statistical operator. We now change $Q \rightarrow Q - b$ on the left hand-side, where b is given in Eq. (3.20):

$$\begin{aligned} & \int dQ \left[\tilde{J}(\hat{p}, Q) \right]_{NR}^2 \hat{\rho}_{NR}(\hat{p}) \left[e^{-R(\hat{p}-(Q-b), Q-b)} e^{-\beta \hat{H}_{RC}(\hat{p}-(Q-b))} \right. \\ & \quad \left. - e^{-R(\hat{p}, Q)} e^{-\beta \hat{H}_{RC}(\hat{p})} \right] = 0. \end{aligned} \quad (\text{D.8})$$

We now expand the exponentials to order $1/c^2$ to obtain:

$$\int dQ \left[\tilde{J}(\hat{p}, Q) \right]_{NR}^2 \hat{\rho}_{NR}(\hat{p}) \left[\left(\frac{\beta}{8m^3} - a_3 \right) (\hat{p} - (Q - b))^4 - \left(\frac{\beta}{8m^3} - a_3 \right) \hat{p}^4 \right] = 0, \quad (\text{D.9})$$

which has the solution:

$$a_3 = \frac{\beta}{8m^3}. \quad (\text{D.10})$$

This concludes the determination of the map rCD to order $1/c^2$. A remark is in order. This result follows from the ansatz in Eq. (D.6): we will briefly discuss the freedom in the choice of the ansatz in Sec. D.4.

D.3 rcdCSL

In the previous section we have identified the map rCD to order $1/c^2$. We can now define the rcdCSL model to order $1/c^2$ by following the procedure of Sec. 3.3 for the non-relativistic cdCSL model. We impose Eqs. (3.34), (3.35), where we again assume a \mathbb{R} valued noise field, and in place of Eq. (3.36) we set:

$$J(\hat{p}, Q) = J_{NR}(\hat{p}, Q) \exp(-\beta \hat{p}^4 / 8m^3 c^2), \quad (\text{D.11})$$

where $J_{NR}(\hat{p}, Q)$ is the operator in Eq. (3.36). The rcdCSL model dynamics, in the second quantized formalism, is then defined by Eqs. (3.37), (3.38) and the corresponding dynamical map is given by Eq. (3.39).

D.4 Higher order corrections

The derivation of the operator $\tilde{J}(\hat{p}, Q)$ in Sec. D.2 (which we denote as $J(\hat{p}, Q)$ in Sec. D.3) can be extended to higher order relativistic corrections. The rcdCSL model dynamics, in the second quantized formalism, is again defined by Eqs. (3.37), (3.38), with the corresponding dynamical map given by Eq. (3.39). We start from Eq. (D.8), which is valid to arbitrary order in $1/c^{2n}$ with n positive integer. We introduce the following compact notation

$$R = \sum_{n=1} \frac{R^{(n)}}{c^{2n}} \quad (\text{D.12})$$

$$\xi_s = e^{-R(\hat{p}-(Q-b), Q-b)} = 1 + \sum_{n=1} \frac{\xi_s^{(n)}}{c^{2n}}, \quad (\text{D.13})$$

$$\Theta_s = e^{-\beta \hat{H}_{RC}(\hat{p}-(Q-b))} = 1 + \sum_{n=1} \frac{\Theta_s^{(n)}}{c^{2n}}, \quad (\text{D.14})$$

$$\xi = e^{-R(\hat{p}, Q)} = 1 + \sum_{n=1} \frac{\xi^{(n)}}{c^{2n}}, \quad (\text{D.15})$$

$$\Theta = e^{-\beta \hat{H}_{RC}(\hat{p})} = 1 + \sum_{n=1} \frac{\Theta^{(n)}}{c^{2n}}, \quad (\text{D.16})$$

It is straightforward to obtain the condition to order $1/c^{2n}$ from (D.8):

$$\int dQ \left(\sqrt{\tilde{D}(Q)} J(\hat{p}, Q) \right)_{NR}^2 \hat{\rho}_{NR}(\hat{p}) F(\xi, \Theta) = 0, \quad (\text{D.17})$$

where

$$F(\xi, \Theta) = \xi_s^{(n)} + \Theta_s^{(n)} + \sum_{j=1}^{n-1} \xi_s^{(j)} \Theta_s^{(n-j)} - \left(\xi^{(n)} + \Theta^{(n)} + \sum_{j=1}^{n-1} \xi^{(j)} \Theta^{(n-j)} \right). \quad (\text{D.18})$$

Using the condition given in Eq. (D.17) we can obtain the $\xi^{(n)}$ iteratively from the lower order correction $\xi^{(j)}$ with $j < n$, by setting $F(\xi, \Theta) = 0$. We have seen that for the first relativistic correction, i.e. to order $1/c^2$, Eq. (D.18) reduces to

$$\xi_s^{(1)} + \Theta_s^{(1)} - \left(\xi^{(1)} + \Theta^{(1)} \right), \quad (\text{D.19})$$

which can be set to 0 by setting $\xi^{(1)} = -\Theta^{(1)}$. However, already at order $1/c^4$ we get a more complicated condition:

$$\xi_s^{(2)} + \Theta_s^{(2)} + \xi_s^{(1)} \Theta_s^{(1)} - \left(\xi^{(2)} + \Theta^{(2)} + \xi^{(1)} \Theta^{(1)} \right). \quad (\text{D.20})$$

We leave for future research, the determination of the explicit expressions for $\xi^{(n)}$. In addition, from the Eqs. (D.12),(D.15) we can obtain the expression for R to each order in $1/c^{2n}$:

$$\sum_{n=1} \frac{\xi^{(n)}}{c^{2n}} = \sum_{k=1} \frac{1}{k!} \left[\sum_{j=1} \frac{R^{(j)}}{c^{2j}} \right]^k \quad (\text{D.21})$$

There is a particularly important question we have not yet addressed: what is the residual freedom in the determination of $\xi^{(n)}$ and thus of $R^{(n)}$? The answer to this question, i.e. characterizing the dynamics that leads to an asymptotic Gibbs state, may not be trivial. In particular, we want to fix higher order corrections without introducing new free parameters in the dynamics: r_C and T should be the only free parameters of the dynamics to all orders in $1/c^{2n}$ (this is the case for the first relativistic correction to order $1/c^2$). We leave the answer to this question for future research.

D.5 Comparison with fully relativistic collapse models

We have obtained a relativistic collapse models with the noise field selecting a preferred reference frame: for example the noise can be identified with a non-quantum background cosmological field. In particular, the interaction with the stochastic field solves the issue of constant energy production of Galilean boost covariant models. This is in stark contrast with previous relativistic collapse models: these models are fully Lorentz-covariant and do not suppress particle/antiparticle interactions. These models, based on the Schwinger-Tomonaga equation, had for a long time suffered from a non-physical constant energy production in conflict with experimental data[6]: only recently this problem was solved with the introduction of a non-standard quantum operator [84]. In particular, a relativistic extension of the CSL was considered in [83].

Besides providing a simple resolution to the energy production issue, the preferred reference frame approach can be also used to define the ontology in a natural way: the relation between the wave-function and matter in physical space. For example, the preferred reference frame can be used to define the following matter-density ontology[6]:

$$m(x, t) = \sum_{i=1}^N m_i \int dy_1 \dots dy_N \delta(x - y_i) |\psi_t(y_1, \dots, y_N)|^2, \quad (\text{D.22})$$

where $m(x, t)$ denotes the mass density in \mathbb{R}^3 for N with masses m_i and $\psi_t(y_1, \dots, y_N)$ is the wave-function in the preferred reference frame of the noise field. This fixes the matter-density on the whole manifold. On the other hand, the matter density ontology for the Lorentz covariant models proposed in the literature is defined with the help of the light cone [81].

There is another benefit of the preferred reference frame approach: the theory has a straightforward non-relativistic limit and relativistic corrections are easy to evaluate. In particular, the first relativistic correction to order $\mathcal{O}(1/c^2)$ puts the predictions of this model within reach of current experiments.

We will analyze in detail the properties of the rdCSL model (collapse mechanism, amplification mechanism) and investigate the connection with the relativistic CSL considered in [83] in a future work.

Bibliography

- [1] John S. Bell. *Speakable and unspeakable in Quantum mechanics: Collected papers on quantum philosophy*. Cambridge university press, 2004.
- [2] Detlef Dürr, Sheldon Goldstein, and Nino Zanghì. *Quantum physics without quantum philosophy*. Springer Science & Business Media, 2012.
- [3] GianCarlo Ghirardi. *Sneaking a look at God’s cards: unraveling the mysteries of Quantum mechanics*. Princeton University Press, 2005.
- [4] Leslie E. Ballentine. The statistical interpretation of Quantum mechanics. *Reviews of Modern Physics*, 42(4):358, 1970.
- [5] Erwin Schrödinger. Die gegenwärtige Situation in der Quantenmechanik. *Naturwissenschaften*, 23(49):823–828, 1935.
- [6] Angelo Bassi and GianCarlo Ghirardi. Dynamical reduction models. *Physics Reports*, 379(5):257–426, 2003.
- [7] Angelo Bassi, Kinjalk Lochan, Seema Satin, Tejinder P Singh, and Hendrik Ulbricht. Models of wave-function collapse, underlying theories, and experimental tests. *Reviews of Modern Physics*, 85(2):471, 2013.
- [8] GianCarlo Ghirardi, Alberto Rimini, and Tullio Weber. Unified dynamics for microscopic and macroscopic systems. *Physical Review D*, 34(2):470, 1986.
- [9] Stephen L. Adler. *Quantum theory as an emergent phenomenon: The statistical mechanics of matrix models as the precursor of Quantum field theory*. Cambridge University Press, 2004.
- [10] Roger Penrose. On gravity’s role in quantum state reduction. *General relativity and gravitation*, 28(5):581–600, 1996.
- [11] Marko Toroš, Sandro Donadi, and Angelo Bassi. Bohmian mechanics, collapse models and the emergence of classicality. *Journal of Physics A: Mathematical and Theoretical*, 49(35):355302, 2016.
- [12] Christoph Simon, Vladimír Bužek, and Nicolas Gisin. No-signaling condition and quantum dynamics. *Physical Review Letters*, 87(17):170405, 2001.
- [13] Giulio Gasbarri, Marko Toroš, and Angelo Bassi. Structure of collapse models. (*in preparation*), 2017.

- [14] Marko Toroš, Giulio Gasbarri, and Angelo Bassi. Colored and dissipative continuous spontaneous localization model. (*in preparation*), 2017.
- [15] Marko Toroš and Angelo Bassi. Bounds on collapse models from matter-wave interferometry. *arXiv preprint arXiv:1601.03672*, 2016.
- [16] Marko Toroš and Angelo Bassi. Bounds on collapse models from matter-wave interferometry: Computational details. *arXiv preprint arXiv:1601.02931*, 2016.
- [17] Giulio Gasbarri, Marko Toroš, and Angelo Bassi. Galilean covariant Gaussian maps. (*in preparation*), 2017.
- [18] Marko Toroš, Giulio Gasbarri, and Angelo Bassi. Relativity and classicalization maps. (*in preparation*), 2017.
- [19] Stephen L. Adler and Angelo Bassi. Collapse models with non-white noises. *Journal of Physics A: Mathematical and Theoretical*, 40(50):15083, 2007.
- [20] Stephen L. Adler and Angelo Bassi. Collapse models with non-white noises: II. particle-density coupled noises. *Journal of Physics A: Mathematical and Theoretical*, 41(39):395308, 2008.
- [21] Hermann Weyl. Quantenmechanik und gruppentheorie. *Zeitschrift für Physik*, 46(1-2):1–46, 1927.
- [22] Kuang-chao Chou, Zhao-bin Su, Bai-lin Hao, and Lu Yu. Equilibrium and nonequilibrium formalisms made unified. *Physics Reports*, 118(1-2):1–131, 1985.
- [23] Lajos Diósi. Landau’s density matrix in quantum electrodynamics. *Foundations of Physics*, 20(1):63–70, 1990.
- [24] Lajos Diósi. Calderia-Leggett master equation and medium temperatures. *Physica A: Statistical Mechanics and its Applications*, 199(3-4):517–526, 1993.
- [25] Leon Isserlis. On a formula for the product-moment coefficient of any order of a normal frequency distribution in any number of variables. *Biometrika*, 12(1/2):134–139, 1918.
- [26] Alberto Barchielli. Applications of quantum stochastic calculus to quantum optics. *Quantum Probability and Related Topics*, 6:111–125, 1991.
- [27] Angelo Bassi. Collapse models: analysis of the free particle dynamics. *Journal of Physics A: Mathematical and General*, 38(14):3173, 2005.
- [28] Angelo Bassi, Detlef Duerr, and Martin Kolb. On the long time behavior of free stochastic Schrödinger evolutions. *Reviews in Mathematical Physics*, 22(01):55–89, 2010.
- [29] Lajos Diósi and Luca Ferialdi. General non-Markovian structure of Gaussian master and stochastic Schrödinger equations. *Physical review letters*, 113(20):200403, 2014.
- [30] Lajos Diósi. Models for universal reduction of macroscopic quantum fluctuations. *Physical Review A*, 40(3):1165, 1989.
- [31] Philip Pearle. Combining stochastic dynamical state-vector reduction with spontaneous localization. *Physical Review A*, 39(5):2277, 1989.

- [32] GianCarlo Ghirardi, Philip Pearle, and Alberto Rimini. Markov processes in Hilbert space and continuous spontaneous localization of systems of identical particles. *Phys. Rev. A*, 42:78–89, Jul 1990.
- [33] Lajos Diósi. Relativistic theory for continuous measurement of quantum fields. *Physical Review A*, 42(9):5086, 1990.
- [34] Andrea Smirne and Angelo Bassi. Dissipative continuous spontaneous localization (CSL) model. *Scientific Reports*, 5:12518 EP –, Aug 2015. Article.
- [35] Angelo Bassi, Emiliano Ippoliti, and Bassano Vacchini. On the energy increase in space-collapse models. *Journal of Physics A: Mathematical and General*, 38(37):8017, 2005.
- [36] Angelo Bassi and Luca Ferialdi. Non-Markovian dynamics for a free quantum particle subject to spontaneous collapse in space: General solution and main properties. *Physical Review A*, 80(1):012116, 2009.
- [37] Luca Ferialdi and Angelo Bassi. Dissipative collapse models with nonwhite noises. *Physical Review A*, 86(2):022108, 2012.
- [38] John S. Bell et al. On the Einstein-Podolsky-Rosen paradox. *Physics*, 1(3):195–200, 1964.
- [39] Alain Aspect, Philippe Grangier, and Gérard Roger. Experimental tests of realistic local theories via Bell’s theorem. *Phys. Rev. Lett.*, 47:460–463, Aug 1981.
- [40] Alain Aspect, Philippe Grangier, and Gérard Roger. Experimental realization of Einstein-Podolsky-Rosen-Bohm *Gedankenexperiment* : A new violation of Bell’s inequalities. *Phys. Rev. Lett.*, 49:91–94, Jul 1982.
- [41] Alain Aspect, Jean Dalibard, and Gérard Roger. Experimental test of Bell’s inequalities using time - varying analyzers. *Phys. Rev. Lett.*, 49:1804–1807, Dec 1982.
- [42] Stefan Nimmrichter, Klaus Hornberger, Philipp Haslinger, and Markus Arndt. Testing spontaneous localization theories with matter-wave interferometry. *Phys. Rev. A*, 83:043621, Apr 2011.
- [43] Klaus Hornberger, John E. Sipe, and Markus Arndt. Theory of decoherence in a matter wave Talbot-Lau interferometer. *Phys. Rev. A*, 70:053608, Nov 2004.
- [44] Klaus Hornberger. Thermal limitation of far-field matter-wave interference. *Phys. Rev. A*, 73:052102, May 2006.
- [45] Philip Pearle. Ways to describe dynamical state-vector reduction. *Phys. Rev. A*, 48:913–923, Aug 1993.
- [46] Björn Brezger, Markus Arndt, and Anton Zeilinger. Concepts for near-field interferometers with large molecules. *Journal of Optics B: Quantum and Semiclassical Optics*, 5(2):S82, 2003.
- [47] Michele Sclafani. *Molecular beam methods for quantum optics experiments: sources, detection schemes and coherent manipulation*. PhD thesis, Universität Wien, 2013.

- [48] Sandra Eibenberger, Stefan Gerlich, Markus Arndt, Marcel Mayor, and Jens Tüxen. Matter-wave interference of particles selected from a molecular library with masses exceeding 10 000 amu. *Phys. Chem. Chem. Phys.*, 15:14696–14700, 2013.
- [49] Philip Pearle and Euan Squires. Bound state excitation, nucleon decay experiments and models of wave function collapse. *Phys. Rev. Lett.*, 73:1–5, Jul 1994.
- [50] Mohammad Bahrani, Andrea Smirne, and Angelo Bassi. Role of gravity in the collapse of a wave function: A probe into the Diósi-Penrose model. *Phys. Rev. A*, 90:062105, Dec 2014.
- [51] Andrea Smirne, Bassano Vacchini, and Angelo Bassi. Dissipative extension of the Ghirardi-Rimini-Weber model. *Phys. Rev. A*, 90:062135, Dec 2014.
- [52] Bassano Vacchini and Klaus Hornberger. Quantum linear Boltzmann equation. *Physics Reports*, 478(4):71–120, 2009.
- [53] Andrea Smirne and Bassano Vacchini. Quantum master equation for collisional dynamics of massive particles with internal degrees of freedom. *Phys. Rev. A*, 82:042111, Oct 2010.
- [54] Sandro Donadi, Dirk-André Deckert, and Angelo Bassi. On the spontaneous emission of electromagnetic radiation in the CSL model. *Annals of Physics*, 340(1):70 – 86, 2014.
- [55] Stephen L. Adler. Lower and upper bounds on CSL parameters from latent image formation and IGM heating. *Journal of Physics A: Mathematical and Theoretical*, 40(12):2935, 2007.
- [56] Stefan Nimmrichter, Klaus Hornberger, and Klemens Hammerer. Optomechanical sensing of spontaneous wave-function collapse. *Phys. Rev. Lett.*, 113:020405, Jul 2014.
- [57] William Feldmann and Roderich Tumulka. Parameter diagrams of the GRW and CSL theories of wavefunction collapse. *Journal of Physics A: Mathematical and Theoretical*, 45(6):065304, 2012.
- [58] Stefan Nimmrichter. *Macroscopic Matter Wave Interferometry (Springer Theses)*. Springer International Publishing, 2014.
- [59] Brian Collett, Philip Pearle, Frank Avignone, and Shmuel Nussinov. Constraint on collapse models by limit on spontaneous X-ray emission in Ge. *Foundations of Physics*, 25(10):1399–1412, 1995.
- [60] Brian Collett and Philip Pearle. Wavefunction collapse and random walk. *Foundations of Physics*, 33(10):1495–1541, 2003.
- [61] Thomas Juffmann, Adriana Milic, Michael Müllneritscha, Peter Asenbaum, Alexander Tsukernik, Jens Tüxen, Marcel Mayor, Ori Cheshnovsky, and Markus Arndt. Real-time single-molecule imaging of quantum interference. *Nature Nanotechnology*, 7:297 – 300, 2012.
- [62] Catalina Curceanu, Beatrix C. Hiesmayr, and Kristian Piscicchia. X-rays help to unfuzzy the concept of measurement. *Journal of Advanced Physics*, 4(3):263–266, 2015-09-01T00:00:00.

- [63] Matteo Carlesso, Angelo Bassi, Paolo Falferi, and Andrea Vinante. Experimental bounds on collapse models from gravitational wave detectors. *arXiv preprint arXiv:1606.04581*, 2016.
- [64] Lajos Diòsi. A universal master equation for the gravitational violation of Quantum mechanics. *Physics Letters A*, 120(8):377 – 381, 1987.
- [65] Vittorio Gorini, Andrzej Kossakowski, and Ennackal C. G. Sudarshan. Completely positive dynamical semigroups of n-level systems. *Journal of Mathematical Physics*, 17(5):821–825, 1976.
- [66] Goran Lindblad. On the generators of Quantum dynamical semigroups. *Communications in Mathematical Physics*, 48(2):119–130, 1976.
- [67] Alexander S. Holevo. A note on covariant dynamical semigroups. *Reports on mathematical physics*, 32(2):211–216, 1993.
- [68] Alexander S. Holevo. On conservativity of covariant dynamical semigroups. *Reports on Mathematical Physics*, 33(1-2):95–110, 1993.
- [69] Alexander S. Holevo. On translation-covariant quantum Markov equations. *Izvestiya: Mathematics*, 59(2):427–443, 1995.
- [70] Alexander S. Holevo. Covariant quantum Markovian evolutions. *Journal of Mathematical Physics*, 37(4):1812–1832, 1996.
- [71] EB Davies. d. funct. *Analysis*, 6:318, 1970.
- [72] Alexander S. Holevo. Statistical decision theory for Quantum systems. *Journal of Multivariate Analysis*, 3(4):337–394, 1973.
- [73] Leslie L. Foldy. Synthesis of covariant particle equations. *Physical Review*, 102(2):568, 1956.
- [74] R.A. Krajcik and Leslie L. Foldy. Relativistic center-of-mass variables for composite systems with arbitrary internal interactions. *Physical Review D*, 10(6):1777, 1974.
- [75] Claus Lämmerzahl. The pseudodifferential operator square root of the Klein–Gordon equation. *Journal of mathematical physics*, 34(9):3918–3932, 1993.
- [76] Karol Kowalski and Jakub Rembieliński. Salpeter equation and probability current in the relativistic Hamiltonian Quantum mechanics. *Physical Review A*, 84(1):012108, 2011.
- [77] Leslie L. Foldy and Siegfried A. Wouthuysen. On the Dirac theory of spin 1/2 particles and its non-relativistic limit. *Physical Review*, 78(1):29, 1950.
- [78] Erdal Inonu and Eugene P. Wigner. On the contraction of groups and their representations. *Proceedings of the National Academy of Sciences*, 39(6):510–524, 1953.
- [79] Heinz-Peter Breuer and Francesco Petruccione. *The theory of open quantum systems*. Oxford University Press on Demand, 2002.

- [80] Charles G. Darwin. LI. The dynamical motions of charged particles. *The London, Edinburgh, and Dublin Philosophical Magazine and Journal of Science*, 39(233):537–551, 1920.
- [81] Daniel J. Bedingham, Detlef Dürr, GianCarlo Ghirardi, Sheldon Goldstein, Roderich Tumulka, and Nino Zanghì. Matter density and relativistic models of wave function collapse. *Journal of Statistical Physics*, 154(1-2):623–631, 2014.
- [82] Stefan Nimmrichter and Klaus Hornberger. Macroscopicity of mechanical quantum superposition states. *Physical review letters*, 110(16):160403, 2013.
- [83] Philip Pearle. Relativistic dynamical collapse model. *Physical Review D*, 91(10):105012, 2015.
- [84] Daniel J. Bedingham. Relativistic state reduction dynamics. *Foundations of Physics*, 41(4):686–704, 2011.